Spastin regulates microtubule dynamics and is required for normal motor and cognitive functions

Dissertation

Zur Erlangung des Doktorgrades der Naturwissenschaften vorgelegt im Fachbereich Biologie der Fakultät für Mathematik, Informatik und Naturwissenschaften der Universität Hamburg

von
André Teixeira Lopes
aus Chaves, Portugal

Hamburg
2017

Day of oral defense: 23rd June 2017

Gutachter:

Prof. Dr. Matthias Kneussel

Prof. Dr. Christian Lohr

Prüfungskommission:

Prof. Dr. Susanne Dobler

Junior Prof. Dr. Esther Diekhoff

Dr. Torben Hausrat

Dr. Michaela Schweizer

PD Dr. Sabine Hoffmeister-Ullerich

Eidesstattliche Versicherung

Declaration on oath

Hiermit erkläre ich an Eides statt, dass ich die vorliegende Dissertationsschrift selbst verfasst und keine anderen als die angegebenen Quellen und Hilfsmittel benutzt habe.

I hereby declare, on oath, that I have written the present dissertation by my own and have not used other than the acknowledged resources and aids.

Unterschrift / Signature

Hamburg, den 18 Mai 2017

Table of contents

Abstract 6
1 Introduction 8
1.1 Brain organization and function 8
1.2 Synapse formation in the CNS 9
1.3 Chemical neurotransmission 10
1.4 Clinical features and epidemiology of HSP 12
1.5 Autosomal Dominant HSP 12
1.6 Pathophysiology of HSP 13
1.7 Neuronal cytoskeleton: microtubules and actin 14
1.8 Microtubule-severing enzymes 17
1.9 Mechanisms of microtubule severing 19
1.10 Roles of spastin in the nervous system 20
1.11 Cellular functions of spastin 20
1.12 Mouse models of hereditary spastic paraplegia 21
1.13 Intracellular protein transport 22
1.14 Microtubule modifications and kinesin-mediated transport 24
1.15 Polyglutamylation of microtubules 26
1.16 Detyrosination and tyrosination of microtubules 26
1.17 Acetylation of microtubules 27
1.18 Role of the hippocampus in learning and memory 27
1.19 Microtubule stability and memory 28
1.20 AMPA receptor trafficking 30
1.21 Related defects and disease 32
1.22 Aims of the research project 33
2. Material and methods 35
2.1 Chemicals 35
2.2 Apparatus 35
2.3 Media and solutions 37
2.4 Antibodies 40
2.4.1 Primary antibodies 40
2.4.2 Secondary antibodies 41
2.5 Vectors 41
2.6 Olygonucleotides 42
2.7 Molecular biological methods 42

2.7.1 Transformation of DH5alpha competent cells 42
2.7.2 Isolation of plasmid-DNA from DH5alpha competent cells (midipreps) 43
2.7.3 Determination of DNA concentration and purity 43
2.7.4 Agarose Gel Electrophoresis 43
2.7.5 DNA sequencing 44
2.7.6 Genotyping PCR of spastin knockout mice 44
2.8 Cell Biology and immunocytochemistry 45
2.8.1 Preparation of primary cultures of hippocampal neurons 45
2.8.2 - Calcium phosphate-based transfection of neurons 46
2.8.3 Immunocytochemistry on hippocampal neurons 46
2.9 Image and tracking analysis 47
2.10 Biochemical experiments 48
2.10.1 Mouse brain differential centrifugation 48
2.10.2 Lysates of Cultured Neurons 48
2.10.3 Preparation of Proteins Samples for SDS electrophoresis 49
2.10.4 SDS-poly-acrylamide gel electrophoresis (SDS-PAGE) 49
2.10.5 Western blotting analysis 50
2.10.6 Electron microscopy 50
2.10.7 Pharmacological manipulation of microtubule stability 51
2.11 Histology and immunohistochemistry 52
2.12 Behavior experiments 53
2.12.1 Subjects and housing 53
2.12.2 Horizontal grid test 53
2.12.3 Pole test 54
2.12.4 Grip Strength test 54
2.12.5 Accelerating Rotarod Test 55
2.12.6 Y-maze spontaneous alternation 55
2.12.7 T-maze confined alternation 55
2.12.8 Contextual Fear Conditioning 56
3. Results 59
3.1 General phenotypical characterization of the spastin knockout mouse 59
3.2 Spastin -/- mice show age-dependent motor impairments 61
3.3 Working memory impairments in mice lacking spastin 63
3.4 Impaired contextual fear memory in spastin-depleted mice 65
3.5 Synapse formation in spastin -/- neurons 68

3.6 Altered dendritic spine formation in spastin knockout neurons ...71
3.7 Minor perturbations in synaptic structure of spastin -/- neurons ..72
3.8 Reduced surface expression of GluA2-containing AMPA receptors in spastin (-/-) neurons 74
3.9 Microtubule stability in neurons lacking spastin 76
3.10 Longer microtubules in neurons lacking spastin 78
3.11 Microtubule dynamics in neurons lacking spastin 79
3.12 Altered GluA2-containing AMPA receptor transport in spastin (-/-) neurons 80
3.13 Altered KIF5C motility in spastin (-/-) neurons 81
3.14 Altered mitochondria transport in dendrites from spastin (-/-) neurons 82
3.15 Synaptophysin transport is altered in spastin (-/-) neurons 84
3.16 Taxol-induced stability of microtubules decreases surface GluA2-containing AMPA receptor levels 85
4. Discussion 88
4.1 Characterization of spastin knockout mouse 88
4.2 Implications of spastin depletion on motor neuron function 89
4.3 Impact of spastin depletion on cognitive function 90
4.4 Impact of a lack of spastin on contextual fear learning 92
4.5 Role of spastin in synapse formation and maintenance 94
4.6 Impact of microtubule deletion on microtubule dynamics 95
4.7 Microtubule stabilization affects the surface distribution of AMPA receptors 97
4.8 Regulation of microtubule-dependent intracellular transport by spastin 99
5. Conclusions and future directions 103
6. References 106
7. Appendix 115
7.1 List of figures 115
7.2 List of tables 116
7.3 Abbreviations 116
8. Acknowledgements 120

Abstract

The distribution of membrane proteins to specific subcellular domains poses particular challenges to the protein trafficking machinery of nerve cells. Most transmembrane proteins are transported over long distances from the soma into axons and dendrites. This intracellular transport is driven in an ATP-dependent manner by kinesin and dynein motor proteins along microtubules.

Microtubules are polymeric cytoskeletal structures with variable lengths, which can grow or shrink resulting in a dynamic cellular network. Neurons contain both stable and dynamic pools of microtubules that can be regulated by microtubule severing proteins. Spastin, a member of AAA ATPase family, encoded by the *SPAST* gene, is one of these severing proteins expressed in neurons.

Microtubule function can be modulated by microtubule associated proteins and different post-translational modifications of tubulin subunits. Notably, tubulin polyglutamylation promotes microtubule severing through spastin.

Here, I used a mouse model lacking spastin to analyze the role of microtubule severing proteins regarding motor protein-dependent transport of glutamate receptors. In hippocampal spastin knockout neurons, I observed increased microtubule stability and altered microtubule dynamics. Additionally, the transport of glutamate receptors was diminished. Consequently, glutamate receptor levels at the cell surface were significantly reduced. Behavioral analysis showed impaired motor performance and specific learning and memory deficits in spastin knockout mice.

These data suggest that microtubule severing provides an important mechanism to maintain the cell surface delivery of synaptic proteins. This might explain the cognitive deficits observed in mice lacking the microtubule-severing protein spastin.

Chapter 1

Introduction

1 Introduction

1.1 Brain organization and function

The central nervous system (CNS) of mammals is divided into two major structures: the brain and the spinal cord.

The brain is a complex organ that has the astonishing ability to process and store information that it receives from the environment and also to regulate the internal homeostasis. The complexity of the brain is not only functional but also structural with almost 100 billion neurons organized in different regions [1].

The brain can be further subdivided into hindbrain, midbrain and forebrain. Based on their functions and anatomical differences these three brain regions can be divided in multiple subregions [2].

The neuron is the structural and functional unit of the nervous system made of a soma that contains the nucleus and the cytoplasm. The soma of the neuron extends outwards to form processes termed as dendrites, which can branch further and originate small protrusions called dendritic spines. Neuronal cells have a single axon that conveys information away from the soma towards the nerve terminal or bouton. Dendritic spines and the bouton of the nerve terminal form a connection known as synapse that allows the transmission of information between neurons. Neurons can be organized in distinct layers like in the hippocampus and the cerebral cortex or clusters, known as “nuclei” in the CNS. The specific connectivity among different neurons within an area of the brain or with other brain regions is fundamental for the proper function of the brain.

The CNS also contains non-neuronal cells such as glial cells that have a supportive function to the neurons and include macroglia and microglia. The macroglial cells comprise astrocytes that supply energy to neurons and are involved in the clearance of released neurotransmitters from the synaptic cleft. Another member of the macroglia family are the myelinating cells of the CNS, the oligodendrocytes. These cells participate in the isolation of the axons, thus ensuring the unidirectionality of the action potential. Microglia are the immune cells of the CNS and become active during episodes of acute inflammation.

1.2 Synapse formation in the CNS

Synaptogenesis is the process by which the formation of functional synapses occurs. This biological process originates during embryonic development and lasts until the early postnatal period. Later on, synapses can be strengthened and stabilized, or weakened and eliminated, processes that largely underlying learning and memory function [3].

Neuronal cells start to express pre- and postsynaptic proteins prior to the formation of new synapses. The bi-directional signaling between the pre- and the postsynapse is important for the organization of synaptic components at newly formed synaptic contacts. The formation of synaptic contacts occurs rapidly in the range of 1-2 hours, with the mobilization of the pre- and postsynaptic terminals within 10-20 minutes.

The initial contact between the axon and dendrites is achieved through filopodia-like processes. The interaction between the two synaptic compartments can be mediated via the axonal protein neurexin and the dendritic protein, neuroligin. The timing and positioning of neurexin-neuroligin interactions determine the formation of the synapse.

The assembly of neuronal compartments involves the trafficking of various types of vesicles or the recruitment of individual proteins that are trapped and accumulate either at the active zone membrane or at the postsynaptic density [4-6].

The formation of neuronal connections is regulated by different signaling molecules that guide axons and dendrites to come closer and form a synapse. An important group of signaling molecules includes the cell-surface adhesion molecules (CAM) that regulate the initial steps of synapse formation [7, 8].

The early accumulation of several types of vesicles at the newly forming synapses might be the triggering mechanism for the formation of a fully functional presynaptic compartment. Proteins such as SYNCAM and neuroregulin are important players in the assembly of the active zone membrane [9].

Some presynaptic components like synaptophysin, Bassoon, Picollo, and RIM or components of the vesicle exocytotic machinery are the first to be transported to the presynaptic side through the axon. At the same time,

proteins of the postsynaptic density, namely the PSD95 scaffolding family, start to accumulate in the dendritic spine [10, 11].

Closely after, the accumulation of postsynaptic density protein 95 (PSD95) α-amino-3-hydroxy-5-methyl-4-isoxazolepropionic acid receptor (AMPA) and N-methyl-D-aspartate receptor (NMDA) receptors are mobilized directly into the postsynaptic density or to the vicinity of the dendritic spine.

Newly formed synapses undergo a process of maturation that will change their shape and their composition of receptors. For instance, glutamate receptors accumulate initially on filopodia-shaped dendritic spines or on dendritic shafts, which then develop into mature dendritic spines. Mature dendritic spines can be classified into stubby, thin, branched and mushroom type [12].

The presynaptic bouton will also undergo a process of maturation in which it grows in size with more accumulation of synaptic vesicles.

Not all the pre- and postsynaptic components need to be synthesized in the soma and to be transported through long-range transport mechanisms. For instance, local protein synthesis may also supply the dendritic spine with various components if their mRNAs are available. Some examples include CAMKIIα, Shank, NR1 and GluR1/2 whose abundant mRNAs in dendrites can be locally translated.

Synapses employ different neurotransmitters such as glutamate (excitatory), which depolarizes the postsynaptic cell, or GABA (inhibitory), which leads to hyperpolarization of the membrane [13]. The assembly of synaptic connections in the CNS is not static and responds to plastic changes that modify the neuronal circuits. During the developmental stage, the axon communicates with several dendrites, but later on, many of these contacts will be eliminated (synaptic pruning) [14]. Although not a determining factor during the assembly of the synapse, synaptic activity plays an important role in the final selection and maintenance of fully functional synapses [3, 15, 16].

1.3 Chemical neurotransmission

The nervous system of vertebrates contains mainly chemical synapses, and the main focus of this study will be on this type of synapse. The synapse

works by converting an electrical signal, the action potential, into chemical signals. Therefore, neurotransmitters are released into the space between the presynaptic bouton and a dendritic spine, called the synaptic cleft. These chemical signals are then postsynaptically converted back to electrical impulses by binding to postsynaptic neurotransmitter receptors. In more detail, the generated action potential reaches the presynaptic terminal causing the opening of voltage gated calcium channels and influx of calcium ions. The calcium ions bind to calcium sensors and trigger the release of neurotransmitters by membrane fusion of the docked vesicles with the active zone plasma membrane. Released neurotransmitters activate specific receptors at the postsynaptic membrane, which allows the formation of a new action potential [17].

The primary neurotransmitters are glutamate, GABA, dopamine, serotonin and glycine. They are synthesized in the soma and loaded into synaptic vesicles that can be transported by specific motor proteins toward the presynaptic terminal. Neurotransmitter receptors can be classified into ionotropic or G-protein coupled. G-protein coupled receptors, also known as metabotropic, bind to the neurotransmitter and undergo conformational changes yielding an intracellular response. Another family of neurotransmitter receptors is the ionotropic receptors that allow ions to pass through a channel pore when bound to the agonist. Some examples include NMDA-type and AMPA-type glutamate receptors [18].

Depending on which type of receptor the neurotransmitter binds to, they induce fast synaptic transmission through ligand gated receptors or slower synaptic transmission, when metabotropic receptors are activated.

Neurotransmitters can be removed from their receptors through one of three ways: they can be cleaved by different enzymes located at the synaptic cleft, recycle back to the presynaptic terminal or simply diffuse away. The reversibility of the binding of neurotransmitters to their receptors is important; otherwise a permanent interaction would lead to constant activation of the receptor, which causes neurotoxic effects.

1.4 Clinical features and epidemiology of HSP

Hereditary spastic paraplegias (HSP) are a heterogeneous group of neurodegenerative disorders clinically characterized by progressive weakness and spasticity of the lower limbs [19]. In most cases of HSP, the spasticity is the consequence of progressive retrograde axonopathy, which affects mainly the longest nerve fibers of the corticospinal tracts. Compared to other causes of spastic paraplegia such as spinal injury or multiple sclerosis, the muscle strength of HSP patients seems not to be affected, despite an increased muscle tonus of the legs.

Neuronal loss has been also reported in some cases of HSP, but so far there is no evidence that this is involved in the etiology of the disease.

From the available epidemiologic studies, the incidence of HSP is estimated at 3-10 patients per 100,000 inhabitants in Europe and can be inherited by autosomal dominant, autosomal recessive and x-linked recessive mechanisms [20-22].

Not only does the mode of inheritance vary, but also the onset of the disease ranges from early childhood up to 70 years of age. The progressive impairment of locomotion in HSP patients can make them dependent on walkers or even a wheelchair at some point in their lives.

Traditionally, HSP forms are classified into uncomplicated (pure) HSP and complicated cases. The pure form of HSP includes mild sensory problems of the lower limbs, urinary urgency and mild cognitive deficits. In addition to spastic paraplegia, complicated forms of HSP comprise a broader number of abnormalities such as ataxia, optic atrophy, mental retardation, dementia and epilepsy among others.

1.5 Autosomal Dominant HSP

So far, 224 *SPAST* mutations have been described in the literature. They include nonsense, missense, frame shift, splice side and large deletion mutations. Mutations in the *SPAST* gene that encodes spastin, a microtubule-severing enzyme, account for up to 45% of all cases of autosomal dominant HSP.

Patients suffering from autosomal dominant HSP start to display the first symptoms in childhood, which persists throughout life. In most cases, the disease progresses slowly and on average the loss of mobility occurs 20 years after the first symptoms.

Patients who suffer from this type of HSP for several years develop urinary dysfunction, deceased vibration sense, muscle wasting of the lower limbs and cerebellar ataxia.

There are also reports of patients presenting progressive cognitive decline, which starts at 40 years of age and can progress to overt dementia by the age of 60-80 years [23-26].

1.6 Pathophysiology of HSP

The main pathophysiological hallmark of HSP is the progressive degeneration of long axons from the ascending and descending pathways of the spinal cord [27]. A possible explanation for the observed axonopathy is that many of the mutated genes in HSP (SPG30/KIF1A, SPG10/KIF5A) encode for important players in axonal transport of organelles, receptors and other cargoes. Due to the unique and challenging neuronal morphology with axons reaching up to one meter in length in humans, minor defects in the transport might have profound effects on the proper neuronal function [28-30].

Supporting the hypothesis of altered transport in HSP pathology, some of the mutated genes found in HSP patients encode for motor proteins such as KIF5A that has been linked to a pure form of HSP. KIF5A is a kinesin motor responsible for the anterograde transport of cargoes along the microtubules in axons and dendrites [30].

Data stemming from *in vitro* studies show that mutant forms of KIF5A bind microtubules with less affinity or the motility of this kinesin is reduced, leading to an impairment of the kinesin-dependent transport, which ultimately can cause terminal degeneration of axons.

Studies conducted in Drosophila and zebrafish overexpressing wild-type spastin showed that this microtubule-severing protein has an important role on synaptic function and axonal growth [31, 32]. Also, data from a mouse model with a deletion mutation in the *SPAST* gene leading to a premature

stop codon showed evidence for axonal transport defects leading to mitochondria accumulation and altered organization of the cytoskeleton [33, 34].

In conclusion, it appears that mutations in the *SPAST* gene, a key player in the maintenance of the microtubule cytoskeleton might negatively affect the transport of various cargoes along the axon and dendrites.

1.7 Neuronal cytoskeleton: microtubules and actin

Microtubules are major components of the cytoskeleton and important for establishing the unique polarized structure of the neuron.

Microtubules are formed by the end-to-end polymerization of α- and β-tubulin subunits followed by binding of GTP and assembly of an assymetrical protofilament. Thirteen protofilaments bind in a parallel orientation and form a 24nm wide helical cylinder, which is the microtubule. The end of the microtubule that terminates in a β-tubulin subunit is called “plus end” of the microtubule, while the other end that terminates in α-tubulin is known as “minus end”. Over time, the GTP is hydrolyzed in the lattice to GDP-tubulin, that then curls and peels off the “plus end” tip causing the depolymerization (shrinkage) of the microtubule (Figure 1).

Microtubules are differentially oriented in dendrites and axons. Dendritic microtubules have a mixed orientation, with the same percentage of microtubules directing their plus end toward the soma or toward the nerve terminals. On the other hand, axons have uniformly oriented microtubules that direct their plus ends away from the cell body [35-37].

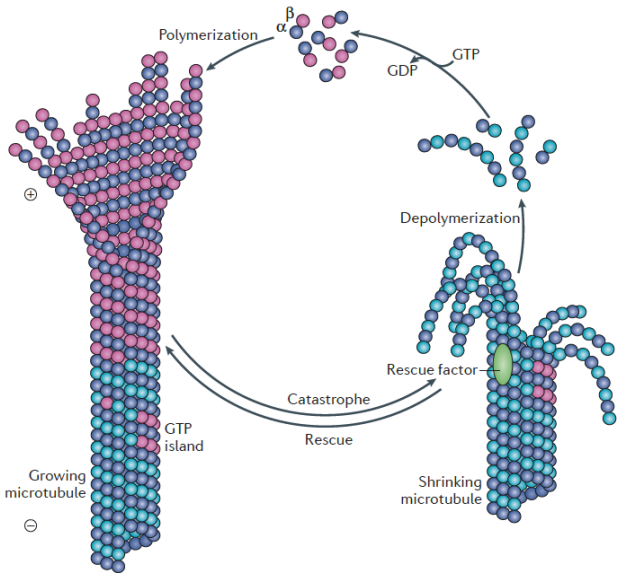

Figure 1: The tubulin assembly-disassembly cycle. Microtubules can undergo dynamic phases of growth (polymerization) or shrinkage (depolymerization). During the growth phase, the tubulin dimer binds 2 molecules of GTP. The tip of the growing end of the microtubules contains a GTP-Cap that protects them from disassembling. After GTP hydrolysis, the GTP-cap is lost leading to rapid depolymerization (catastrophe event) [38].

The type of microtubule-associated proteins (MAPs) that binds to microtubules is also different between axons and dendrites. MAP2 binds preferentially to dendritic microtubules, whereas the Tau protein is mainly found in axons. MAP binding not only shows a certain specificity in the axon-dendritic compartments, but also controls the density, elongation and stability of microtubules that regulate the transport of molecular cargoes [39].

The nervous system relies on the cytoskeleton to achieve proliferation, migration and differentiation of neuronal cells. The cytoskeleton has to cope with constant changes as neurons develop dendrites, an axon and establish contacts with other neurons.

The generation of new microtubules is based on "*De novo*" microtubule formation and involves the microtubule nucleation mediated by the γ-tubulin ring complex (γ-TuRC) that acts as a template. New microtubules can also be generated from pre-existing microtubules through a process of severing that is mediated by several enzymes [40].

As a result of the microtubule severing process, two new microtubule fragments are generated and can be mobilized for further outgrowth. However, the minus ends of the newly generated fragments are unstable and depolymerize, unless stabilized by the protein complex CAMSAP/Patronin/Nezha. The CAMSAP protein family is involved in neuronal polarity, axon differentiation and dendritic branching [41].

This stabilization can also take place at the plus end and requires the binding of proteins of the CLASP family. For instance, CLASP2 is involved in axon outgrowth and neuronal polarity and is highly expressed in neuronal tissues [41].

Despite undergoing the similar steps of growing and depolymerization, the dynamics of both microtubule ends differs. For instance, the plus end terminating by a β-tubulin is involved in microtubule dynamics and the microtubules from this end grow faster but also depolymerize faster (Figure 2).

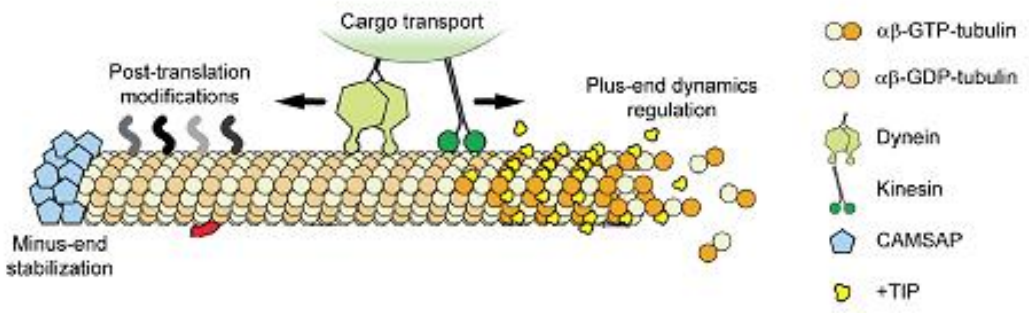

Figure 2: Dynamics of microtubule polymerization and cargo transport. Schematic representation showing the different microtubule-interacting proteins and post-translational modifications of tubulin in polymerizing microtubules [42].

Microtubules are organized in bundles with different inter-filament spacing found among dendrites and the axon. The axon is compacted neuronal process with 20nm inter-filament spacing, whereas dendrites are sparsely compacted (65nm). MAP proteins like Tau and MAP2 play an important role in this bundling process, keeping the proper organization of microtubules [43].

Due to its rigid structure, microtubules grow in straight lines, making the process of growing perpendicular to the dendritic shaft unlikely to occur. One exception appears to be when microtubules enter into spines [44].

Recent studies suggest that the actin cytoskeleton mediates these transient entries. Drebrin A, an actin-binding protein has been suggested to be a link between microtubule plus ends and actin [45].

The importance of the microtubule cytoskeleton in the nervous system is highlighted by several disorders related to microtubule defects. Mutations in the gene encoding microtubule severing proteins (spastin, katanin and fidgetin), microtubule-associated proteins (Tau) and microtubule-based motor proteins (dynein and kinesin) have been linked to several neurodegenerative disorders [46].

1.8 Microtubule-severing enzymes

The remodeling of microtubules in dendrites or axons is critical for the development of neurons and in response to plasticity changes. Neurons express three microtubule-severing enzymes: katanin, spastin and fidgetin. These proteins belong to the AAA superfamily of P loop ATPases that form hexameric rings on the surface of microtubules and use ATP as a source of energy to cleave microtubules into small tracks.

Additionally, microtubule-severing enzymes are critical microtubule regulators and play an important role in mitosis, meiosis, cell migration, morphogenesis and cilia biogenesis [47].

Katanin, was the first microtubule severing enzyme to be characterized and was initially purified from sea urchin eggs and is ubiquitously expressed in protozoa, higher plants and animals [48]. This protein is formed by two subunits: p60-katanin, the catalytic domain, and p80-Katanin, the targeting/regulatory subunit. Recent studies suggest that Drosophila and mammalian neurons also contain a p60-katanin-like protein responsible for microtubule polymerization and stabilization of dendrites throughout early neuronal development. At later stages, it is involved in microtubule depolymerization and dendritic pruning [49, 50].

Spastin has been studied since mutations in the *SPG4* gene were found in HSP patients [51-53]. Spastin comprises four domains: the AAA ATPase catalytic domain, the microtubule-binding domain (MTBD), the microtubule interacting and trafficking domain (MIT) and the hydrophobic region (HR) (Figure 3). It has also been reported that spastin has alternative functions; namely in membrane trafficking and fluidity through the interaction with different binding partners [54].

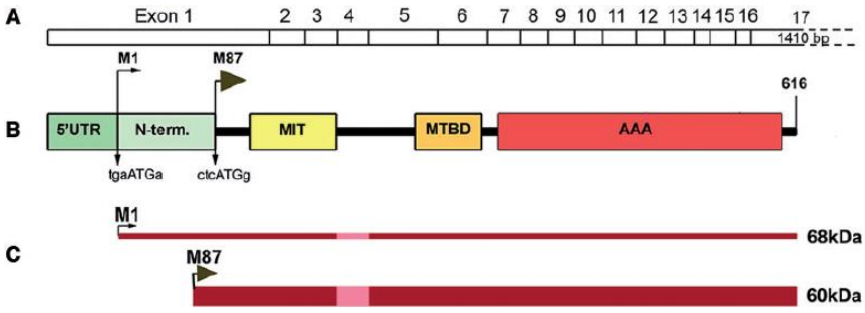

Figure 3: Schematic representation of the spastin domains. A) Exons 1 to17 of spastin. B) Spastin functional domains: N-term=N-terminal; MIT=microtubule interacting and trafficking domain; MTBD=microtubule binding domain; AAA=ATPase associated with various cellular activities. C) Representation of M1 and M87 spastin isoforms depending on the initiation starting codon. The thickness of the dark red line represents the relative amount of each spastin isoform. The light red line represents the regions that are absent after the alternative splicing of exon 4 [55]

Finally, fidgetin is another protein involved in the severing of microtubules. It is encoded by the *FIGN* gene and was initially found as a spontaneous mutation in mice with a characteristic “head-shacking-and-circling” behavior [56]. Studies in Drosophila by overexpressing fidgetin led to the destruction of microtubules and *FIGN* knockdown in fetal cortical neurons enhanced microtubule elongation [57]. These findings might be of great interest as fidgetin can be used as a therapeutic tool to promote the microtubule elongation of diseased axons.

1.9 Mechanisms of microtubule severing

Several studies show that the severing activity of spastin, katanin and fidgetin is based on the binding of AAA ATPase domain to the C-terminal region of the tubulin tail followed by hydrolysis of ATP to pull the tail of the tubulin through the central hexameric pore. While moving through the pore, tubulin is unfolded and the ligations between the tubulin subunits are weakened and cleaved. Mutations in the pore-loop region inhibit the severing of microtubules, although the mutants still bind microtubules indicates that the hexameric ring is the catalytic core of the severing proteins [58, 59].

The majorities of posttranslational modifications of tubulin occur in the C-terminal region of the tubulin tails and are regulatory mechanisms of the severing process. For example, spastin binds preferentially to microtubules enriched in polyglutamylated tubulin. The addition of negatively charged glutamine groups to the C-terminal region of the tubulin tails enhances binding to the positive charged hexameric ring of spastin [60]. Recent work on the effects of different lengths of polyglutamylated chains on severing activity has shown that spastin responds biphasically to the glutamate number on tubulin. Initially increasing the number of glutamates added to the tubulin tails enhances the severing activity of spastin. However, side chains with more than 7 glutamates results in a marked reduction in the severing of microtubules [61].

In the case of katanin, one of the main regulatory factors for severing of microtubules is acetylation, another posttranslational modification of tubulin and the presence of the MAP protein Tau. Katanin preferentially severs microtubules enriched in acetylated tubulin and with reduced levels of Tau. Katanin requires ATP for dimerization of the two Katanin domains, is stimulated by the presence of the microtubule substrate (alpha- and beta-tubulin) and is inhibited by high concentrations of polymerized tubulin [62].

Regarding the mechanism of severing, fidgetin seems to preferentially sever the labile fraction of microtubules containing tyrosinated tubulin as opposed to the other severing proteins, spastin and katanin, that show a binding preference for stable microtubule fractions [57].

1.10 Roles of spastin in the nervous system

Spastin is highly enriched in the central nervous system and it is differentially expressed among the different areas of the brain. Brain regions such as the cortex and hippocampus show higher levels of spastin expression, whereas others like the cerebellum show no detectable levels of this protein [63].

Data revealed by immunostainings using a spastin antibody have shown that spastin expression is restricted to neurons. Within the cell spastin was found in the cytoplasm, endosomes and endoplasmatic reticulum (ER) [64].

Spastin seems to work together with katanin in the regulation of axonal morphology by increasing the number of branching sides. Immunostainings against spastin confirmed its localization at the nascent branch sides. This may prompt to suggest that by increasing the amount of microtubule fragments, spastin may generate a mobile fraction of microtubules that can be delivered to the growing branches [65].

Recent data from *Drosophila* have shown that spastin participates in the amplification of microtubules in bouton-like projections of the axon, suggesting that spastin might be involved in the formation of synapses [32]. The severing activity of spastin and katanin is not restricted to the axon. Several studies have pointed out that both proteins work alongside to modify the morphology of dendrites. For example, spastin null mutants in *Drosophila* have reduced branching of dendrites in sensory neurons [66].

1.11 Cellular functions of spastin

The spastic gait 4 gene (*SPG4*) encodes for spastin, a member of the AAA ATPase superfamily and has a predicted molecular weight of 67.2 kDa. As a result of alternative initiation codon sites within exon 1, the M87 spastin isoform can be generated, which lacks the first 87 amino acids. Additionally, these two isoforms can undergo alternative splicing of exon 4, thus generating two additional isoforms (M1ΔEx4 and M87ΔEx4).

The hydrophobic region of spastin is only present in the full-length isoform (M1-spastin) and interacts with membrane adaptor proteins like receptor expression-enhancing protein 1 (REEP1), atlastin and nuclear auto-antigen

14 (NA 14). These interacting proteins then can direct spastin to different cellular compartments, thereby spatially restricting the severing activity of spastin.

Additionally, spastin also has important interacting partners involved in membrane remodeling. Together with ESCRT-III (endosomal sorting complex required for transport) and VPS4 (vacuolar protein sorting-associated protein 4), spastin participates in the nuclear envelope sealing and spindle disassembly.

Spastin is also involved in the early secretory pathway and regulates trafficking between the endoplasmatic reticulum toward the Golgi complex.

Among the known spastin isoforms, M87 spastin is recruited to the midbody and endosomes, where it mediates endosomal tubulation.

Papadopoulos *et al.* have shown that spastin is also important for lipid metabolism, namely on the lipid droplet formation. The M1 spastin isoform can be sorted from the endoplasmatic reticulum to the lipid droplets. Mutated versions of M1 spastin led to reduced lipid droplet size and clustering. It was also reported that the downregulation or upregulation of spastin in *Drosophila* caused a reduction in triacylglycerol levels [67].

Overall, spastin is an important regulator of the microtubule cytoskeleton, microtubule-dependent transport of various cargoes, shaping of membrane organelles and lipid metabolism.

1.12 Mouse models of hereditary spastic paraplegia

In order to get more insight into the pathogenesis of the hereditary spastic paraplegia associated with mutations of *SPAST* gene, two murine models of hereditary spastic paraplegia have been generated and characterized.

Tarrade *et al.* generated a mouse model with a deletion of the exons 5-7 of the *SPAST* gene. Both homozygous and heterozygous spastin knockout mice did not display any changes in body weight, although spastin homozygous mice were infertile. They found axonal swellings in the white matter of the spinal cord from spastin mutant mice that became more overt with age. These axonal swellings were not reported in the sciatic nerve, indicating that this phenotype was specific to the central nervous system. Within the axonal

swellings, an accumulation of various organelles such as mitochondria and peroxisomes was found, possibly due to defective axonal transport [33, 34].
These aberrant structures found in the spinal cords of spastin mutant mice had an impact on the motor capabilities as showed by several motor tests.
Since there is still a lack of evidence for the occurrence of truncated forms of spastin in HSP patients, a different laboratory generated a new mouse model for HSP bearing a missense point mutation previously described in HSP patients (c.1092+2T>G) [68].
Interestingly, they also identified the previously described axonal swellings in cultured cortical neurons and spinal cord. They also reported gait deficits in the spastin homozygous mice, which matched the pathophysiologic defects found in the CNS neurons of HSP patients. For the first time, they also studied the transport of two cargoes: the amyloid precursor protein (APP) and mitochondria. As expected, the anterograde transport of both cargoes was perturbed by the mutant form of spastin, which resulted in an increase in stalled cargoes [68].
Taken together, data from these two mouse models show that the regulation of the microtubule cytoskeleton by spastin is crucial for the maintenance of proper axonal transport.
In summary, the available mouse models recapitulate important pathophysiological features of the HSP, such as the impairment of motor cognitive performance. However, the role of spastin in the central nervous system on higher brain functions, such as learning and memory, has not been addressed so far.

1.13 Intracellular protein transport

In eukariotic cells, motor proteins such as kinesins and dyneins transport various cargoes. This includes organelles, for example mitochondria or membrane vesicles containing different protein complexes. These motor proteins walk along the microtubules using ATP, as a chemical energy. So far, 45 genes that encode kinesins have been identified in humans, 38 of those specifically expressed in the brain [69].

Kinesins are known as anterograde motors, meaning that they transport cargoes toward the plus ends at the cell periphery.

The human genome contains 15 genes that encode for dynein motors, but cytoplasmatic dynein on its own is involved in all long distance intracellular transport processes. The remaining members of this superfamily are responsible for transport in flagella and cilia. Unlike kinesins, dynein motor proteins transport cargoes toward the minus-end of microtubules, which are oriented toward the soma [70].

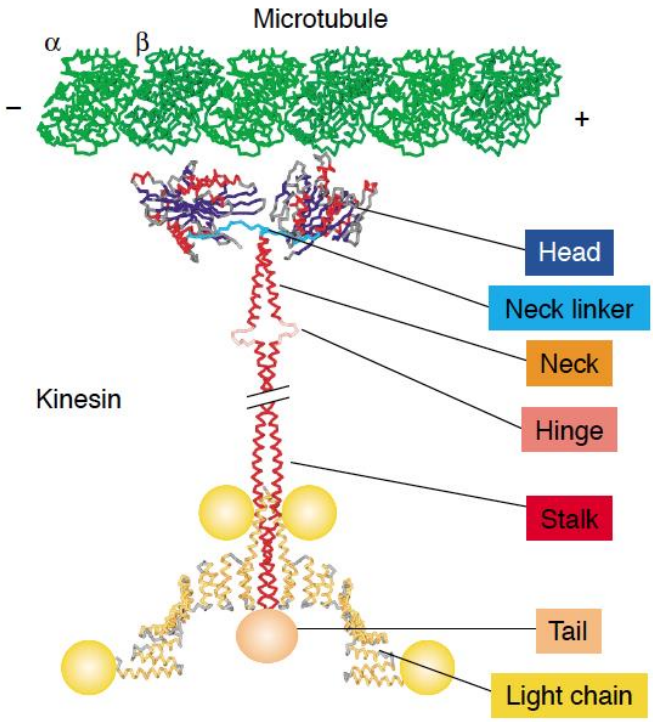

Figure 4: Subunit composition of KIF5 motor protein. The diagram shows composition and organization of KIF5 bound to a protofilament of a microtubule. Each heavy chain of a kinesin motor protein consists of a head that binds ATP and interacts with the microtubules, a neck linker that undergoes conformational changes after ATP hydrolysis, a neck and a stalk domain that causes the dimerization of the motor domains [71].

In this scientific project I focused on the transport of different cargoes carried out by the kinesin-1 motor protein, also known as KIF5.

KIF5 was the first kinesin to be identified, and since its discovery many studies followed on its motility and cargo binding [72].

Like most kinesins, KIF5 is a heterotetramer formed by a dimer of kinesin heavy-chain subunits (KHCs) and a dimer of kinesin light chain subunits (KLCs). Each KHC subunit has a N-terminal kinesin motor domain, a neck domain, a coiled-coil stalk and a C-terminal cargo-binding domain. The neck participates in the homodimerization step and controls the processivity of the motor protein. The stalk domain enables the motor protein to adopt a folded shape or an inactive state (autoinhibition). Each motor domain has two binding sites: one binds to the microtubule track and the other to ATP (Figure 4) [73-79].

The movement of the motor protein is accomplished by binding of the motor domain to the microtubule, followed by a "hand-over-hand" walk mechanism. While one head domain is still bound to the microtubules, the other one takes a step forward. This movement is repeated several times and is powered by the hydrolysis of ATP, which causes conformational changes in the neck domain, thus leading the forward movement of the motor domain [75, 80].

One feature of motor proteins is their highly processive activity. They can be bound to microtubules through several cycles of ATP hydrolysis, processing toward the plus end for a few seconds until they finally detach.

On average, a kinesin motor protein can take more than 100 steps, each step (0,08 nm) corresponding to the distance between 2 consecutive β-tubulins aligned in a protofilament [81].

Motor proteins were also observed to navigate differently along microtubules that contain different tubulin isotypes, different post-translational modifications of tubulin or bound to specific MAPs [82, 83].

1.14 Microtubule modifications and kinesin-mediated transport

Microtubules are very heterogeneous in their composition, being a common target for multiple posttranslational modifications (Figure 5). These modifications change both the structure of the microtubules, the interaction with microtubule-associated proteins, and motor proteins.

Neuronal cells express several motor proteins. Some move in both dendrites and axon (i.e, kinesin-2 and -3), others are restricted to the axon (kinesin-1). Since the transport mediated by motor proteins is regulated by different

tubulin posttranslational modifications, this raises the possibility of heterogeneous populations of microtubules in different cellular compartments, which may explain the unique distribution of motor proteins [81].

As mentioned before, the C-terminal regions of tubulin tails are the binding sites for several kinesins, MAPs, and also the positions where post-translational modifications of tubulin occur. Additionally, there are different tubulin isoforms that can distinctly regulate the binding of motor proteins. The combination of different MAPs, PTMs and tubulin isoforms may regulate the motility and directionality of motor proteins [83, 84].

Regarding the stability, microtubules can be categorized in dynamic microtubules and stable microtubules. Usually PTMs like polyglutamylation, detyrosination and acetylation are present in stable microtubules, although on its own tubulin modifications do not increase microtubule stability. The more dynamic population of microtubules has high levels of tyrosinated tubulin [85].

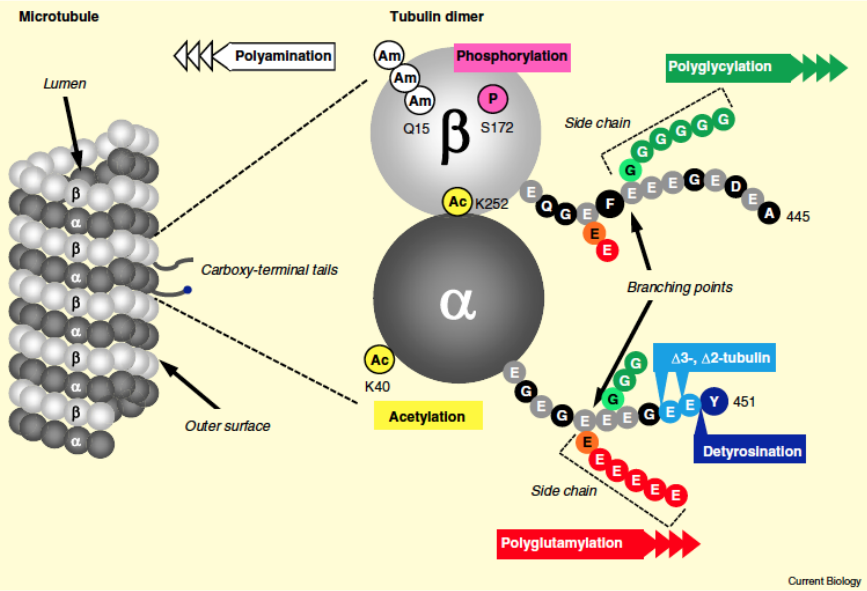

Figure 5: Most common tubulin posttranslational modifications. The C-terminal region of the tubulin tail is a preferential target for posttranslational modifications. Acetylation occurs preferentially at α-tubulin K40 and β-tubulin K252; Polyamylation at Q15 and phosphorylation at S172 of the β-tubulin; Polyglutamylation/Polyglycylation within the C-terminal tails of α- and β-tubulins; Detyrosination/Tyrosination in the C-terminal tail of α-tubulin [86].

1.15 Polyglutamylation of microtubules

Polyglutamylation is abundant in neurons, but it is also found in centrioles and cilia. Enzymes known as TTLL (tubulin tyrosine ligase-like) proteins add negatively charged glutamate to the C-terminal tail of α- and β-tubulin. The polyglutamylated chains may vary in length, from 1 to 20 glutamyl units and also in location, since glutamates can be added to different locations or tubulin isotypes. The recruitment of enzymes with polyglutamylase activity to microtubules is mediated by PGS1 proteins. For instance, a mouse deficient in PGS1 named ROSA22 had reduced levels of α-tubulin polyglutamylation [87, 88].

Some studies suggest that the length of polyglutamylated side chains may regulate the binding of MAPs and motor proteins to microtubules. Boucher and colleagues have shown that the binding of MAP2 and Tau is enhanced when side chains of 1-3 glutamyl units are present. On the contrary, longer chains inhibit the binding of those proteins to microtubules [89].

Interestingly, the effect of the chain length of polyglutamylation on the binding of KIF5 was also reported. Short chains consisting of up to 3 glutamyl units increased the binding of KIF5, whereas longer chains impair its binding [90].

1.16 Detyrosination and tyrosination of microtubules

Most α-tubulins with a terminal tyrosine can undergo detyrosination, with the exception of TUBA4A and TUBA8. The removal of this terminal tyrosine is catalyzed by a cytosolic carboxypeptidase (CCP) and the tyrosination of detyrosinated tubulins is carried out by tubulin tyrosine ligase (TTL). Tyrosinated and detyrosinated tubulins are differentially distributed in the neuron. Proximal segments of the axons are enriched in detyrosinated tubulin, whereas tyrosinated microtubules are commonly found in growth cones [91-94].

Data from live-cell imaging show that the motor protein KIF5 binds with higher affinity to detyrosinated microtubules than tyrosinated microtubules [95].

1.17 Acetylation of microtubules

Acetylation occurs on the lysine 40 of α-tubulin. Microtubule acetylation was reported to have an effect on kinesin-based transport. By inhibiting tubulin deacetylase, the binding of kinesin was enhanced after adding AMP-PNP, which is used to stabilize microtubules and microtubule associated proteins [87].

Data from binding assays also showed that KIF5 interacts with lower affinity to microtubules with low levels of acetylation, and the enzymatic activity of KIF5 is regulated by this post-translational modification of tubulin [96].

The impact of acetylation on the transport of JIP1, one of the cargoes of KIF5, was also evaluated.

Hippocampal neurons were treated with tubacin, a drug that increases the levels of acetylation through the inhibition of the α-tubulin deacetylase.

In control neurons, kinesin-1 and its cargo JIP1 accumulate in neurites with higher levels of acetylation. However, the hyperacetylation induced by tubacin disrupted this distribution pattern, suggesting that the selectivity of the motor protein was lost [96].

Altogether, several PTMs can be present on the same microtubule, increasing the number of combinatorial effects of these tubulin modifications.

This may affect differentially not only the binding of motor proteins but also of microtubule-associated proteins. Since the majority of the described PTMs are reversible changes, they may act as regulatory mechanisms to regulate the binding of motor proteins in response to dynamic changes in the neuron.

1.18 Role of the hippocampus in learning and memory

The hippocampus is a brain region localized in the medial temporal lobe. Its name originates from its resemblance to an inverted seahorse.

The hippocampus can be subdivided into three regions: the dentate gyrus (DG), the cornu ammonis 1 (CA1) and cornu ammonis 3 (CA3).

The hippocampus belongs to the limbic system and has an important function in the consolidation of short-term learning and long-term memory. It has an important role in spatial learning and memory [97, 98].

Place cells present in the hippocampus are activated based on the spatial location of the animal and encode information about particular objects or behaviors associated with different places. The hippocampus is not only involved in the recall of memory associated to specific locations but also in the temporal organization of episodes [99, 100].

Another important function of the hippocampus is the generation of new neurons in adulthood, a biological process known as adult neurogenesis. For many years it was thought that the process of generating new neurons from precursor cells was limited to the embryonic development period of the brain. Later, studies showed adult neurogenesis in the dentate gyrus of the adult brain. These newly formed neurons can migrate and incorporate into the pre-existing brain network and may be recruited to the formation of new memories [101].

The first evidence of the involvement of the hippocampus in memory formation came from the study of patients with lesions in this brain structure and other regions of the limbic system. A famous study of the patient HM that underwent a bilateral hippocampal resection due to untreatable epilepsy, led to important insights about the role of the hippocampus in memory processes. This patient displayed loss of memories related to autobiographical experiences and could not recall recent memories. However the past experiences like childhood episodes were still conserved. These findings suggested a role of the hippocampus in memory encoding, but not in long-term storage of episodic memory [102].

Several neurodegenerative and developmental disorders, associated with a deficient memory have been linked to alterations in the hippocampus.

In Alzheimer´s disease, the most common neurodegenerative disorder, one of the first symptoms is the loss of hippocampal-dependent memories [103].

1.19 Microtubule stability and memory

Neuronal cells are known for their highly polarized structure that originates after a long maturation process. At the same time, these cells undergo constant cytoskeletal modifications in order to cope with the changes that occur in the organism. This ability is known as neuronal plasticity and has

been extensively studied in the last years. These synaptic changes are thought to form a coding mechanism and storage of information that is assumed to underlie learning and memory processes [104].

Some studies have reported that microtubule dynamic or stability affect long-term potentiation, a process that leads to an increase in synaptic strength through recruitment of AMPA receptors to the dendritic spine upon high frequency stimulation. This long-term potentiation protocol is used to mimic *ex vivo* the processes underlying memory formation.

Increasing the microtubule stability upon treatment with paclitaxel or increasing the microtubule instability with nocodazol interferes with long-term potentiation [105, 106].

Shumyatsky and colleagues have shown that the depletion of stathmin, a protein that controls microtubule polymerization had a profound impact on LTP and ultimately impaired fear memory in mice [105].

Another group has studied the impact of the contextual fear conditioning paradigm, a behavior task used to study hippocampal-dependent memory, on different microtubule fractions identified in neurons. They reported that brain samples from mice which have been trained for this behavior task contain an increase of dendritic microtubules (MAP fraction) and of the cold-stable fraction (overstable microtubule fraction commonly found in neurons). Remarkably, they were also able to control the time spent by each mouse freezing (a read-out of learning and memory formation associated to a specific context) depending on the pharmacological manipulation of microtubule stability [107].

Uchida and colleagues further reported biphasic changes in microtubule stability after performing contextual fear conditioning in mice. After mice have been trained for this behavioral task, brain samples were collected and processed in order to quantify the levels of detyrosinated versus tyrosinated tubulin, a read-out assay of stable microtubules versus more labile microtubules, respectively. Shortly after testing, they identified an increase in the levels of tyrosinated tubulin, in contrast with increased levels of detyrosinated tubulin observed 8 hours after training. In combination, these data suggest that during the learning phase, the microtubule cytoskeleton is

more plastic and later on, during the consolidation phase, the stability of microtubules increases [108].

1.20 AMPA receptor trafficking

Synaptic plasticity is thought to be the cellular mechanism that underlies learning and memory processes. These plastic modifications that take place at the synapse are highly regulated and rely on the concentration and integration of AMPA receptors into the plasma membrane [109].

There are four genes encoding the AMPA receptors subunits GluA1-4. After translation of the messenger RNA that encodes for the different subunits, the proteins are folded in the endoplasmatic reticulum. AMPA receptor subunits establish contacts with each other and dimerize. The AMPA dimers will be associated in tetramers forming homo-tetramers or hetero-tetramers. The specific subunit composition of the AMPA receptor determines the electric current elicited at the postsynaptic cell and the trafficking pathway.

GluA2/3 AMPA receptors are continuously transported into the dendritic spine, whereas GluA1/2 receptors are mobilized to the postsynaptic membrane upon acute stimulation [110].

After the formation of AMPA homo- or hetero-tetramers is completed at the ER, these protein complexes are sorted in the trans-Golgi network, loaded into vesicles and shuttled to the dendritic compartment (Figure 6).

The long-range transport of AMPA receptors along the microtubule cytoskeleton is carried out by kinesins. The kinesin KIF5 transports AMPA GluA2-type receptors bound to the adaptor protein GRIP1 (GluA2-receptor interacting protein 1) [111].

The delivery of AMPA receptors to the plasma membrane of the dendritic spine requires the interaction of the microtubule cytoskeleton with the actin cytoskeleton since the spine is a structure highly enriched in actin filaments. Myosin V is a major motor protein responsible for the transport of GluA2 receptors along the actin filaments toward the postsynaptic density.

The last step of receptor targeting is the integration of the transported AMPA receptors into the membrane by exocytosis. Exocytosis of AMPA receptors is

mediated by proteins from the SNARE family like SNAP23 and syntaxin4 [112].

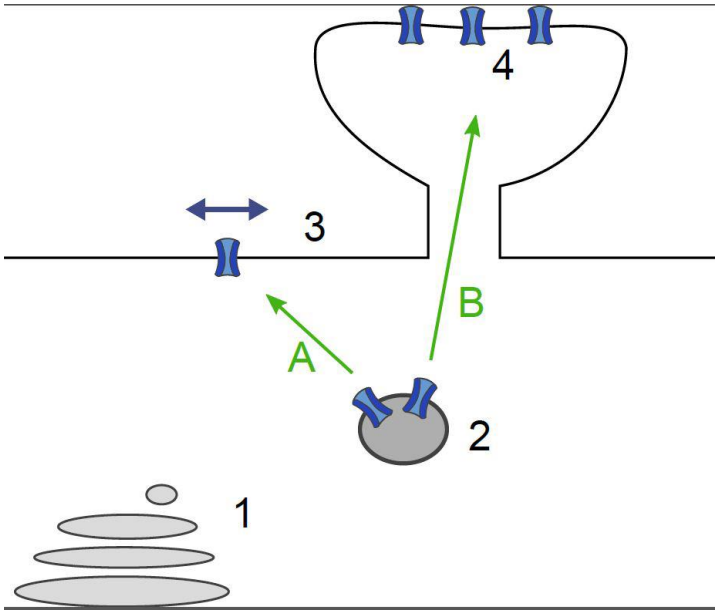

Figure 6: Alternative routes of AMPA receptor trafficking to the synapse.
AMPA receptors are loaded into vesicles (2), assembled in the trans-Golgi network (1). Two alternative mechanisms for AMPA receptor delivery have been described. The AMPA receptors can be inserted in the extrasynaptic side (3) and move to the spine head by lateral diffusion (route A) or the vesicles can be directly transported into the postsynaptic density of the dendritic spine (4) (Route B).

However, the regulation of AMPA receptor delivery is still not completely understood.

Some studies have reported that vesicles containing the receptors are delivered at the dendritic shaft and then, laterally diffuse into the spine membrane. This mechanism would circumvent the direct positioning of vesicles under the postsynaptic density membrane.

Nevertheless, there are also reports of active and direct transport of AMPA receptors into and within the spines [111, 113, 114].

1.21 Related defects and disease

One of the biggest challenges of neuronal survival is the maintenance of efficient long-range transport of cargoes throughout the whole life of an organism.

Since neuronal transport is carried out by several motor proteins and relies on the stability and dynamics of the microtubule cytoskeleton and defects in motor proteins can lead to several pathologic conditions.

As mentioned before, the C-terminal region of the tubulin tail is a major target for several post-translational modifications that might affect the final properties of the microtubule [87].

Several mouse models carrying defects in the microtubule cytoskeleton have been studied in detail. The PCD mouse model carries a mutation in one of the deglutamylase enzymes, CCP1, that removes glutamate residues. This mouse model displayed degeneration of the Purkinje cells of the cerebellum and ataxic behavior. Interestingly, increased polyglutamylation levels of α-tubulin were found in the cerebellum 2014 [115].

Mutations of KIF5A, which transports various cargoes including mitochondria, causes the spastic paraplegia type 10 (SPG10), in which the motor neurons are affected [116].

Another key regulator of microtubule stability are the microtubule-associated proteins that bind to the C-terminal region of the tubulin tail and stabilize the microtubules. One of the best studied MAP proteins is Tau, the protein encoded by the *MAPT* gene. Mutations in this gene lead to hyperphosphorylation and detachment of Tau followed by destabilization of microtubules.

Another pathogenic outcome is the accumulation of hyperphosphorylated Tau and formation of toxic neurofibrillary tangles within the cell body. The malfunction of Tau is associated with several disorders such as Alzheimer´s disease or Fronto-temporal dementia [117].

1.22 Aims of the research project

The most common form of hereditary spastic paraplegia (HSP) is associated with mutations in the *SPAST* gene that encodes spastin, a microtubule-severing enzyme. However, the underlying subcellular mechanisms are poorly understood. A tempting explanation for the cause of this disease is that the impaired severing activity of spastin would alter the microtubule cytoskeleton organization and function and thus affect several biological processes in the neuron.

One of the first symptoms described in HSP is the progressive loss of the motor neuron function of the lower limbs. Interestingly, this motor impairment can be followed by deficits in cognitive function in adulthood and even dementia in later stages of the disease.

Despite breakthroughs in the understanding of the mechanisms that underlie the etiology of HSP in recent years, many questions remain unanswered.

While previous efforts mainly focused on investigating the role of spastin in motor neuron function, none of the studies addressed the role of microtubule severing by spastin in cognitive function.

This research project seeks to address the following questions: 1) How does microtubule stability and its dynamics change after spastin depletion? 2) Does spastin affect the mechanisms governing the intracellular protein transport of cargoes? 3) Does spastin play a role in cognitive function?

In order to tackle these questions, spastin knockout mice and their wild type littermates underwent a detailed biochemical, structural and behavioral analysis.

Chapter 2

Materials and Methods

2. Material and methods

2.1 Chemicals

All high-quality reagents were purchased from the following supliers: SIGMA-Aldrich (Taufkirchen, Germany), Roche (Mannheim, Germany), Carl Roth GmbH & Co. KG (Karlsruhe, Germany), Life Technologies (Darmstadt, Germany), VWR (Darmstadt, Germany), Merck (Darmstadt, Germany) and AppliChem (Darmstadt, Germany).

2.2 Apparatus

2-photon microscope for time lapse imaging: Olympus Fluoview F1000 MPE (Olympus, Hamburg, Germany).

Epifluorescent Microscope: Zeiss Axiovert 200M (Zeiss, Jena, Germany), Sony CCD-Camera 12. Monochrome w/o IR-18 (Diagnostic Instruments Inc., Sterlings Heights, USA), MetaVue Imaging Software (Visitron Systems, Puchheim, Germany).

Transmission Microscope: Zeiss Axiovert 25 (Zeiss, Jena, Germany).

DNA gel imager: Intas Gel Imager (Intas, Göttingen, Germany).

Agarose gel chambers: Owl Seperation Systems B2 and B1A (Thermo Fisher Scientific, Asheville, USA).

Bacterial culture incubator: Innova 3200 Platform Shaker (New Brunswick Scientific, Nürtingen, Germany).

Cell culture incubators: HeraCell 150/150i (Thermo Fisher Scientific, Asheville, USA).

Vibratome: Leica VT 1000S (Leica, Mannheim, Germany)

Cell culture sterile hood: SterilGARD Class II TypA/B3 (Baker Company, Sanford, USA).

Centrifuge rotors: JA-10, JA-25.5 (Beckman Coulter, Krefeld, Germany).

Centrifuges: Ultracentrifuge L7 (Beckman Coulter, Krefeld, Germany), 5417C (Eppendorf, Hamburg, Germany), MC6 Minifuge (Sarstedt, Nümbrecht, Germany).

Confocal Microscope: Olympus Fluoview F1000 (Olympus, Hamburg, Germany), Olympus Fluoview Software Version 2.1b (Olympus, Hamburg, Germany).

-20°C Freezer: G 3513 Comfort (Liebherr, Ochsenhausen, Germany).

-80°C Freezer: MDF-U74Vultra low temperature freezer (Sanyo, Osaka, Japan).

Laboratory scales: Sartorius LC-6201 (Sartorius, Göttingen, Germany), Mettler AE240 (Mettler -Toledo, Giessen, Germany).

Microtiter plate reader: Infinite 200 PRO NanoQuant (Tecan, Männedorf, Switzerland).

PCR machine: PTC – 200 Peltie Thermal Cycler (MJ Research, Waltham, USA).
pH Meter: SevenEasy (Mettler - Toledo, Giessen, Germany).

Platform shaker: Promax 2020 (Heidolph Instruments, Kelheim, Germany), WS5 (Edmund Bühler GmbH, Hechingen, Germany).

Power supplies: Power Pac 200 (BioRad, Munich, Germany).

Refrigerator: G 5216 Comfort (Liebherr, Ochsenhausen, Germany).

Rolling incubator: TRM5-V (IDL GmbH & Co. KG, Nidderau, Germany).

SDS-PAGE chambers: Mini-PROTEAN Tetra Electrophoresis System (BioRad, Munich, Germany).

Semi dry blotter: V20 Semi-Dry Blotter (SCIE-PLAS, Cambridge, UK).

Sequencer: ABI Prism 377. DNA Sequencer (Applied Biosystems, Darmstadt, Germany).

Spectrophotometer: NanoQuant plate for Infinite 200 PRO NanoQuant (Tecan, Männedorf, Switzerland).

Thermo mixer: Thermomixer 5436 (Eppendorf, Hamburg, Germany).

Vortex: REAX 2000 (Heidolph Instruments, Kelheim, Germany).

Water bath: GFL-1012 (GFL, Burgwedel, Germany).

Western blot chemiluminescence reader: Intas ChemoCam (Intas, Göttingen, Germany).

Laminar flow cabinet: Thermo Fisher Scientific GmbH, Dreieich, Germany

2.3 Media and solutions

The water used to prepare the solutions was purified using a Milli-Q-System (Millipore, Schwalbach/Ts, Germany) to the degree of "*Aqua bidest*" purity.
The pH of the solutions was adjusted using NaOH, KOH and HCl solutions.
For sterilization, solutions were autoclaved at 121°C and 2.1 bar over a time period of 20 min. Alternatively, solutions were sterile filtered using filter tips with a pore size of 0.22 µm (Millipore, Schwalbach/Ts, Germany).

Blocking solution (immunocytochemistry, immunohistochemistry)
5 % (w/v) bovine serum albumin diluted in 1 x PBS.

Homogenization Buffer (brain homogenates)

20 mM HEPES, 100 mM CH_3CO_2K, 40 mM KCl, 5 mM EGTA, 5 mM $MgCl_2$, pH 7.2, protease inhibitor (Roche Complete), 2 mM mg ATP, 5 mM DTT and 1 mM PMSF.

Blocking Buffer (immunoblotting)
5 % (w/v) dry milk or 5 % (w/v) bovine serum albumin (BSA) in 1x TBST.

D-MEM/F-12 complete (neuronal cell culture)
500 ml D-MEM/F-12 (1:1, w/o L-Glu, Invitrogen, # 21331020), 10 % (v/v) FCS, 2 mM L-glutamine (Invitrogen), 25 ug/ml pyruvate (Sigma, #P-2256), 50 µg/ml penicilin/streptomycin (Invitrogen).

Neuronal culture medium (neuronal cell culture)
500 ml neurobasal-A medium (Invitrogen #10888), 25 µg/ml pyruvate (Sigma, #P-2256), 2 mM L-Glutamine (Invitrogen), 50 µg/ml penicilin/streptomycin (Invitrogen).

HEPES Buffer (neuronal transfection)
135 mM NaCl, 5 mM KCl; 2 mM MgCl2, 2 mM $CaCl_2$, 10 mM HEPES, pH 7.4, 15 mM (D)-Glucose, diluted in H_2O.

LB-medium (growth medium bacteria)
10 g trypton, 5 g of yeast extract, 5 g NaCl, add 1000 ml H_2O, pH 7.5, sterilization by autoclaving.

LB-Agar (growth medium bacteria)
LB medium with 1.5 % (w/v) agarose (autoclaved), after autoclaving cool to 50°C and add the antibiotic: ampicillin (100 µg/ml) or kanamycin (50 µg/ml). Pour the mixture into petri dishes and let harden. Storage at 4°C.

4 % PFA solution (immunocytochemistry, immunohistochemistry)
4 g PFA, 4 g sucrose, add 1000 ml 1x PBS; warm up the solution up to 60°C and add NaOH dropwise until the solution clears. Adjust the pH to 7.2.

1x PBS

8 g NaCl, 0.2 g KCl, 1.44 g Na_2HPO_4, 0.24 g KH_2PO_4, add 1000 ml H_2O, pH 7.5, sterilization by autoclaving.

SDS Running Buffer (10x) (western blot)
250 mM tris, 2.5 M glycin, 1 % (w/v) SDS, diluted in H_2O, pH 8.3.

SDS Sample Buffer (western blot)
220 mM tris (pH 6.8), 40 % (v/v) glycin, 8 % (w/v) SDS, 0.8 % (w/v) bromophenol, diluted in H_2O, before use add 8 µl of beta-mercaptoethanol per 100 µl of buffer.

Phosphate buffer
170 mM KH_2PO_4, 720 mM K_2HPO_4, sterilization by autoclaving

Stripping Buffer (immunodetection)
25 mM Glycin; 1 % SDS; pH 2.0; diluted in H_2O.

TAE (50x) (agarose gel electrophoresis)
2 M tris-HCl (pH 8.0); 100 mM EDTA; diluted in H_2O.

TBST (10X) (western blot)
200 mM tris (pH 7.5), 1.5 M NaCl 2% (v/v) tween-20, diluted in H_2O.

Western Blot Buffer (western blot)
20 %(v/v) methanol; 250 uM tris; 192 uM glycin; add 1000 ml H_2O, pH 8.4.

10x DNA Loading Buffer (PCR genotyping)
7.5 g ficoll; 0.125 g bromophenol blue; add 50 ml H_2O (aliquots stored at -20°C).

2x HBS (neuronal cell transfection)
1.6 g NaCl; 0.074 g KCl; 0.027 g Na_2HPO_4*2 H_2O; 0.2 g dextrose; 1 g HEPES; add 100 ml H_2O; pH 7.05 (steril filtered, aliquoted and stored at -20°C).

SOB buffer

2 % (w/v) bacto tryptone (competent cells), 0.5 % (w/v) yeast extract, 10 mM NaCl, 2.5 mM KCl, 10 mM $MgCl_2$, 10 mM $MgSO_4$, pH 6.7 (KOH).

2.4 Antibodies

The following antibodies were used for immunocytochemistry (ICC), immunohistochemistry (IHC) and western blotting (WB).

2.4.1 Primary antibodies

Antibodies	Specie	Dilution	Incubation time and temperature	Reference
GluA2	monoclonal, mouse	1:500 (WB) 1:300 (ICC)	ON, 4°C 2h, RT	Millipore (Massachusetts USA)
spastin	monoclonal, mouse (clone sp606)	1:500 (WB)	ON, 4°C	Abcam (Cambridge, UK)
detyrosinated tubulin	polyclonal, rabbit	1:20000 (WB)	1h, RT	Milipore (Massachusetts, USA)
polyglutamylated tubulin	monoclonal, mouse (clone GT335)	1:5000 (WB) 1:200 (IHC)	1h, RT ON, 4°C	Adipogen (Liestal, Switzerland)
alpha tubulin	monoclonal, mouse	1:5000 (WB) 1:200 (IHC)	1h, RT ON, 4°C	Abcam (Cambridge, UK)
α-tyrosinated tubulin	monoclonal, mouse (clone TUB-1A2)	1:5000 (WB)	1h, RT	Sigma Aldrich (Buchs, Switzerland)
NSE	polyclonal, chicken	1:5000 (WB)	1h, RT	Novus Biologicals (Littleton, USA)
PSD95	monoclonal, mouse	1:1000 (WB) 1:2000 (ICC)	2h, RT 2h, RT	Thermo fisher scientific, (Massachusetts, USA)

synaptophysin	polyclonal, guinea pig	1:1000 (WB) 1:2000 (ICC)	ON, 4°C 2h, RT	Synaptic systems (Göttingen, Germany)

Table 2.4.1: List of used primary antibodies in this study

2.4.2 Secondary antibodies

Antibodies	Specie	Dilution	Incubation time and temperature	Reference
α- mouse HRP-conjugated	goat	1:10000 (WB)	1h, RT	Dianova (Hamburg, Germany)
α- rabbit HRP-conjugated	goat	1:10000 (WB)	1h, RT	Dianova (Hamburg, Germany)
α- chicken HRP-conjugated	goat	1:2500 (WB	1h, RT	Dianova (Hamburg, Germany)
α- guinea pig HRP-conjugated	goat	1:10000 (WB)	1h, RT	Dianova (Hamburg, Germany)
α- rabbit CY2	donkey	1:500 (ICC) 1:500 (IHC)	1h, RT	Dianova (Hamburg, Germany)
α- mouse CY3	goat	1:500 (ICC) 1:500 (IHC)	1h, RT	Dianova (Hamburg, Germany)
α- mouse CY5	goat	1:500 (ICC)	1h, RT	Dianova (Hamburg, Germany)
α-rat-Cy5	donkey	1:500 (ICC)	1h, RT	Dianova (Hamburg, Germany)

Table 2.4.2: List of used secondary antibodies

2.5 Vectors

The following vectors were used for the transfection of hippocampal neurons:

Name	Source	Use
pEGFP-C1	Clontech	Expression of eEGFP-C1 in neurons

EB3-pEGFP	Anna Akhmanova, Faculty of Science, Utrecht, The Netherlands	Expression of EB3-pEGFP in neurons
pEGFP-spastin	M. Kneussel, ZMNH, Hamburg, Germany	Expression of pEGFP-spastin in neurons
KIF5-tomato-pex26	M. Kneussel, ZMNH, Hamburg, Germany	Expression of KIF5-tomato-pex26 in neurons
GluA2-mCherry	Addgene (Plasmid #24001)	Expression of GluA2-mCherry in neurons
Synaptophysin-eGFP	M. Kneussel, ZMNH, Hamburg, Germany	Expression of in synaptophysin - eGFP neurons

Table 2.5: List of used vectors

2.6 Olygonucleotides

The following oligonucleotides were used for sequencing and PCR and were supplied by the company Eurofins, Germany:

Name	5'-3´- Sequence	Use
PLR41	AAGTCATGGCAGTCTTTCTGGCT	Genotyping of spastin knockout mice
PLR89	CACATGGTGGCTCATAACCATTTA	Genotyping of spastin knockout mice
PLR169	ATTTGCAAAAACTACTTGCTATTAA ATTCC	Genotyping of spastin knockout mice

Table 2.6: List of used unmodified olynucleotides for PCR genotyping.

2.7 Molecular biological methods

2.7.1 Transformation of DH5alpha competent cells

For the DNA amplification, DH5alpha competent cells were transformed with different expression vectors. The purified vectors were subsequently used for further transfection of neurons. The transformation protocol was adapted from Inoue *et al.* 1990 [118]. Briefly, 50 ng of plasmid DNA was added to 50 µl of DH5alpha competent cells and incubated for 20 minutes on ice. Following a heat shock and successive incubation on ice for 2 minutes, 250 µl of SOC medium was added to the DNA solution. The cells were allowed to grow for 1 hour at 37°C and then centrifuged at 20 000 x g for a few seconds. 200 µl of

supernatant were discarded and the pellet together with the remaining supernant was resuspended gently. The obtained suspension was plated onto agarplates containing antibiotic to select clones containing the Plasmid DNA of interest. These agar plates were incubated overnight at 37°C. On the next day, positive clones were transferred to 250 µl of LB medium containing the antibiotic and grown overnight at 37°C.

2.7.2 Isolation of plasmid-DNA from DH5alpha competent cells (midipreps)

200 ml LB media (containing an appropriate antibiotic) were inoculated with a single colony and incubated overnight at 37°C at 200 rpm. The cultures were pelleted by centrifugation (centrifuge; company) at 10000 rpm, for 15 minutes, at 4°C. The plasmid DNA was isolated following the instructions of the Qiagen Midi preparation kit (company). The DNA was eluted from columns by addition of prewarmed (50°C) 200 µl tris-HCl (10 mM, pH 8.0). Finally, the DNA pellet was resuspended in steril H_2O and the DNA concentration determined.

2.7.3 Determination of DNA concentration and purity

The isolated Plasmid-DNA was resuspended in steril water and a quantitative and qualitative analysis was followed. A nanodrop spectrophotometer (Nanoquant Infinite M200pro) was used to take measurements of absorbance at 260 nm and 280 nm. To assess the purity of the DNA the ratio of A260/A280 was calculated. Only DNA with a ratio between 1.8 and 2 was used. The final concentration of DNA was based on the equation: 1 OD_{260} unit = 50 µg/ml

2.7.4 Agarose Gel Electrophoresis

The PCR products obtained after the genotyping of wildtype and Spastin knockout mice underwent a gel electrophoresis separation based on their size and charge. The separated DNA bands were visualized with ethidium bromide staining, under UV-Light exposure. Agarose gels were prepared with a concentration of 4%. For the preparation of the gels, agarose was dissolved

by heating, in required electrophoresis buffer (1 x TAE buffer), and 0.5 mg/ml ethidium bromide was added. Samples were mixed with 10 x DNA loading buffer and loaded into the wells. DNA fragments are separated at constant voltage (100 V) in 1 x TAE buffer and Hyperladder I (Bioline, Luckenwalde, Germany) was used as a size marker.

2.7.5 DNA sequencing

The sequencing of DNA was a service provided by the Sequencing Unit under the supervision of Dr. Sabine Hoffmeister-Ullerich from the Center for Molecular Neurobiology Hamburg (ZMNH, Hamburg, Germany). To do that, a protocol based on the Sanger Sequencing was carried out using an ABI Prism 377 DNA-Sequencer (Applied Biosystems, Darmstadt, Germany) combined with the BigDye Terminator v1.1 Cycle Sequencing Kit (Applied Biosystems, Darmstadt, Germany).

2.7.6 Genotyping PCR of spastin knockout mice

The genotyping of wildtype, heterozygeous and homozygeous spastin mice required 3 spastin oligonucleotides (PL41, PL89 and PL169). The resulting amplified PCR product has a size of 223 base pairs for the wildtype allel. For the detection of the Spastin knockout allele the following primers were used (see Figure 2.6) and the respective amplification product has a size of 432 base pairs. The genomic DNA was isolated from tail biopsies using the Quick Extract Buffer (Biozym Scientific GmbH, Hessisch Oldendorf, Germany). 2 µl of extracted DNA were used for a final volume of 50 µl. The composition of the master mix reaction mixture was the following:

Components per tail biopsy	Components per tail biopsy (µl)
Genomic DNA	2
10x DNA loading buffer	5
2,5 mM dNTPs (Invitrogen, Carlsbad, USA)	1
Primer PLR 41 10 pmol/µl	2
Primer PLR 89 10 pmol/µl	2
Primer PLR 169 10 pmol/µl	2

5 U/l Taq polymerase (Invitrogen, Carlsbad, USA)	0.25
Steril H_2O	35.75

Table 2.7.6: Components of the master mix reaction mixture for genotyping PCR of spastin knockout mice

Spastin genotyping was performed on mouse genomic DNA by separate amplification of wildtype and knockout alleles.
The amplification conditions used were as follows:
Step 1: 95°C for 2 minutes
Step 2: 95°C for 25 seconds
Step 3: 65°C for 45 seconds
Step 4: 72°C for 1minute and 15 seconds (49 cycles from step 2 to 4)
Step 5: 72°C for 10 minutes
Step 6: 4°C ∞
After the PCR (Polymerase Chain Reaction) reaction, the amplification product was separated through agarose electrophoresis and the separated bands were analyzed.

2.8 Cell Biology and immunocytochemistry

2.8.1 Preparation of primary cultures of hippocampal neurons

One day prior to the preparation, 12 mm sterile glass coverslips (#P231.1, Roth) were placed into 24-well-plates and coated with Poly-D-lysine (sigma P7886) (50 µg/ml) over night at 37°C. On the next day, the coverslips were rinsed twice with 500 µl sterile H_2O and 1 ml complete neurobasal medium was added to each well and preheat the 24-well-plates to 37°C before plating the cells. The embryos at embryonic stage E16.0 were carefully dissected and stored in hibernate buffer until PCR genotyping results were known.
Then, the hibernate buffer was replaced by HBSS at 4°C and hippocampi were dissected out, transferred to 1 ml 0.05 % trypsin/EDTA solution (Invitrogen #14025050) and incubated for 1 minute at 37°C. Trypsin was removed and the hippocampi washed with DMEM containing serum and kept in HBSS medium. The hippocampi were gently dissociated into cells using fire

polished Pasteur pippetes. The estimation of cell density was calculated using a Neubauer Counting Chamber (4 x 4 grid x 1000). 60000 were plated out per well in 6 well plate and 24 well plates and stored at 37°C in a cell incubator. The cells were kept in these conditions for up to 20 days without changing the medium.

2.8.2 - Calcium phosphate-based transfection of neurons

For transfection of primary culture of hippocampal neurons at DIV5 to DIV22 the calcium phosphate method adapted from Kohrman *et al.* 1999 was used [119]. 2 µg Plasmid DNA was mixed with 6.5 µl 2 M $CaCl_2$ solution and 18.75 µl of steril H_2O. The DNA solution was added dropwise to 25 µl 2x HBS under vortex agitation and incubated at room temperature for 10 minutes. After the incubation time, 750 µl of the conditioning medium was removed and kept at 37ºC and 5 % CO_2. Then, the neuronal cells were incubated with the DNA solution until a fine precipitate formed (this step normally takes 15 minutes). The calcium precipitate is removed by rinsing the cells twice with pre-warmed 2 x HEPES buffer. The hippocampal neurons were cultured in the original medium at 37ºC at 5 % CO_2 for up to 22 days.

2.8.3 Immunocytochemistry on hippocampal neurons

Cultured hippocampal neurons were fixed in 4% paraformaldehyde/ 4% sucrose diluted in phosphate buffered saline (PBS) for 10 minutes. Subsequently, the cells were rinsed three times in PBS and permeabilized for 4 minutes in PBS containing 0.5 % triton-x-100, followed by one hour incubation in PBS containing 1 % BSA to avoid non-specific antibody binding. Neurons were incubated for one hour in primary antibodies diluted in blocking buffer at room temperature or overnight at 4°C, washed 3 times with PBS and incubated in secondary antibodies and DAPI diluted in blocking buffer for 1 hour. After washing 3 times with PBS, the coverslips were mounted using mounting media (Aqua poly mount, Polysciences, PA, USA) on slides.
This protocol was followed for all the standard immunocytochemistry, except for surface GluA2 staining when cells were incubated with the primary

antibody under non-permeabilizing conditions for 2 hours followed by permeabilisation for 4 minutes and blocking with 1% BSA.

2.9 Image and tracking analysis

For time-lapse imaging, coverslips with the transfected neurons were mounted into a live cell imaging chamber containing conditioned medium and kept at constant temperature of 37°C and 5 % CO_2 levels in an incubator coupled to the spinning disk microscope.

To observe the transport of GluA2, KIF5C and synaptophysin clusters, neurons at DIV11 were transfected with respective constructs and analysed 24 h later.

In order to examine microtubule dynamics, neurons at DIV11 were transfected with the microtubule-plus end marker EB3-GFP and analysed 24 h later.

For mitochondria movement analysis, DIV7 neurons were labeled with 100 nM Mitotracker RedCMXRos (Life technologies, Darmstadt, Germany) for 15 minutes, washed with HEPES buffer and kept in conditioning medium at 37°C and 5 % CO_2 during the time-lapse imaging.

Time-lapse Images were acquired using a Nikon spinning disc microscope (Visitron, Puchheim, Germany) equipped with a 60 x and 100 x objective and 488 nm, 561 nm argon lasers. For final analysis, captured LSM images were exported as TIF images.

KIF5 single particle mobility, mitochondria mobility, and EB3-GFP comet growth of sequential images were quantified manually using ImageJ (ImageJ, NIH, USA). Kymographs were generated using the Multiple Kymograph plugin for Fiji (ImageJ, NIH, USA). Student´s *t* test was used for statistical analysis unless stated otherwise and was carried out using SPSS (PASW Statistics 18.0, IBM, New York, USA). The velocity and run length frequency distributions of motile KIF5 particles were performed using Graphpad Prism (Graphpad Software, Inc., San Diego, CA).

All the immunofluorescence quantifications were performed on the Metamorph 6.3 r7 software (Molecular Devices, Sunnyvale, CA) or using the ImageJ software. Co-imunnostaining of both pre- and postsynaptic markers were quantified by thresholding the signal and applying a separation filter to isolate the seperated puncta. Further, the number and fluorescent intensity of

the puncta per cell were measured. For the surface receptor staining, ROI were drawn manually in a given channel and superimposed on the complementary channel. *p<0.05; **p<0.01; ***p<0.001.

2.10 Biochemical experiments

2.10.1 Mouse brain differential centrifugation

Spastin -/- mice and their +/+ littermates were sacrificed using CO_2 and brains were isolated and placed in 1.5 ml ice-cold Homogenization Buffer (20 mM HEPES, 100 mM potassium acetate, 40 mM KCl, 5 mM EGTA, 5 mM $MgCl_2$, pH 7.2, protease inhibitor (Roche Complete, Sigma-Aldrich, Hamburg, Germany), 2 mM mg ATP, 5 mM DTT and 1 mM PMSF) and homogenized with a 26 G needle syringe. The homogenate was centrifuged for 10 minutes at 1000 x g (JA 20 or JS 13.1 Beckman). The supernatant (S1) was centrifuged for 10 minutes at 10000 x g (JA 20 or JS 13.1 Beckman) and pellet (P1) was discarded. Subsequently, the supernatant was collected into a new tube (S2) and the pellet (P2) was resuspended in the homogenization buffer. The collected samples were diluted with 4 x sample buffer and boiled at 95°C for 10 minutes, and either used immediately or stored at -80°C.

2.10.2 Lysates of Cultured Neurons

80000 neurons were plated in 24-well plates per well. Cells between DIV4 and DIV21 were washed with pre-warmed PBS and lysed with homogenization buffer. The cells were harvested from the dish using a cell scraper and the lysate was centrifuged at 1000 x g for 10 minutes. The supernatant was subsequently collected, boiled with 4x sample buffer for 10 minutes at 95°C and used directly for western blotting analysis or snap frozen with liquid nitrogen and stored at -80°C.

2.10.3 Preparation of Proteins Samples for SDS electrophoresis

Total protein concentrations were determined using the Bicinchoninic Acid (BCA) method based on the instructions provided by the Protein Assay form BioRad.

Briefly, the absorbances of the standards and the samples whose concentration is unknown were measured using a monocromator (Nanoquant Infinite M200 Pro, Tecan, Switzerland). The final protein concentration of the samples was determined through the standard curve based on the absorbance values of the standards versus their protein concentration.

For the biochemical analysis, spastin +/+ and -/- lysates were standardized to the same protein concentration by addition of homogenization buffer. The protein samples were mixed with 4x sample buffer, boiled at 95°C for 10 minutes, snap frozen with liquid nitrogen and stored at -80°C.

2.10.4 SDS-poly-acrylamide gel electrophoresis (SDS-PAGE)

The separation process of proteins was based on their molecular size after migrate through a SDS-poly-acrylamide gel when an electrical field was applied. For the experiments 8% or 10% SDS-PAGE gels were used.

For the gel preparation, glass plates were assembled following the instructions provided by Biorad and the resolving gel solution of the desired concentration was poured between the two glasses. After the gel polymerization, the remaining volume above the gel was filled up with stacking gel and a comb with the desired size was inserted. After the second step of polymerization, the gels were placed in a vertical electrophoresis chamber (Mini-Protean III Systems, Biorad, Munich, Germany) containing SDS running buffer. The protein samples were loaded as well as a protein marker (Precision Plus Protein Standards Dual Color, Biorad, Munich Germany). The electrophoresis process was conducted at constant voltage of 95 V while the proteins where running through the stacking gel and increased up to 120 V for the protein separation in the resolving gel. When the bromophenol front reached the bottom of the gel, the separation of proteins was concluded, the gel removed and used for western blotting analysis.

2.10.5 Western blotting analysis

Western blotting technique was used to transfer proteins previously separated on SDS-PAGE to PVDF membranes (Millipore, Frankfurt, Germany). The proteins were electrophoretically transferred at 250 mA for 2 hours, or overnight at 40 mA using a Wet-Blot Mini Trans-Blot Cell device (Biorad, Munich, Germany) to a PVDF membrane previously activated by methanol immersion. The transferred proteins stay bound to the surface of the membrane, making them accessible for further immunoblotting analysis.

For the protein analysis, primary antibodies were used which recognize a specific epitope on the protein of interest. First, the membrane was blocked using a blocking buffer containing milk (5 %) or bovine serum albumin (5 %) in TBS-T to avoid non-specific binding of antibodies to the surface of the membrane. Then, the membrane was incubated with the primary antibody (diluted either in 5 % milk or 5 % BSA in TBS-T) for 1 hour at room temperature or overnight at 4°C. To detect the antigen-antibody interaction, a horseradish peroxidase (HRP) – labeled secondary antibody (diluted either in 5 % milk or 5 % BSA), which binds to the first antibody was applied for 1 hour. In order to visualize the immunoreactive bands, the membrane was incubated with immobilon western HRP substrate (Merck, Millipore, Frankfurt, Germany) leading to light release, which was visualized by a chemiluminescence detection system (INTAS Chemo Cam 3.2, Göttingen, Germany).

The acquired images were saved as TIF files and processed using Photoshop 6.0.1. Finally, the intensities of individual bands were measured using the ImageJ software (ImageJ, NIH, USA).

2.10.6 Electron microscopy

Adult spastin +/+ and -/- mice were anesthetized and transcardially perfused with a mixture of 4 % paraformaldehyde and 1 % glutaraldehyde in 0.1 M Phophate buffer at pH 7.4. Then, the brains from spastin +/+ and -/- brains were processed using a vibratome (Leica VT 1000S) to obtain 100 µm thick sections. These brain sections were rinsed three times in 0.1 M sodium

cacodylate buffer (pH 7.2-7.4) (Sigma-Aldrich) and incubated with 1 % osmium tetroxide (Science Services) in cacodylate buffer for 20 minutes on ice. The osmication of sections was followed by dehydration through ascending ethyl alcohol concentration steps and rinsed twice in propylene oxide (Sigma-Aldrich). Infiltration of the embedding medium was performed by immersing the pieces first in a mixture of 2:1 of propylene oxide and Epon (Carl Roth) then in a 1:1 mixture and finally in neat Epon and hardened at 60°C for 48 hours. Ultrathin sections (60 nm) were observed using a EM902 transmission electron microscope (Zeiss, Germany) equipped with a CCD in lens 2K digital camera and running the ImageSP software (Tröndle, Moorenweis, Germany).

Primary hippocampal neurons, cultured on Aclar (TED PELLA), were fixed and embedded and polymerized on already polymerized Eponslides. Thereafter the Aclar was drawn off and ultrathin sections were prepared and investigated as described above.

Defined microtubules in dendrites of similar size and orientation were traced using the ImageJ software. Distances between adjacent microtubules traces were measured prior to statistical analysis.

For the ultrastructural analysis in the CA1 region of the hippocampus, only synapses with intact synaptic plasma membranes with recognizable pre- and postsynaptic density and clear defined synaptic vesicle membranes were used.

Synaptic vesicles were classified as docked if there was a distance of 0 nm between the synaptic vesicle membrane and the membrane of the active zone.

The active zone membrane was defined as the part of the plasma membrane that contained a clear density opposed to the postsynaptic density and docked synaptic vesicles.

2.10.7 Pharmacological manipulation of microtubule stability

Primary hippocampal neurons prepared from spastin +/+ and -/- E16.0 embryos were transfected with eEGFP-C1 at DIV10 and maintain in culture at 37°C and 5 % CO_2. At DIV13, the neurons were incubated with 2 different

concentrations of Taxol (10 nM and 100 nM) and the control neurons only with the vehicle (DMSO) for 2 hours. The hippocampal neurons were rinsed twice with HEPES buffer and kept in conditioned medium in the incubator. 20 hours after the treatment, the neurons were fixed for 10 minutes with 4 % PFA / 4 % sucrose, rinsed in PBS and incubated for two hours with the primary antibody anti-GluA2 in non-permeabilizing conditions in 1 % BSA. After the incubation time, the neurons were rinsed three times in 1 x PBS, permeabilized with 0.25 % Triton-X-100 incubated with the secondary antibody and mounted in Aqua Mounting.

2.11 Histology and immunohistochemistry

Mice were transcardially perfused with 4 % phosphate-buffered paraformaldehyde solution (PFA) and brains were carefully removed. They were post-fixed for 2 hours in the same fixative at 4°C, cryopreserved over two days in 30 % sucrose, and frozen on dry ice. The frozen brains were mounted using Tissue Tek (VWR, PA, USA) and sectioned into 30 µm coronal sections using a cryostat. The brain sections were mounted on glass slides and stored at -80°C until further processing.

Immunohistochemistry: Brain sections were washed three times in PBS and permeabilized in 1 % Triton-X-100 (v/v) in PBS for 10 minutes. Antigen blocking was carried out by incubating the sections with 1 % BSA in PBS for one hour. This step was followed by washing with PBS and incubation overnight at 4°C in a humid chamber at 4°C in primary antibodies diluted in the blocking buffer. On the following day, the sections were rinsed three times with PBS prior to incubation in secondary antibodies diluted in the blocking buffer for 2 hours at room temperature (RT). They were rinsed further in PBS and finally mounted in Aqua Poly Mount (Polysciences, Eppelheim, Germany).

Histology: 30 µm thick coronal sections were Nissl-stained using cresyl violet for histological examination. Hippocampal and cortical layers were analysed using the ImageJ software (NIH, Bethesda, MD, USA).

2.12 Behavior experiments

2.12.1 Subjects and housing

Spastin +/+, +/- and -/- mice were bred in a specific-pathogen-free (SPF) facility (Center for Molecular neurobiology (ZMNH), University Medical Center Hamburg-Ependorf, University of Hamburg).

Mice (male and female) were group housed (2-5 mice per cage) under a reversed 12 hour light/dark cycle and divided into 2 different experimental cohorts: 8 and 14 months old at the beginning of the behavioral assessment. Temperature (22 ±1°C) and humidity (50 ± 5 %) in the animal facility were kept constant, and the animals had *ad libitum* access to food and water. The behavioral experiments were conducted during the dark phase of the cycle. All performed behavior tests were approved by the local authorities.

The composition of the middle-aged cohort (8 months) was the following: 23 spastin +/+ mice; 19 spastin +/- mice and 22 spastin -/-. The aged cohort of mice (14 months) consisted of 23 spastin +/+ mice, 21 spastin +/- and 15 spastin -/- mice.

The following table shows the chronological order and duration of behavioral experiments.

Experiment	**Duration (days)**
1 - Pole test	1
2 - Horizontal grid test	1
3 - Grip Strength test	1
4 - Rotarod test	3
4 - Y-maze Spontaneous Alternation	2
5 - T-maze Confined Alternation	2
6 - Contextual Fear conditioning	7

Table 2.9.1: Chronological representation of the behavior experiments and duration.

2.12.2 Horizontal grid test

The horizontal grid test was the behavior test chosen to assess the neuromuscular strength and coordination of spastin mutant mice (+/- and -/-)

and their +/+ littermates. The apparatus consists of a horizontal square metallic grid with the edges covered so that the mice can only grap on the center. The metallic grid was mounted 40 cm above the floor, supported by a metallic vertical bar. A cage filled with saw dust was placed on the floor as a cushion for the falling mouse. The temperature in the room was kept constant at 23 ±1°C and the light at 70 lux. Once the mouse firmly grabbed on the grid with all four paws, the apparatus was carefully inverted so that the mouse would now hang upside down on the center of metallic grid. Each experiment was stopped after 300 seconds. The mouse was videotaped using a fixed video camera (Sony HDR-CX240E, Tokyo, Japan) and the videos were replayed for analysis of the time that a mouse took to fall (latency to fall).

2.12.3 Pole test

Pole test is a commonly test used to study the motor balance and coordination performance in rodents. Mice were placed on top of a 30 cm vertical, 0.9 cm diameter rod while grasping it with the four paws and the head pointing upwards. 24 hours before the testing day, mice were habituated to the pole by performing 3 consecutive trials with an inter-trial interval of 30 seconds. In order to motivate the mice to climb down, nesting material removed from the home cage was placed at the bottom of the rod. On the day of testing, each mouse performed 5 trials and the best performance was used for analysis. Trials were excluded when the mouse slid down or jumped from the top of the pole. The time each mouse took to make a turn of 180 degrees with the head pointing downwards (time to turn), and to reach the ground (time to finish) was quantified for each trial. Each experiment was concluded after 300 seconds.

2.12.4 Grip Strength test

In order to measure the muscle strength, a TSE grip strength meter system from TSE systems (dimensions 40 x 30 x 2.3 cm) was used. Mice were grabbed by the tail and placed on top of the grip by their forelimbs. Once the animal holds on firmly to the grip then this is pulled backwards with a

continuous movement until the mouse releases the grip. The force applied on the grip is automatically displayed on the screen. The test was repeated two more times and the highest values were used later on for statistical analysis.

2.12.5 Accelerating Rotarod Test

Equilibrium sense and motor coordination were monitored on a rotarod apparatus. Mice had to walk on a rotating rod (Acceler, Rotarod for mice, Jones & Roberts, TSE Systems, Bad Homburg, Germany) at constant speed (4 rpm) for two minutes. After two acclimatization trials, each mouse was placed on the rotating rod for four test trials, during which the rotation speed gradually increased from 4 to 40 rpm within four minutes. The performance of the mice on this motor test was evaluated by measuring the latency to fall down.

2.12.6 Y-maze spontaneous alternation

The spontaneous alternation task was used to evaluate spatial working memory and it is based on innate behavior of mice to explore a prior unvisited arm of a Y-maze. The apparatus consists of a Y-shaped maze with three arms arranged in 180° position. Over 10 minutes, each mouse was randomly placed into one arm and allowed to move freely through the maze. Alternation behavior was defined as consecutive entries into each of the three arms in overlapping triplet sets (e.g.: 1, 2, 3 or 2, 1, 3 or 3, 2, 1). The percentage of alternation was calculated as the percentage of actual alternations to the maximum number of arm entries. In order to avoid any bias of the mice through odor cues, the maze was carefully cleaned with 30% ethanol solution.

2.12.7 T-maze confined alternation

In this study, the T-maze confined alternation was used to assess learning and memory features in mice. The apparatus was made of wood and had three arms of equal dimensions (30 x 6 cm). The start arm, enclosed by walls 16 cm high, was perpendicular to two opposing arms. The whole apparatus was elevated 40 cm above the floor. On the training trial, the mouse was

removed from the home cage and placed onto the distal end of the enclosed arm facing the interception of the arms and was allowed to explore the enclosed arm. As soon as the mouse entered one of the arms by placing all four paws into the arm, the operator isolated the mouse in the chosen arm for 30 seconds using a removable wall, perpendicular to the arm walls. After 30 seconds the mouse was put back into the home cage and subsequently placed back into the starting arm in order to choose between left and right arm.

2.12.8 Contextual Fear Conditioning

Fear conditioning is carried out in fear conditioning chambers equipped with shock grid floor and digital NIR video fear conditioning system (MED-VFC-SCT-M, Med Associates Inc, VT, USA) connected to a controller computer. Mice from each genotype and sex were examined in four successive phrases comprising: 1) Conditioned acquisition (day1), 2) Memory for the conditioned background context A (day2), 3) exploration in new background context B (day3) and 4) extinction in the conditioned context A (day4-7).

Day1 (conditioned acquisition): Mice were introduced to the conditioning chambers scented with vanilla odor (RUF Lebensmittelwerk, Quakenbrück, Germany) for 8 minutes and received 3 unconditioned stimulus (US: 1s, 0.25 mA foot shock, trials inter-spaced by 2 minutes inter-trials intervals). Chambers are cleaned with water and ethanol solution between mice to eliminate odor left by the previous animal.

Day2 (context test): To examine the conditioned response to the context, the mice were reintroduced to the training context 24 h later and tested for 5 minutes in the absence of the US.

Day 3 (exploration in a new context): In order to examine whether the freezing behavior of the tested mice is associated to a specific context (context A), the mice were re-introduced to a new context (context B), consisting of contextual properties different to context A.

Day4-7 (extinction of fear conditioning): Mice were re-introduced to the context A without unconditioned stimuli to extinct association of the specific context A and the US (which is described as a form of new learning).

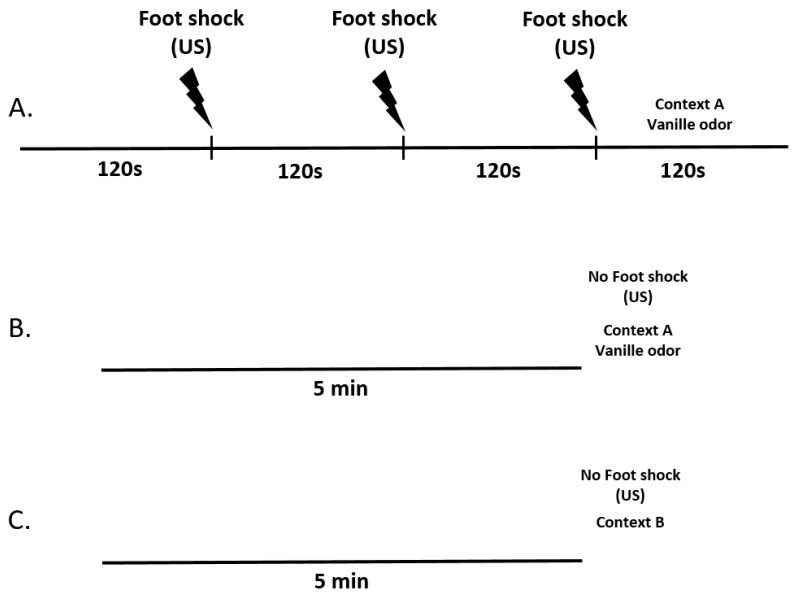

Figure 2.12.8: Experimental design for contextual fear conditioning test. A) Schematic representation of the fear conditioning acquisition in Context A; B) Schematic representation of testing in Context A or Extinction in Context A; C) Schematic representation of testing in a new Context (Context B).

Chapter 3

Results

3. Results

3.1 General phenotypical characterization of the spastin knockout mouse

To investigate the *in vivo* relevance of spastin, a spastin knockout mouse was generated using knockout first embryonic stem (ES) cells obtained from the Knockout Mouse Project repository (KOMP) [120]. Successful gene targeting was confirmed using PCR analysis (Figure 3.1A). Western blot experiments using an antibody against spastin confirmed the loss of this protein in spastin knockout mice (Figure 3.1B). Examination of spastin knockout brain sections by Nissl and DAPI staining revealed normal hippocampal gross morphology and cortical layering (Figure 3.1C and D). In contrast with homozygous mice that are infertile, heterozygous (+/-) spastin mice display no obvious phenotypic changes in their viability or fertility (data not shown).

Regarding the body weight, the spastin mutant (+/- and -/-) mice did not differ from their WT (+/+) littermates (main effect for genotype: $F(2,112)=7.033$; $p<0.001$; followed by restricted analysis and pairwise comparisons. For 8 month old mice: females (+/+) and (+/-) with $p=0.101$ and (+/+) and (-/-) with $p=0.002$; males (+/+) and (+/-) with $p=0.383$ and (+/+) and -/-) with p=0,238. For 14 month old mice: females (+/+) and (+/-) with $p=0.957$ and (+/+) and (-/-) with $p=0.524$; males (+/+) and (+/-) with $p=0.839$ and (+/+) and (-/-) with p=0003 (Figure 3.1E and F). Also, the brain weight analysis revealed no differences between the genotypes (main effect for genotype: $F(2,10)=1.031$; $p=0.392$) (Figure 3.1G).

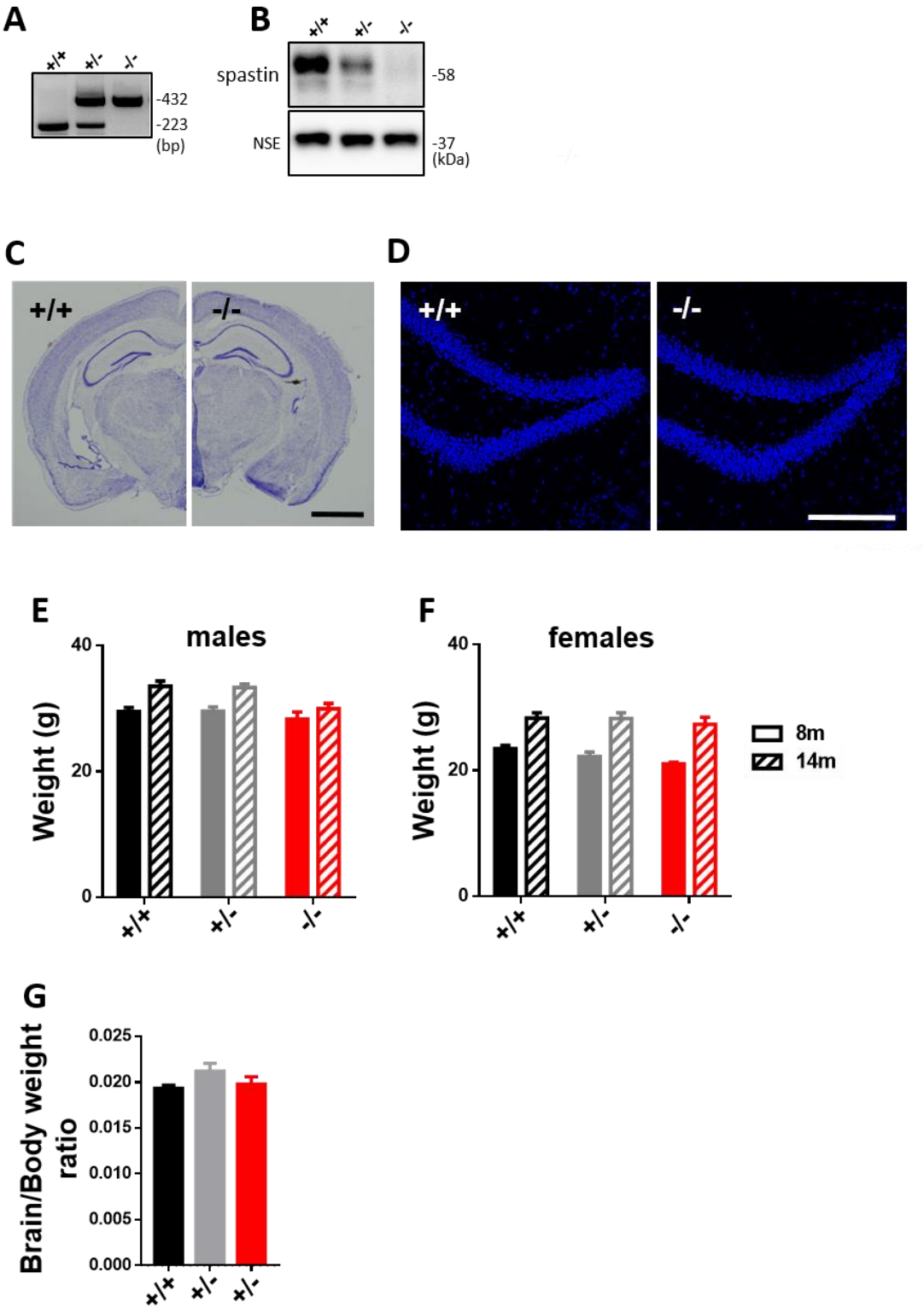

Figure 3.1: General phenotypical characterization of the spastin knockout mouse. (A) PCR genotyping of spastin WT (+/+) and spastin mutant (+/-, -/-) mice. (B) Western blot analysis probed with anti-spastin and anti-NSE (loading control) antibodies. (C) Nissl staining showing intact cortical lamination and thickness (scale bar is 5 mm). (D) Representative

photomicrographs (DAPI counterstaining of nuclei) of coronal hippocampal slices showing grossly normal hippocampal structure and thickness in spastin -/- mice (Scale bar: 200um). (E, F) Representative graphs of body weight for males and females from middle-aged and aged cohorts. (G) Whole brain weight of adult mice from the three genotypes normalized to the body weight. Data represented as mean ± sem.

3.2 Spastin -/- mice show age-dependent motor impairments

As earlier described, mutations in the *SPAST* gene that encodes for spastin are responsible for more than 40% of the autosomal dominate cases of HSP. The most overt phenotype in patients with the spastin mutation is the progressive lower limb spasticity, ataxia and nerve degeneration of long axons. This disorder can be so debilitating that some patients may need the help of walkers to move. Based on what is known about the effects of spastin in humans, I first validated the mouse model by evaluating motor performance of spastin knockout (-/-), heterozygous (+/-) and wildtype mice (+/+) at 8 and 14 months of age using several behavioral motor assays.

The pole test was used to assess the ability of mice to turn around when placed upwards facing the pole, and requires proper limb coordination. 14-month old spastin (-/-) knockout mice showed impaired performance in this test compared to heterozygous and wildtype littermates (main effect for genotype: $F(2,57)=2.59$; $p=0.084$; followed by pairwise comparisons for (+/+) and (-/-) with $p=0.043$) (Figure 3.2 A). The muscle strength was also assessed using the grip strength test. During testing, when mice grasped firmly onto a metallic bar, they were gently pulled backwards until they released it. The force applied was measured and noted for each mouse. The analysis revealed significantly lower values for spastin (+/-) and (-/-) mutant mice when compared to the WT mice (main effect for genotype: $F(2,53)=17.97$; $p<0.0001$; followed by pairwise comparisons for (+/+) and (+/-) with $p<0.0001$ and (+/+) and (-/-) with $p<0.0001$) (Figure 3.2 B). In addition, the horizontal grid test was performed to assess the ability of the mice to hold onto a metallic grid using both hind- and forelimbs. Whereas 8-month old spastin mutant mice did not show any significant impairment in this task compared to their WT littermates, 14-month old spastin (+/-) and (-/-) mice showed decreased latency to fall (8-month old mice: main effect for genotype:

F(2,58)=1.14; p=0.327; followed by pairwise comparison for (+/+) and (+/-) with p=0.344 and (+/+) and (-/-) with p=0.144); 14-month old mice: main effect for genotype: F(2,54)=13.49; p<0.0001; followed by pairwise comparison for (+/+) and (+/-) with p<0.001 and (+/+) and (-/-) with p<0.0001 (Figure 3.2 C).

Further assessment of balance and motor coordination was confirmed using the rotarod test, which consists of a moving rod at accelerating speed. Spastin (-/-) mice showed an impaired performance when compared to control animals at 14 months of age, whereas younger mice at 8 months of age did not show any impairment (8-month old mice: main effect for genotype: F(2,61)=1.07; p=0.351; followed by pairwise comparisons for (+/+) and (+/-) with p=0.269 and (+/+) and (-/-) with p=0.180); 14-month old mice: main effect for genotype: F(2,57)=3.26; p=0.046; followed by pairwise comparisons for (+/+) and (+/-) with p=0.034 and (+/+) and (-/-) with p=0.035; (Figure 3.2D). Taken together, these findings indicate that mice lacking spastin display age-dependent progressive motor performance impairments.

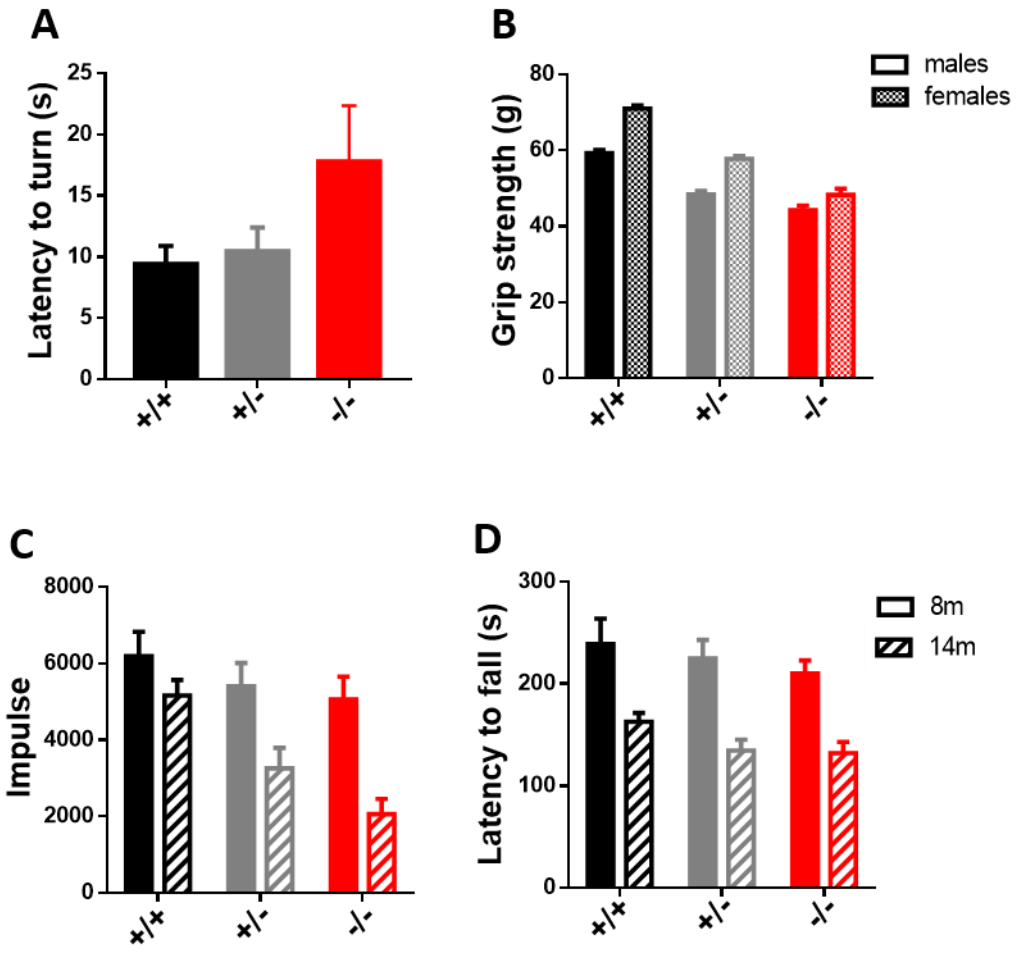

Figure 3.2: Age-dependent progressive impairment of motor performance in spastin -/- mice. (A) Pole test: latency to turn (14-month old mice). (B) Forelimb grip strength in 14-month old mice. (C) Horizontal Grid test performed in 8- and 14-month old mice with body weight as a co-variate. Holding impulse (Impulse) = Body weight x Hang time.(D) Accelerating rotarod test in 8- and 14-month old spastin mice with body weight as a co-variate. The motor performance as indexed by the latency to fall in seconds is depicted. 8-month old cohort: (+/+) = 23 mice; (+/-) = 19 mice; (-/-) = 15 mice. 14-month old cohort: (+/+) = 23 mice; (+/-) = 22 mice; (-/-) = 15 mice. Data represented as mean ± sem.

3.3 Working memory impairments in mice lacking spastin

Working memory was examined using the Y-maze continuous alternation task. Mice were introduced into the maze and the number of arm entries was recorded in order to calculate the alternation score. 8- and 14-month old spastin mutant mice (+/- and -/-) exhibited impaired spontaneous alternation compared with wildtype mice (8-month old mice: main effect for genotype:

F(2,58)=12.56; p<0.0001; followed by pairwise comparisons for (+/+) and (+/-) with p<0.001 and (+/+) and (-/-) with p<0.0001; 14-month old mice: main effect for genotype: F(2,55)=2.46; p=0.09; followed by pairwise comparisons for (+/+) and (+/-) with p=0.249 and (+/+) and (-/-) with p=0.033) (Figure 3.3A). The reduced alternation was not due to changes in overall exploration since total arm entries in spastin knockout mice were comparable with their WT littermates (two-way ANOVA (main effect for genotype: F(2,119)=1.649; p=0.197; 8-month old mice pairwise comparisons for (+/+) and (+/-) with p=0.639 and (+/+) and (-/-) with p=0.615. 14-month old mice (+/+) and (+/-) with p=0.914 and (+/+) and (-/-) with p=0.090 (Figure 3.3B).

Further assessment of working memory was performed using the T-maze confined alternation task. The analysis revealed significantly impaired alternation in 8- and 14-month old spastin (-/-) knockout mice compared with (+/+) controls. (8-month old mice: main effect for genotype: F(1,61)=3.04; p=0.055; followed by pairwise comparisons for (+/+) and (+/-) with p=0.066 and (+/+) and (-/-) with p=0.025; 14 month old mice: main effect for genotype: F(2,46)=4.17; p=0.021; followed by pairwise comparisons for (+/+) and (+/-) with p=0.1 and (+/+) and (-/-) with p=0.006). Additional analysis showed that only the wildtype group alternated at levels significantly above the chance. Spastin (+/-) and spastin (-/-) mice performed at 50% chance level or below, respectively (one sample t-test against 50% chance level: 8-month old mice (+/+): p<0.0001; (+/-) p<0.379; (-/-): p=0.321. 14-month old mice (+/+): p<0.033; (+/-): p=0.727; (-/-): p=0.044 (Figure 3.3C).

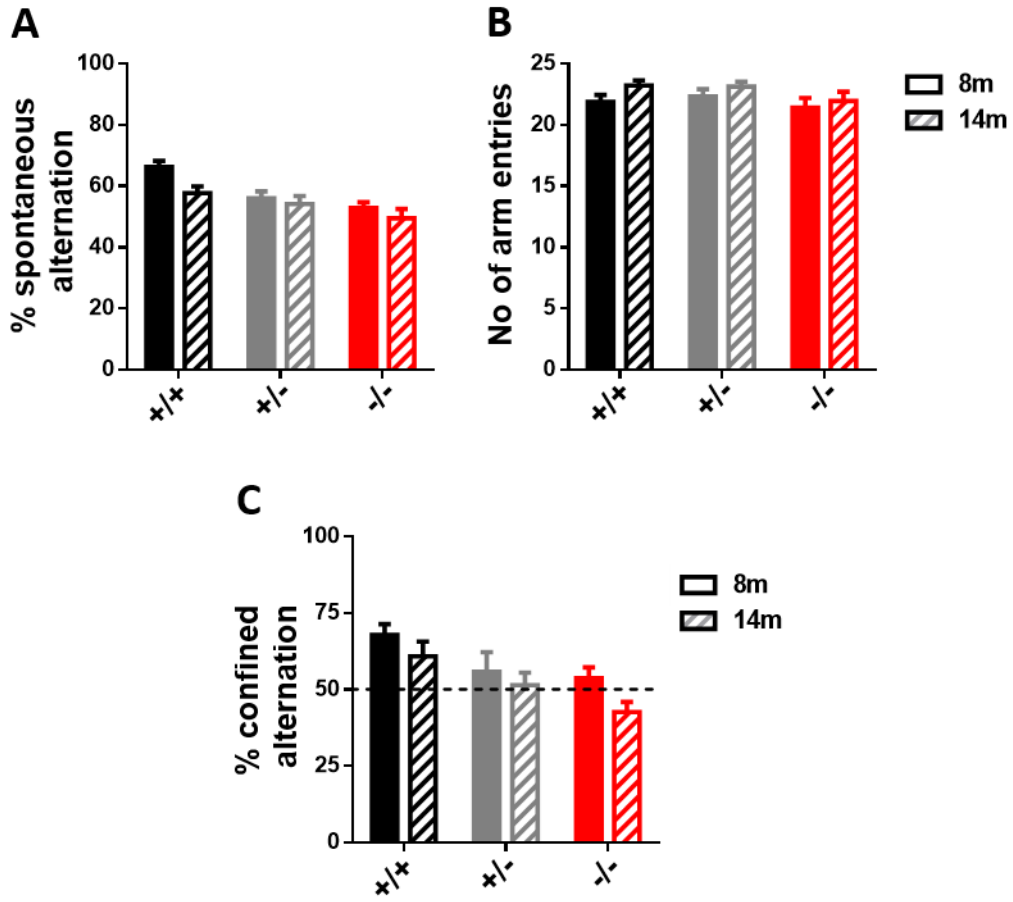

Figure 3.3: Continuous spontaneous and confined alternation behavior in spastin-depleted mice (A) Analysis of the spontaneous alternation in the Y-maze showed a significant difference between spastin (+/+) and spastin mutant (+/- and -/-) mice at 8 and 14 months of age. (B) Intact explorative behavior as depicted by the similar number of arm entries in all genotype groups. (C) Evaluation of working memory in the T-maze showed reduced alternation rates that were more severe at 14 months. The dotted line represents 50% chance level.. 8-month old cohort: (+/+) = 23 mice; (+/-) = 19 mice; (-/-) = 15 mice. 14-month old cohort: (+/+) = 23 mice; (+/-) = 22 mice; (-/-) = 15 mice. Data represented as mean ± sem.

3.4 Impaired contextual fear memory in spastin-depleted mice

In order to study associative learning, the hippocampal-dependent contextual fear conditioning paradigm was used. Here, the pairing of a neutral context (conditioned stimulus, CS) with an aversive shock (unconditioned stimulus, US) elicits a fear response (freezing; conditioned response, CR) (Figure3.4A). Irrespective of age, there was no difference between genotypes in conditioned acquisition as seen in the level of post-shock freezing, suggesting

that spastin is not required for acquisition of contextual fear memories (two-way ANOVA (genotype x age): $F(2,118)=0.328$; $p=0.721$; main effect for genotype: $F(2,118)=1.779$; $p=0.173$) (Figure 3.4B and C). Contextual memory was tested 24 hours after conditioning by re-introducing the mice to the training context for 5 minutes without receiving a foot shock. At the age of 8 months there was no statistical difference regarding the freezing levels between genotypes. Compared to the age-matched wildtype mice, 14-month old spastin mutant mice (+/- and -/-) spent less time freezing. (8- month old mice: main effect for genotype: $F(2,61)=2.09$; $p=0.132$; pairwise comparisons for (+/+) and (+/-) with $p=0.104$ and (+/+) and (-/-) with $p=0.070$; 14 month old mice: main effect for genotype: $F(2,57)=5,5524$; $p=0.006$; pairwise comparisons for (+/+) and (+/-) with $p=0.038$ and (+/+) and (-/-) with $p=0.002$) (Figure 3.4D). In order to test whether the freezing behavior was specific to the conditioning context (context A), mice were placed into a distinct new context (context B) for 5 minutes. Freezing levels in spastin (+/-) and (-/-) mice did not differ from wildtype mice at the age of 8 and 14 months. On the next day, extinction training was performed by re-exposing the mice to the conditioning context (context A) without foot shock for 4 consecutive days. All genotype groups in the 8-month old cohort showed a clear extinction learning profile across the 4 days of testing (Figure 3.4F). Unlike wildtype (+/+) mice, which showed an overt fear extinction learning profile, 14-month old spastin (+/-) and (-/-) mice failed to decrease the freezing response over the course of extinction training (Figure 3.4G). (3 way-ANOVA (day x genotype x age): $F(6,354)=2.021$; $p<0.062$; 8 month old mice: 2-way ANOVA (day x genotype): $F(6,183)=0.862$; $p=0.524$; main effect for genotype: $F(2,61)=0.305$; $p=0.738$. 14-month old mice: 2-way ANOVA (day x genotype): $F(6,171)=2.845$; $p=0.011$; main effect for genotype: $F(1,57)=35.484$: $p<0.0001$; pairwise comparisons (+/+) and (+/-): $p<0.0001$ and for (+/+) and (-/-): $p<0.0001$.

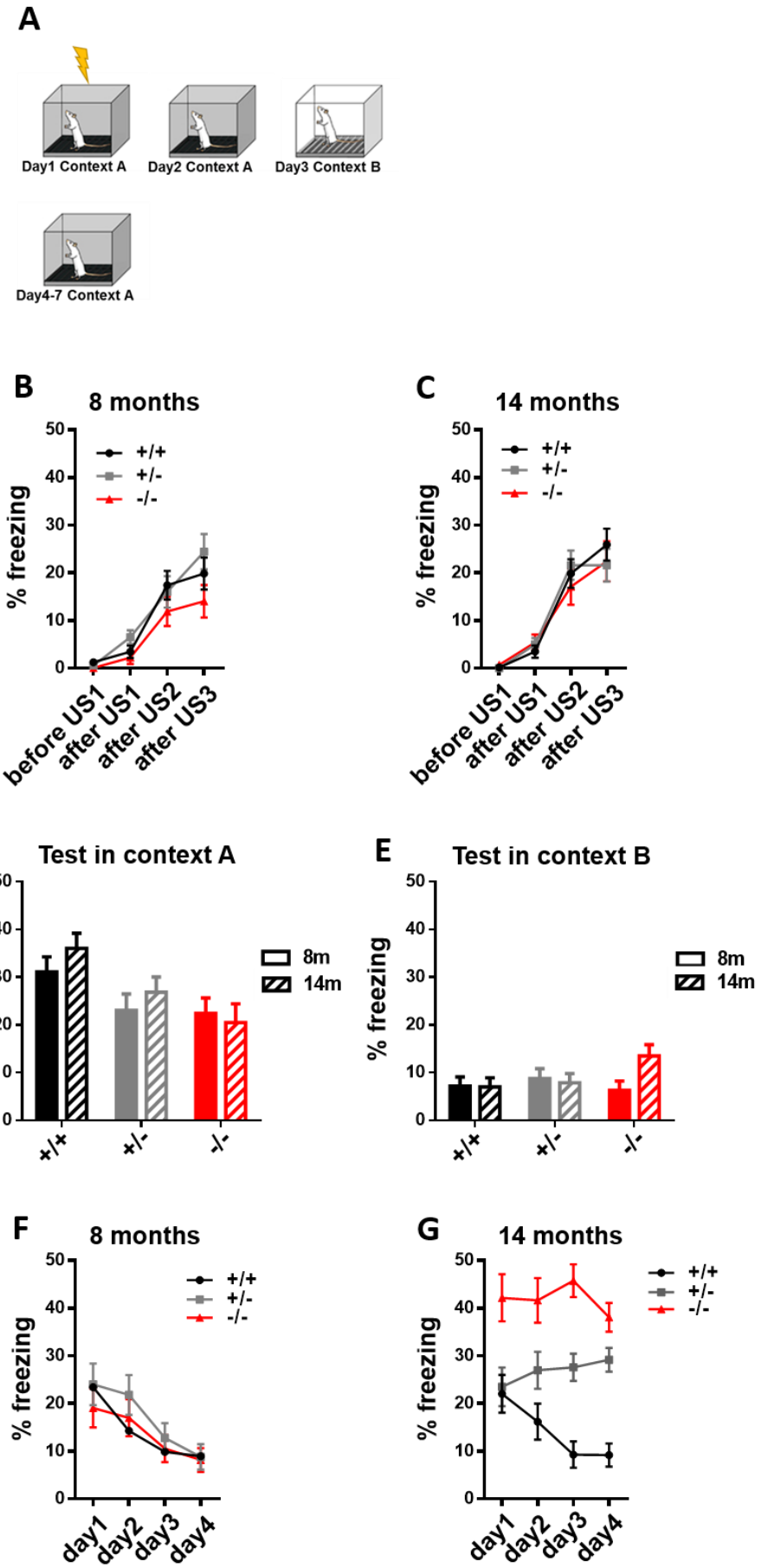
A
Day1 Context A
Day2 Context A
Day3 Context B
Day4-7 Context A
B
8 months
% freezing
+/+
+/-
-/-
before US1
after US1
after US2
after US3
C
14 months
D
Test in context A
8m
14m
E
Test in context B
F
G
day1
day2
day3
day4

Figure 3.4: Altered contextual fear memory and extinction in spastin-depleted mice at 14 months (A) Experiment design of the contextual fear conditioning experiment. (B, C) Spastin (-/-), (+/-) and their (+/+) littermates from both age cohorts were placed in context A and after a 2 minute exposure period they received 3 foot shocks at 2 minute inter-trial intervals. The acquisition of contextual fear as depicted by increased freezing across trials (day1). (D) Context test: 24 hours after the conditioning, the mice were placed into the training context (Context A) and the freezing levels recorded. (E) 24 hours after context test: the mice were placed into a distinct neutral context (context B) and the freezing levels recorded. (F,G) Extinction of contextual fear in spastin (+/+) and spastin mutant (+/- and -/-) mice.. The mice were tested again in context A without receiving a foot shock for the next 4 days and the freezing levels recorded. 8-month old cohort: (+/+) = 23 mice; (+/-) = 19 mice; (-/-) = 15 mice. 14-month old cohort: (+/+) = 23 mice; (+/-) = 22 mice; (-/-) = 15 mice. Data represented as mean ± sem.

3.5 Synapse formation in spastin -/- neurons

Spastin is a microtubule-severing protein that cuts microtubules into shorter fragments, which can be used as nucleation points for further microtubule growth in axons and dendrites. Since microtubules enter spines, it is hypothesized that microtubules may also have a function in spines. Data from Drosophila have shown that spastin regulates the microtubule network and synaptic transmission.

Previous studies have shown that spastin expression increases during embryonic development, but expression levels gradually decline after birth. To determine spastin expression in primary hippocampal neurons, a western blot analysis of spastin expression in cell lysates at different days *in vitro* was performed. Spastin expression levels increased from DIV1 to DIV14, which corresponds to the phase of neurite outgrowth and branching. During maturation of the neurons from DIV14 to DIV20, the spastin expression progressively declined (Figure 3.5A and B).

To examine the effects of spastin depletion on synapse formation, immunolabelling was performed with antibodies raised against the presynaptic marker synaptophysin and the postsynaptic marker PSD95, both specific for glutamatergic synapses (Figure 3.5C). Spastin knockout neurons showed less colocalization of PSD95 and synaptophysin-positive puncta per dendritic

length (merged clusters), indicating that neurons lacking spastin have less excitatory synapses per unit length (Figure 3.5D). Western blotting analysis of P2 homogenates (membrane-enriched fraction) also showed an overall reduction of PSD95 and synaptophysin expression levels (Figure 3.5E and F). These data suggest that spastin may play an important role in synaptogenesis.

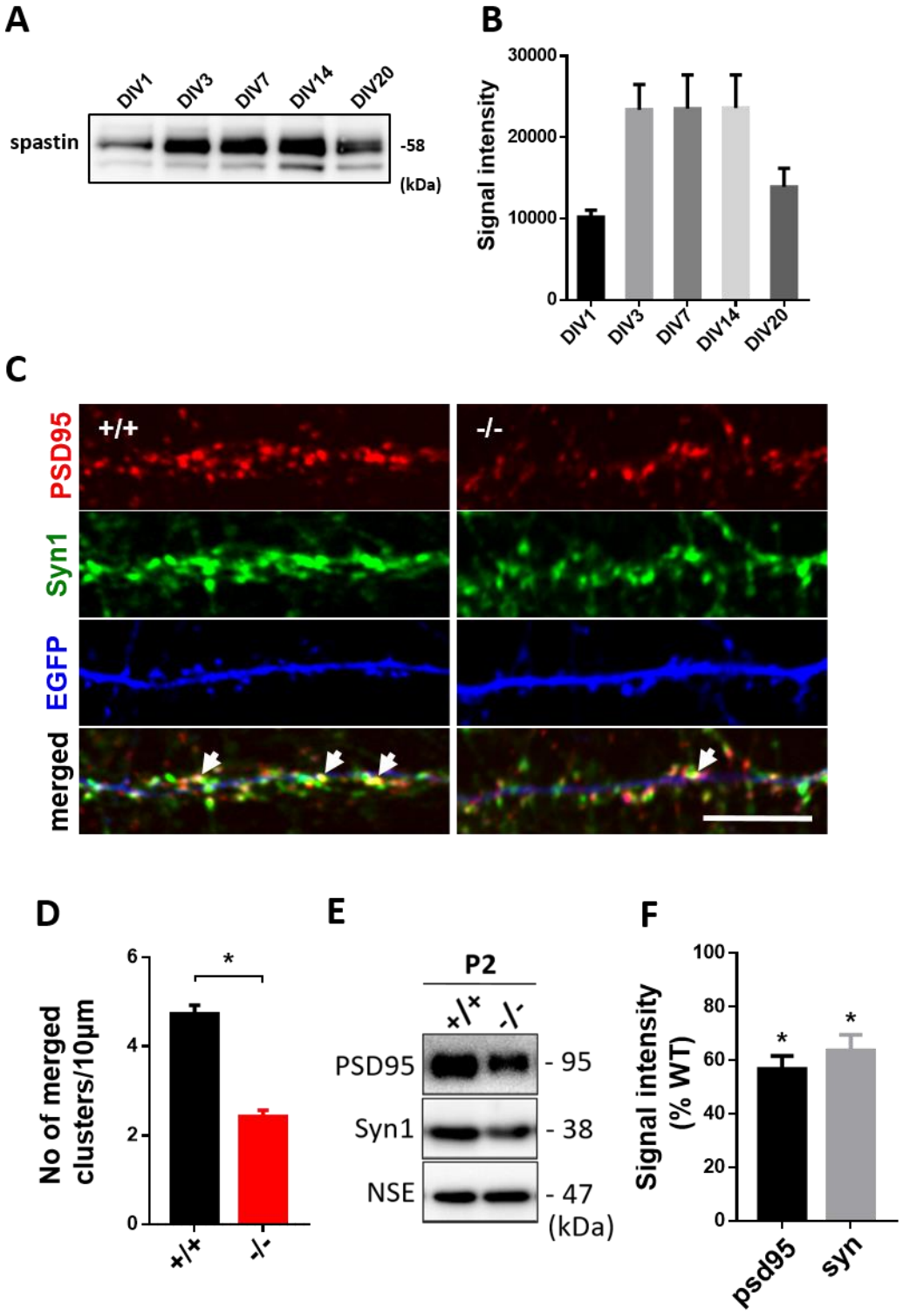

Figure 3.5: Spastin deficiency alters synapse density. (A, B) Representative image of western blotting and corresponding quantification of spastin protein levels in hippocampal neurons from DIV1 to DIV20. (C) Representative images of co-immunostainings of synaptophysin and PSD-95 in hippocampal neurons at DIV18. The arrows indicate colocalization between the two synaptic markers. (D) Quantification of the number of excitatory synapses (merged clusters) per dendritic length (10µm) showed in (B). (E)

Representative western-blots showing endogenous synaptophysin and PSD95 levels in P2 homogenates (membrane-enriched fraction) derived from adult mouse hippocampus after a differential centrifugation protocol. (F) Quantification of the signal clusters shown in (E). Data are normalized to control levels. Scale bar: 5 µm. Statistical significance was determined by Student´s t-test. Data represented as mean ± sem.

3.6 Altered dendritic spine formation in spastin knockout neurons

Dendritic spine morphology and plasticity critically depend on the actin cytoskeleton. However, there are indications that microtubules might influence spine formation. For example, the knockdown of the microtubule-plus end binding protein, EB3, has an impact on spine formation. Furthermore, stabilization of microtubules upon treatment with low doses of taxol altered spine formation [121].

In order to study the function of spastin in dendritic spine formation, hippocampal neurons were transfected at DIV10 with EGFP as a volume marker, fixed at DIV18, and subsequently stained for F-actin using rhodamine-phalloidin toxin (Figure 3.6A). The spine morphometric analysis showed that neurons lacking spastin contained less mature spines (mushroom type), more immature spines (filamentous type) and overall fewer spines per dendritic length unit (Figure 3.6B).Taken together these results demonstrate that spastin depletion affects synapse formation.

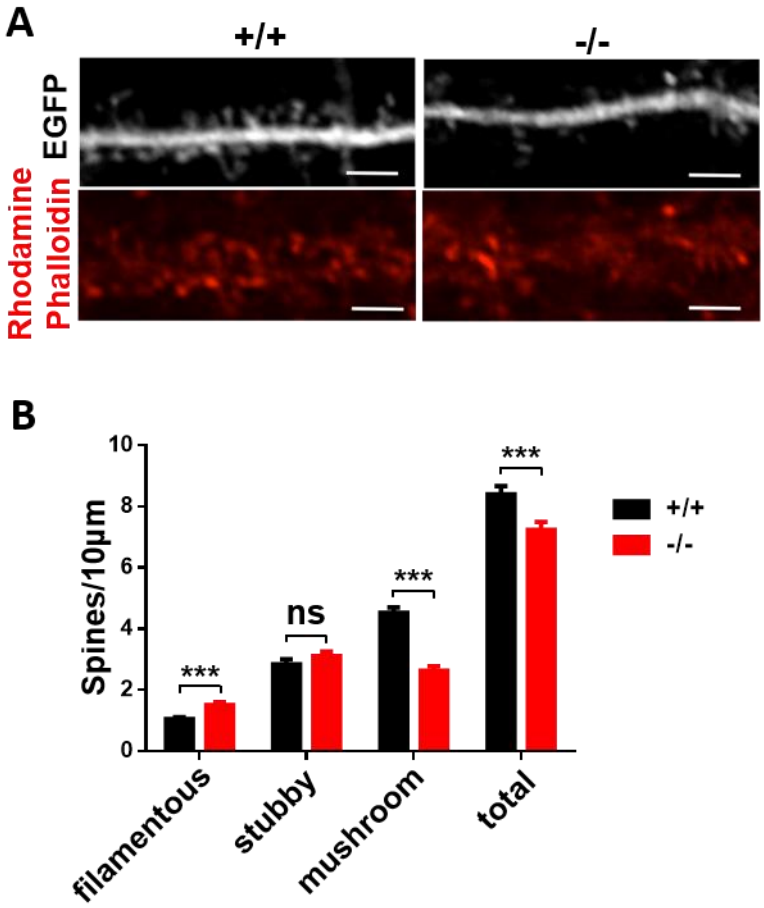

Figure 3.6: Spastin deficiency alters spine morphology. (A) Representative images of EGFP-transfected neurons at DIV10 derived from spastin (+/+) and (-/-) mice. Neurons at DIV18 were fixed and labeled with Rhodamine Phalloidin thus allowing the visualization of dendritic spines. (B) Spine morphometric analysis conducted in hippocampal neurons derived from spastin (+/+) and (-/-) mice. Number of analyzed neurons=30; Scale bar=2 µm. Data represent mean ± sem. Statistical significance was determined by Student´s t-test.

3.7 Minor perturbations in synaptic structure of spastin -/- neurons

To test whether the loss of spastin might impact the transport of synaptic vesicles towards the synaptic terminals, I performed an ultrastructural analysis of synapses from spastin (-/-) and (+/+) hippocampal neurons (Figure 3.7A). The quantifications showed decreased number of undocked synaptic vesicles, but normal number of docked vesicles in spastin (-/-) neurons. Additionally, spastin (-/-) neurons showed a small but significant reduction in synapses and normal active zone length (Figures 3.7B-G).

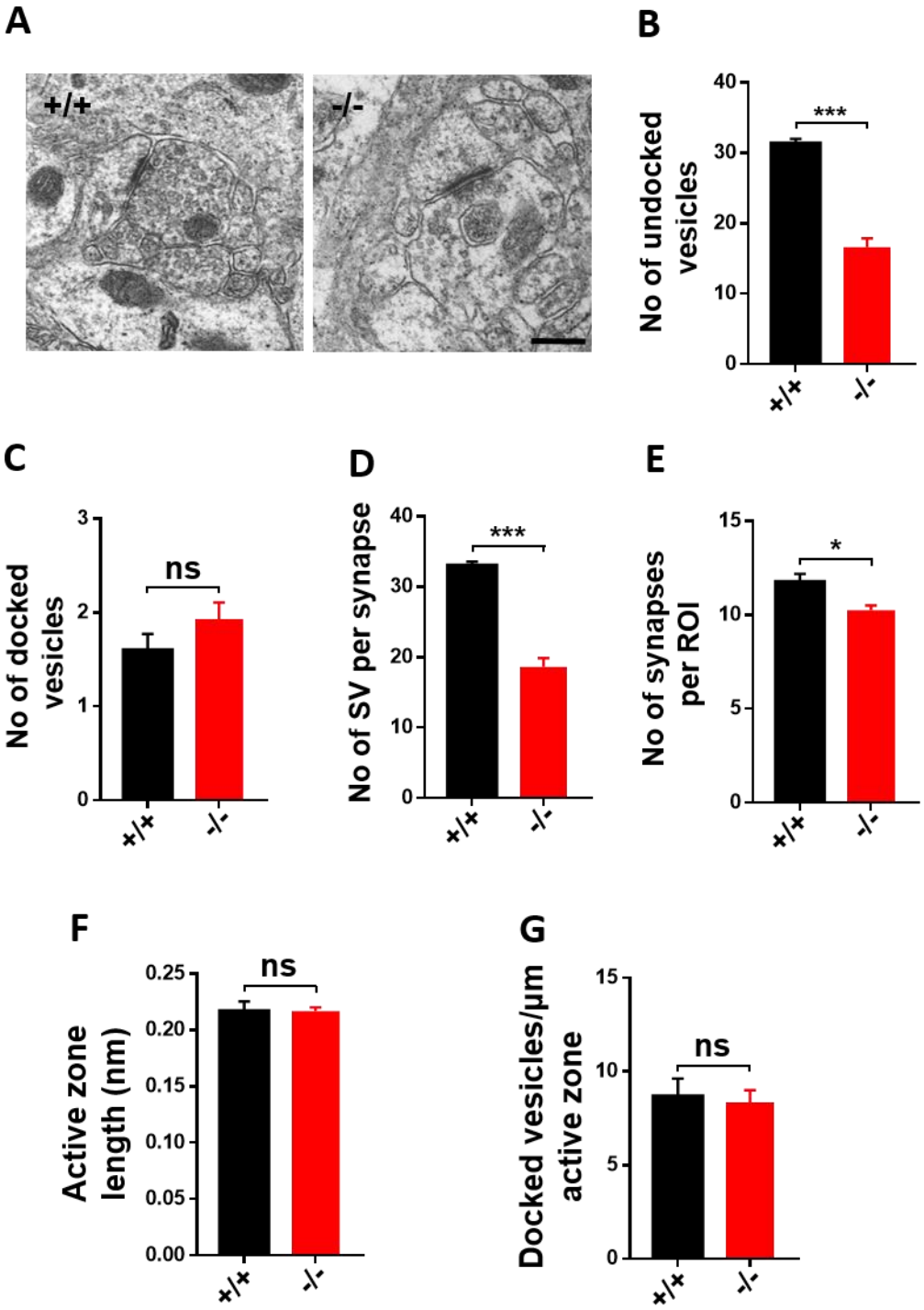

Figure 3.7: Altered distribution of synaptic vesicles in spastin-depleted neurons. (A) Representative electron micrographs of synapses in hippocampal CA1 region of wildtype (+/+) and spastin-depleted (-/-) mice. The density of undocked vesicles (B), docked vesicles (C), and number of synaptic vesicles (D) was quantified per synapse (D). Number of synapses per region of interest (ROI) (E), length of the active zone (F) and number of docked vesicles per active zone length (G) was quantified form 3 mice per genotype. Scale bar=300

nm. Statistical significance was determined by Student´s t-test. Data represented as mean ± sem.

3.8 Reduced surface expression of GluA2-containing AMPA receptors in spastin (-/-) neurons

Since reductions in spine density and morphology may also effect the density of neurotransmitter receptors at the plasma membrane, immunostainings of GluA2-containing AMPA receptors with an antibody against the extracellular N-terminal domain of GluA2 under non-permeabilized conditions were performed (Figure 3.8A). Spastin (-/-) knockout neurons showed a reduction in the total GluA2 fluorescence intensity (Figure 3.8B), number of GluA2 positive puncta (Figure 3.8C) and GluA2 puncta size when compared to wildtype (+/+) neurons (Figure 3.8D).

To test whether a reduction in GluA2 surface levels corresponds to changes in total receptor expression, western blot analysis was employed to compare total expression levels between spastin (+/+) and spastin (-/-) derived brain homogenates (Figure 3.8E). The total expression levels of GluA2-containing AMPA receptors in spastin (-/-) brain lysates were similar to that of the spastin (+/+) controls. However, the crude membrane-enriched fraction (P2) of hippocampal lysates derived from spastin (-/-)mice revealed a reduction of GluA2 expression levels compared to wildtype (+/+) derived fractions (Figure 3.8F and G).

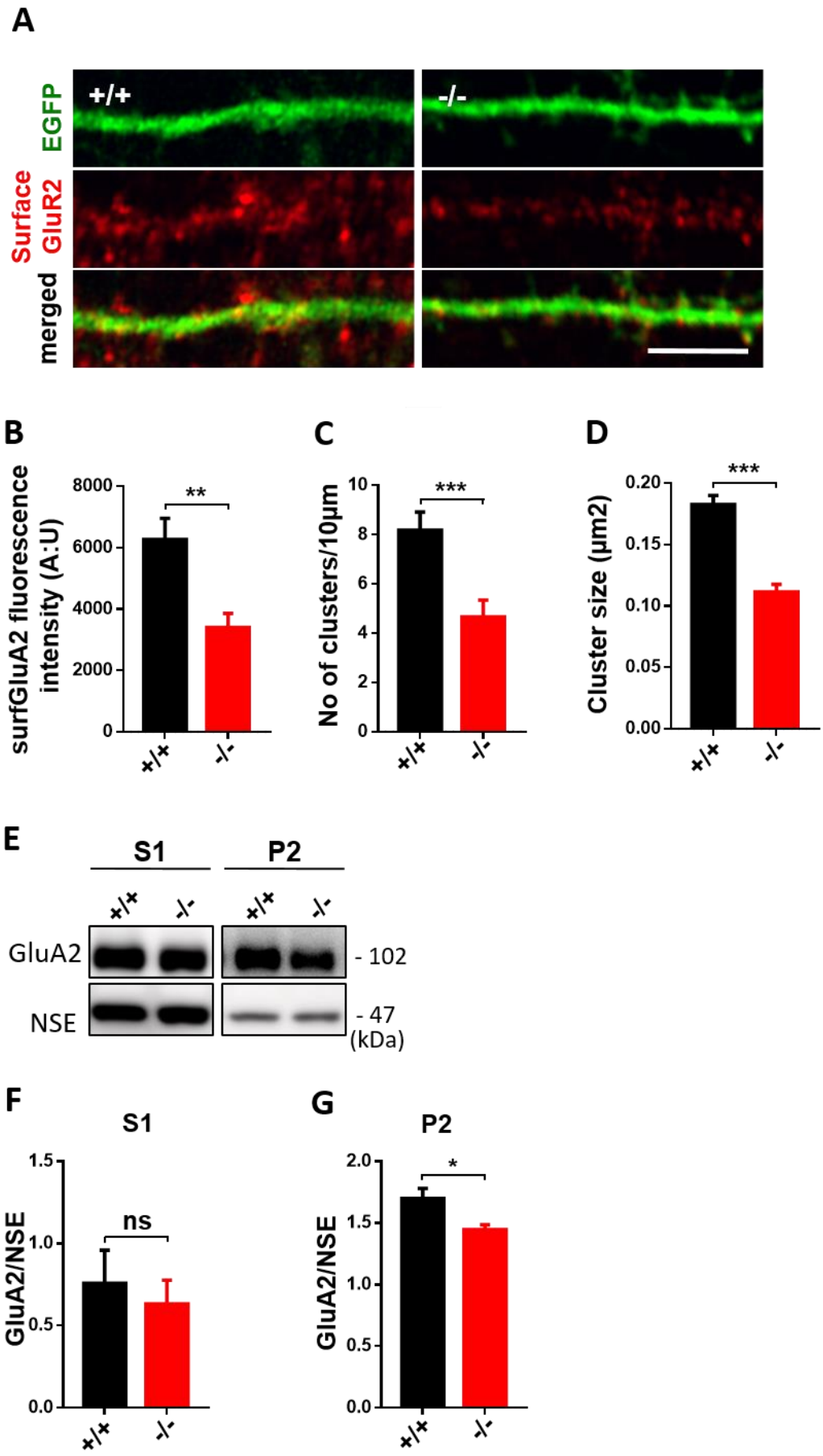
A
+/+
-/-
EGFP
Surface GluR2
merged
B
surfGluA2 fluorescence intensity (A:U)
8000
6000
4000
2000
0
**
+/+
-/-
C
No of clusters/10µm
10
8
6
4
2
0
***
+/+
-/-
D
Cluster size (µm2)
0.20
0.15
0.10
0.05
0.00
***
+/+
-/-
E
S1
P2
+/+
-/-
+/+
-/-
GluA2
NSE
- 102
- 47
(kDa)
F
S1
GluA2/NSE
1.5
1.0
0.5
0.0
ns
+/+
-/-
G
P2
GluA2/NSE
2.0
1.5
1.0
0.5
0.0
*
+/+
-/-

Figure 3.8: Spastin depletion alters cell surface localization of GluA2-containing AMPA receptors. (A) Immunostainings of endogenous expression of surface GluA2 in EGFP-transfected hippocampal neurons at DIV18. (B) Quantification of mean surface fluorescence intensity per area of dendrite. (C, D) Determination of the number and size of GluA2 clusters per 10 µm dendritic length. (E) Representative western blots showing the endogenous levels of GluA2 and NSE as loading control in supernatant (S1) and membrane-enriched fraction (P2) hippocampal homogenates after a differential centrifugation protocol. (F, G) Quantification of GluA2 levels in both protein fractions by western blot analysis. Number of neurons=35. Hippocampal homogenates from 4 mice per genotype. Scale bar=5 µm Statistical significance was determined by Student´s t-test. Data represented as mean ± sem**.**

3.9 Microtubule stability in neurons lacking spastin

Microtubule-severing enzymes, including spastin, have been shown to cut microtubules at distinct regions of the neuron I therefore aimed to analyze the stability of the microtubule cytoskeleton in mice lacking spastin.

Posttranslational modifications of tubulin are used as a read-out for turnover of microtubules. Therefore, the levels of tubulin polyglutamylation and detyrosination were used as markers for stable microtubules, and tubulin tyrosination as a marker for more dynamic microtubules (Figure 3.9C). Western blot analysis of hippocampal lysates showed that spastin (-/-) mice have increased levels of tubulin polyglutamylation. However there were no changes regarding detyrosinated and tyrosinated tubulin, nor in α-tubulin protein levels (Figure 3.9C). Changes in polyglutamylated tubulin levels were also confirmed with immunostainings of the hippocampus CA1 region using the same antibodies (Figure 3.9A).

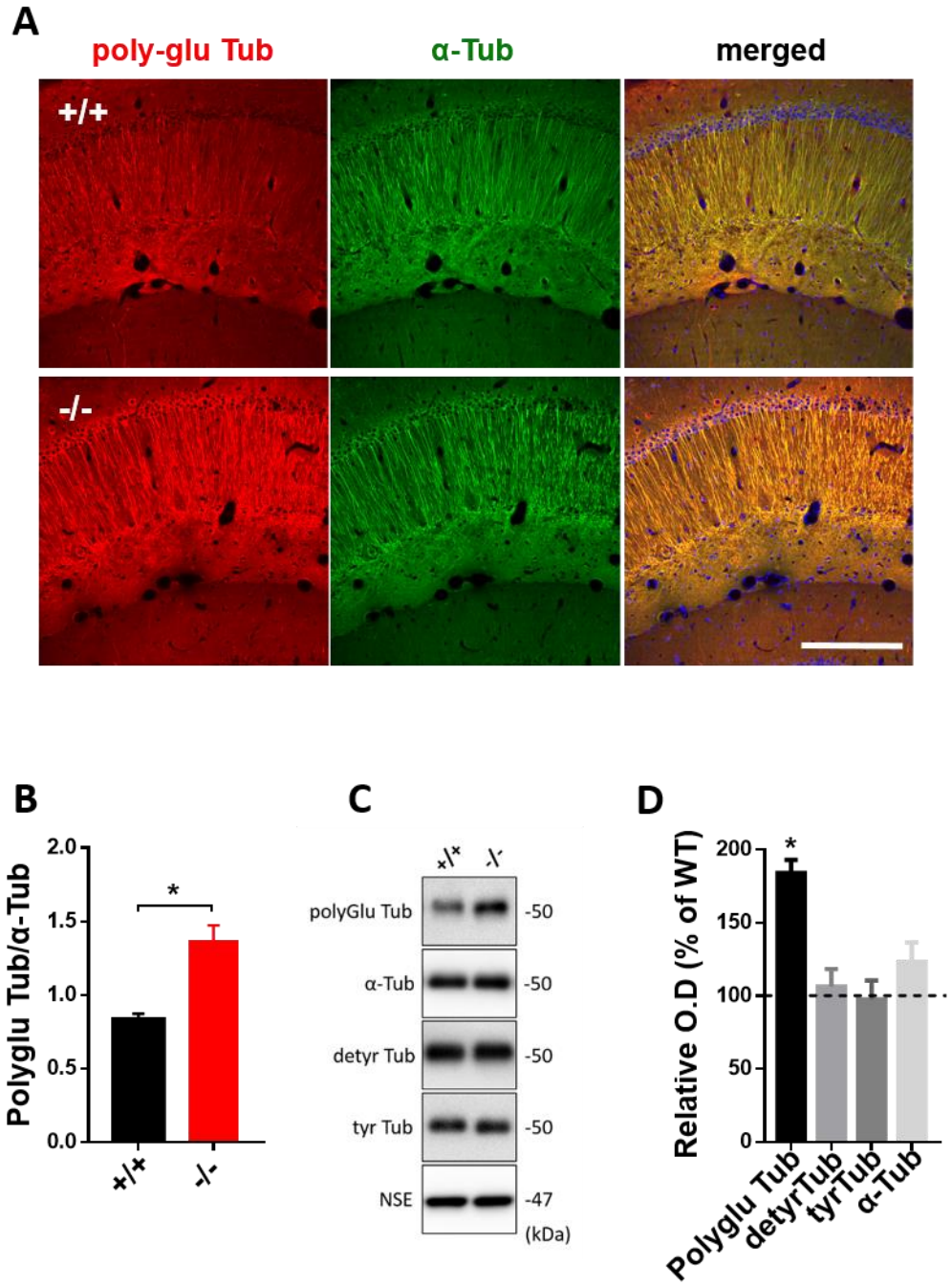

Figure 3.9: Spastin regulates microtubule stability. (A) Representative confocal images of polyglutamylated tubulin and α-tubulin in the CA1 region of the hippocampus of spastin knockout (-/-) and wildtype (+/+) littermates. (B) Quantification of the mean fluorescence intensity levels of polyglutamylated tubulin normalized to α-tubulin levels per ROI. (C,D) Representative western blot and corresponding quantifications of polyglutamylated, detyrosinated and tyrosinated tubulin normalized to α-tubulin levels in hippocampal homogenates from adult mice. Scale bar=200 μm. Statistical significance was determined by Student´s t-test. Data represented as mean ± sem.

3.10 Longer microtubules in neurons lacking spastin

Since the biochemical analysis indicated that microtubules in spastin (-/-) neurons were more stable compared to the wildtype (+/+) neurons, I performed further analyses by investigating the ultrastructure of the microtubule cytoskeleton in spastin (-/-) neurons.

Analysis of DIV14 hippocampal neurons revealed longer microtubules in spastin knockout (-/-) neurons. Furthermore, significantly shorter distances between adjacent microtubules indicated tighter microtubule packing in dendrites of (-/-) neurons (Figure 3.10A-D).

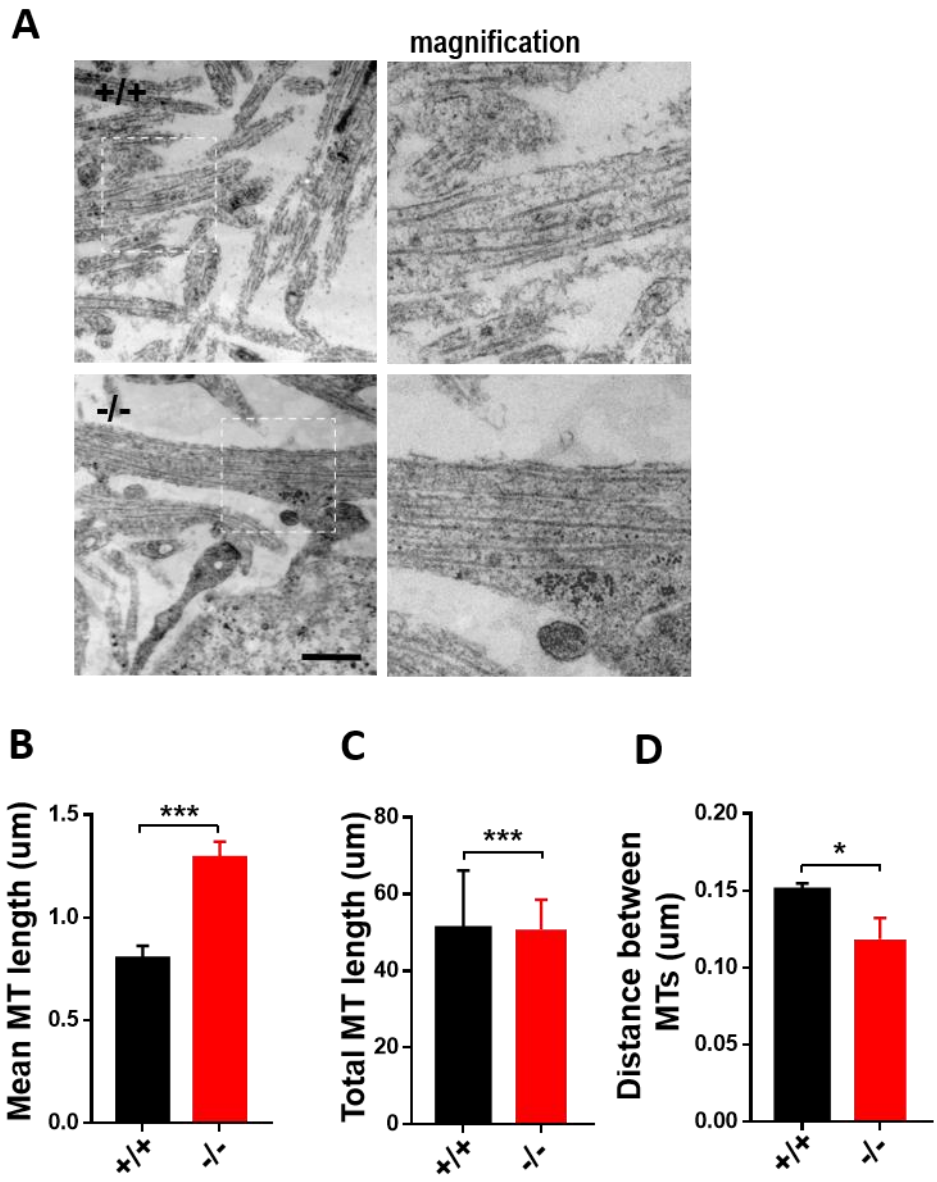

Figure 3.10: Ultrastructural analysis of microtubule cytoskeleton in spastin deficient (-/-) mice and their wildtype (+/+) littermates. (A) Representative electron micrographs of microtubules in DIV14 hippocampal neurons. The boxed regions are shown at higher magnification. (B-D) Quantification of the total microtubule length, the average microtubule length, and the distance between adjacent microtubule traces. Number of analyzed neurons per genotype: 45. Scale bar=300 nm. Statistical significance was determined by Student´s t-test. Data represented as mean ± sem.

3.11 Microtubule dynamics in neurons lacking spastin

To assess the role of spastin in microtubule dynamics, hippocampal neurons at DIV5 were transfected with EGFP-tagged microtubule plus-end-binding protein 3 (EB3), which specifically binds to the polymerizing microtubule plus-end and detaches from the growing +tip when the microtubules depolymerize (catastrophe event). Live imaging analysis showed mobile EGFP-EB3 comets appearing and growing (microtubule polymerization) and disappearing (microtubule depolymerization) (Figure 3.11A). In neurons lacking spastin, the growth rate of EB3 comets was similar to wildtype (+/+) neurons (Figure 3.11B), but the distance of microtubule growth was substantially longer (Figure 3.11C). In addition, the number of EB3 comets per dendritic length was significantly higher in spastin (-/-) compared with wildtype (+/+) neurons (Figure 3.11D).

Taken together, these data indicate that spastin influences microtubule growth by regulating microtubule polymerization/depolymerization rates.

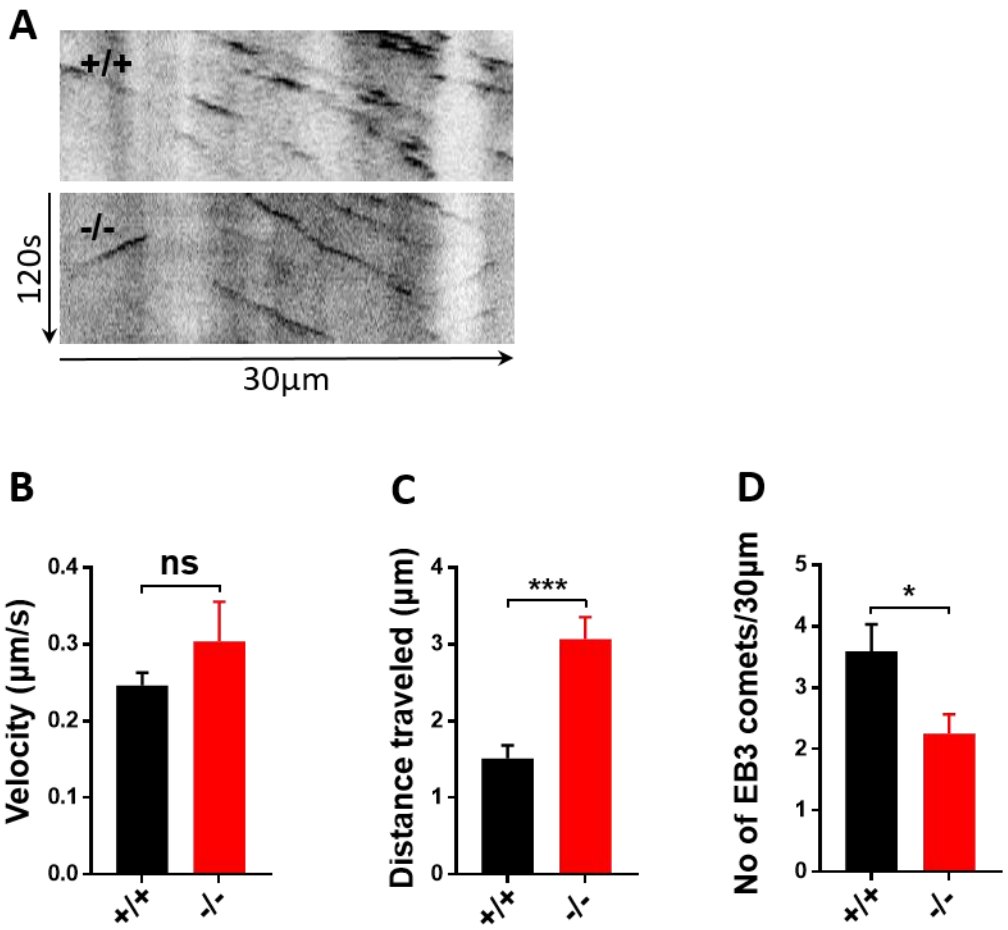

Figure 3.11: The microtubule-severing enzyme spastin regulates microtubule dynamics. (A) Live time-lapse imaging conducted in neurons transfected with the microtubule +tip binding EGFP-EB3 protei. The kymographs illustrate movement of EGFP-EB3 comets in dendrites prior to catastrophe. (B-D) Quantification of EGFP-EB3 comet velocity, run length, and number per unit length. Number of analyzed EGFP-EB3 comets: 55. Statistical significance was determined by Student´s t-test. Data represented as mean ± sem.

3.12 Altered GluA2-containing AMPA receptor transport in spastin (-/-) neurons

The reduction in GluA2 surface levels in spastin (-/-) neurons suggested that spastin depletion might impact the transport of GluA2-containing AMPA receptors along the microtubule cytoskeleton. To address this hypothesis, hippocampal neurons at DIV10 were transfected with mCherry-GluA2. . After 48 hours, the dynamics of mobile GluA2 particles in transfected neurons were analyzed using time-lapse imaging. The analysis revealed decreased velocity (Figure 3.12B), and shorter distances covered (Figure 3.12C) by GluA2

particles in spastin (-/-) neurons. These data indicate that the reduction in GluA2-containing AMPA receptor surface levels in spastin (-/-) neurons may be due to altered microtubule-based transport of the receptor.

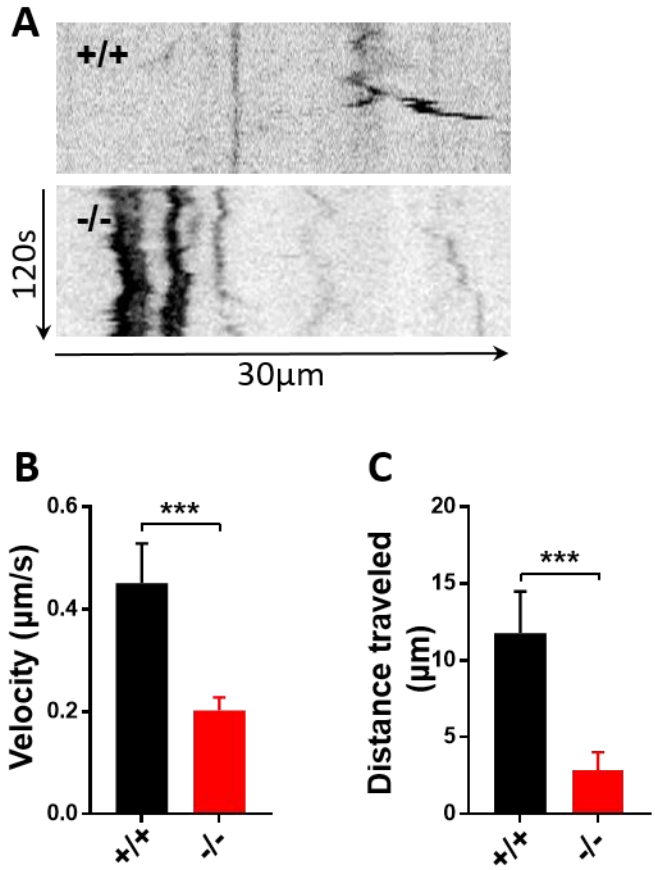

Figure 3.12. Visualization and analysis of mCherry-GluA2 particles by time-lapse imaging. (A) Kymograph depicts dendritic movement of mCherry-GluA2 over time. (B,C) The mean velocity and distance travelled by mCherry-GluA2 particles. Number of analyzed mCherry-GluA2 particles: spastin +/+ neurons =55 particles; spastin -/- neurons=60 particles. Statistical significance was determined by Student´s t-test. Data represented as mean ± sem.

3.13 Altered KIF5C motility in spastin (-/-) neurons

The kinesin motor KIF5C is known to facilitate microtubule-based GluA2-containing AMPA receptor transport. Therefore, I investigated whether the impaired motility of AMPA receptors in spastin (-/-) neurons may stem from changes in KIF5C-based transport.

Hippocampal neurons at DIV5 were transfected with KIF5C-pex-tomato. 48 hours later, KIF5C motility was analyzed using live cell imaging. Similar to the

observations of AMPA receptor motility, KIF5C-tomato-pex particles in spastin (-/-) neurons travelled slower (Figures 3.13A and B), and covered shorter distances (Figure 3.13C) compared with wildtype (+/+) control neurons.

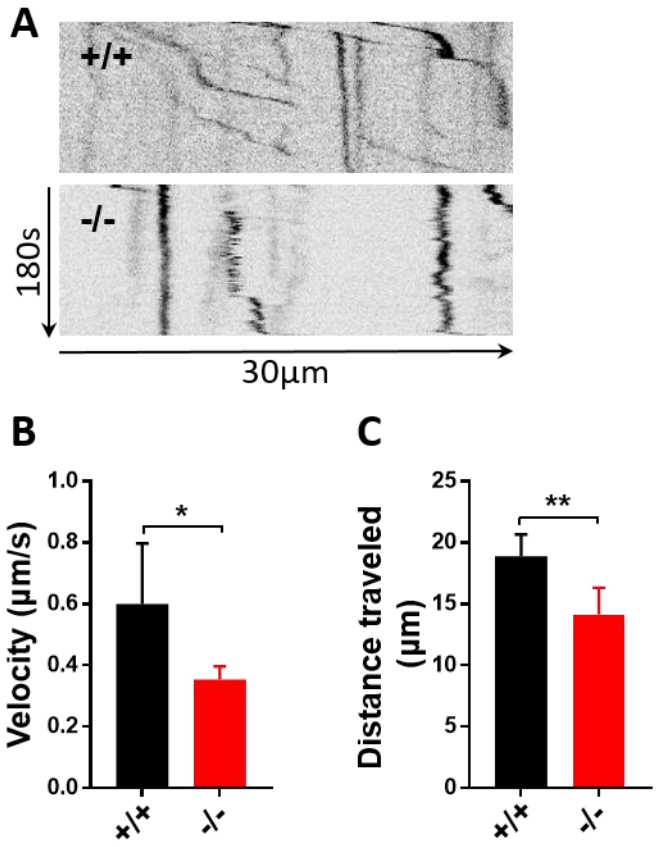

Figure 3.13: The effect of spastin deficiency on KIF5C motility in dendrites. (A) Kymographs illustrating KIF5C-tomato-pex particle mobility in dendrites of wildtype (+/+) and spastin knockout (-/-) neurons. (B) Quantification of velocity and run length of the KIF5C-tomato-pex particles in dendrites. Number of analyzed KIF5C particles: spastin +/+ neurons = 45 particles; spastin -/- neurons = 40 particles. Statistical significance was determined by Student´s t-test. Data represented as mean ± sem.

3.14 Altered mitochondria transport in dendrites from spastin (-/-) neurons

To investigate whether the impaired transport was specific to AMPA receptors, or whether changes in microtubule dynamics might alter general cargo transport, I also analyzed the transport of mitochondria. Hippocampal neurons at DIV7 were incubated with mitotracker, a dye that labels mitochondria in living cells. Following the incubation period, the cells were

subsequently analyzed using time-lapse imaging. I observed that the number of mitochondria within the soma appeared higher in spastin (-/-) neurons, suggesting that the accumulation of this organelle in this cellular compartment was possibly due to altered transport (Figure 3.14A).

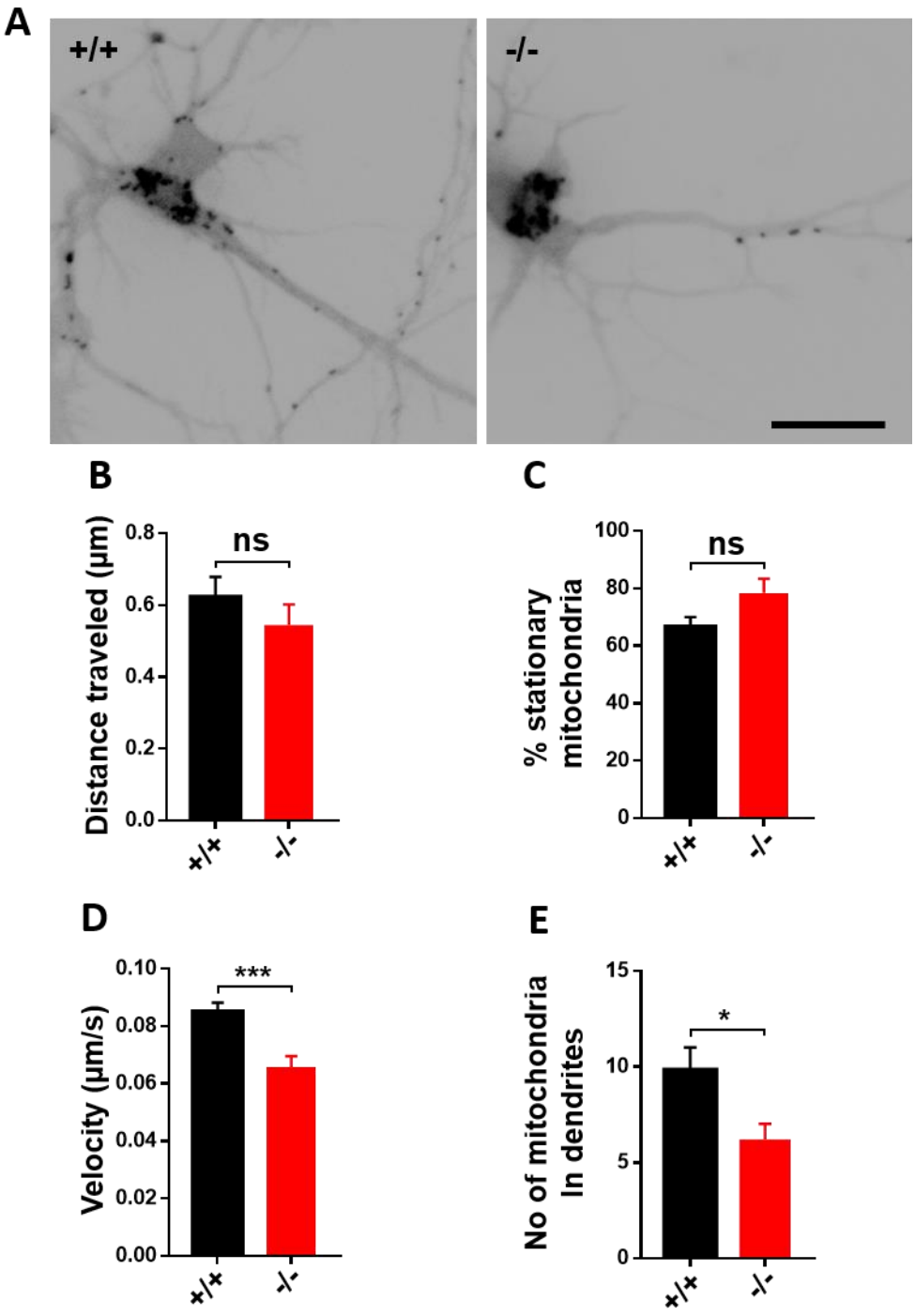

Figure 3.14: Altered intracellular transport of mitochondria in spastin (-/-) neurons. (A) Accumulation of mitochondria in the soma of spastin (-/-) neurons. Analysis of mitochondria movement revealed comparable distance traveled (B) but reduced velocity of mitochondria in spastin (-/-) neurons (C). Although the percentage of stationary mitochondria was similar (D), the number of mitochondria per dendritic length (E) was significantly reduced in spastin (-/-) neurons compared to wildtype (+/+) neurons. Number of analyzed mitochondria per genotype: spastin +/+ neurons =120 mitochondria; spastin -/- neurons =75 mitochondria. Scale=30 µm. Statistical significance was determined by Student´s t-test. Data represented as mean ± sem.

Analysis of mitochondria motility revealed no differences in distance traveled (Figure 3.14B), but a significant reduction in the velocity (Figure 3.14C) in spastin (-/-) neurons. No differences emerged with regard to the percentage of stationary mitochondria (Figure 3.14D), but a significant reduction in the number of dendritic mitochondria was seen in spastin (-/-) neurons (Figure 3.14E).

3.15 Synaptophysin transport is altered in spastin (-/-) neurons

Based on the reduction in the number of synaptic vesicles and corresponding decrease in synaptophysin levels in spastin (-/-) neurons, it is likely that in addition to altered postsynaptic transport, the transport of axonal cargo at the presynaptic compartment might be impaired. I addressed this possibility by transfecting neurons at DIV5 with eGFP-synaptophysin, and performed time-lapse imaging 24 hours later.

Indeed, synaptophysin clusters in spastin (-/-) neurons covered shorter distances but moved at similar velocity compared with wildtype (+/+) neurons (Figure 3.15A, B, C). The proportion of immobile particles was significantly higher in spastin (-/-) neurons (Figure 3.15D). Taken together, these data suggest that spastin malfunction impacts intracellular neuronal transport in both dendrites and axons.

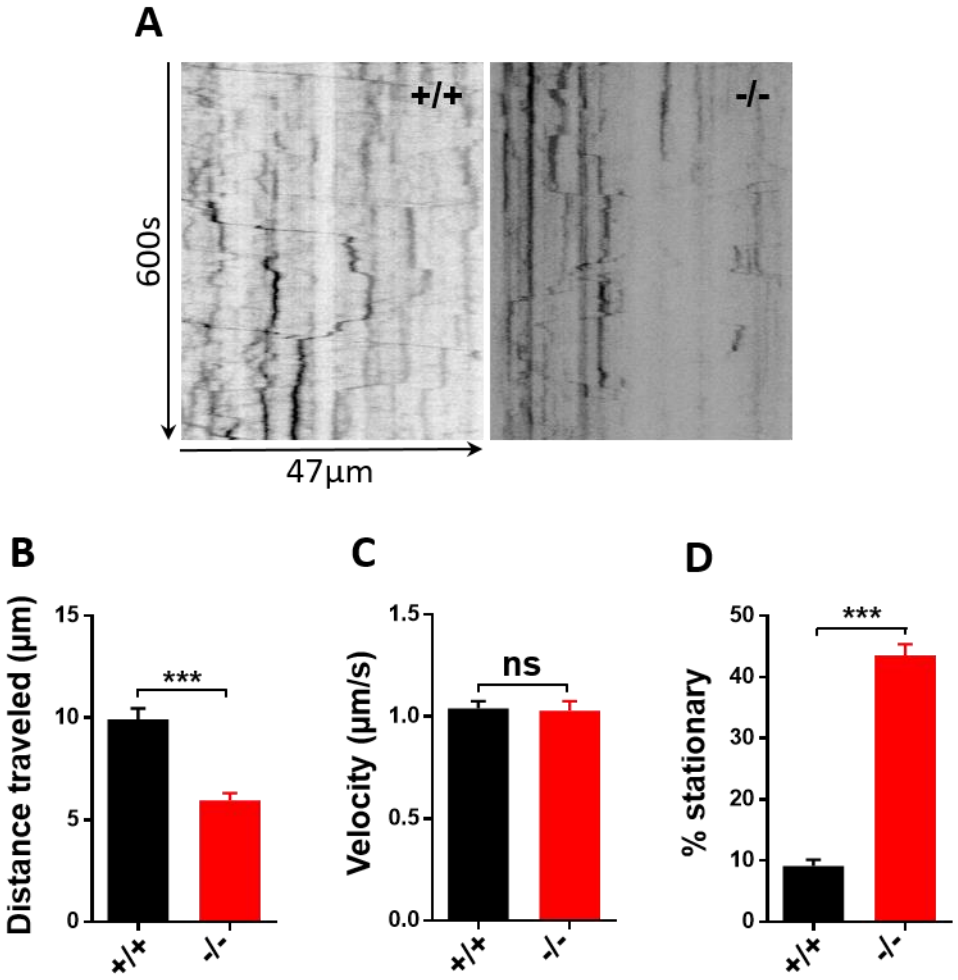

Figure 3.15: Altered axonal transport of synaptophysin in neurons lacking spastin. (A) Representative kymographs of eGFP-synaptophysin movement in wildtype (+/+) and spastin knockout (-/-) neurons. (B) Quantification of distance travelled, velocity of the eGFP-synaptophysin (C) and percentage of stationary particles (D) in axons of wildtype (+/+) and spastin knockout (-/-) neurons. Number of analyzed synaptophysin particles per genotype: spastin (+/+) = 152 particles and spastin (-/-) = 130 particles. Statistical significance was determined by Student´s t-test. Data represented as mean ± sem.

3.16 Taxol-induced stability of microtubules decreases surface GluA2-containing AMPA receptor levels

One hypothesis is that in the absence of spastin, microtubules might be hyperstabilized, leading to impaired neurotransmitter receptor transport. To address this, hippocampal neurons were treated at DIV13 with the microtubule-stabilizing drug taxol for 20 hours using 2 different concentrations (10 nM and 100 nM) (Figure 3.15A). As described in the literature, 10 nM

taxol enhances the polymerization of tubulin, whereas 100 nM taxol has a stabilizing effect on microtubules.

100 nM taxol-treated neurons showed decreased surface GluA2 fluorescence intensity (Figure 3.15B), indicating fewer GluA2 clusters at the cell surface (Figure 3.15C), and smaller clusters per dendritic length (Figure 3.15D). These data matches the data obtained from spastin (-/-) hippocampal neurons, thus highlighting the importance of microtubule dynamics/stability on microtubule-dependent transport processes.

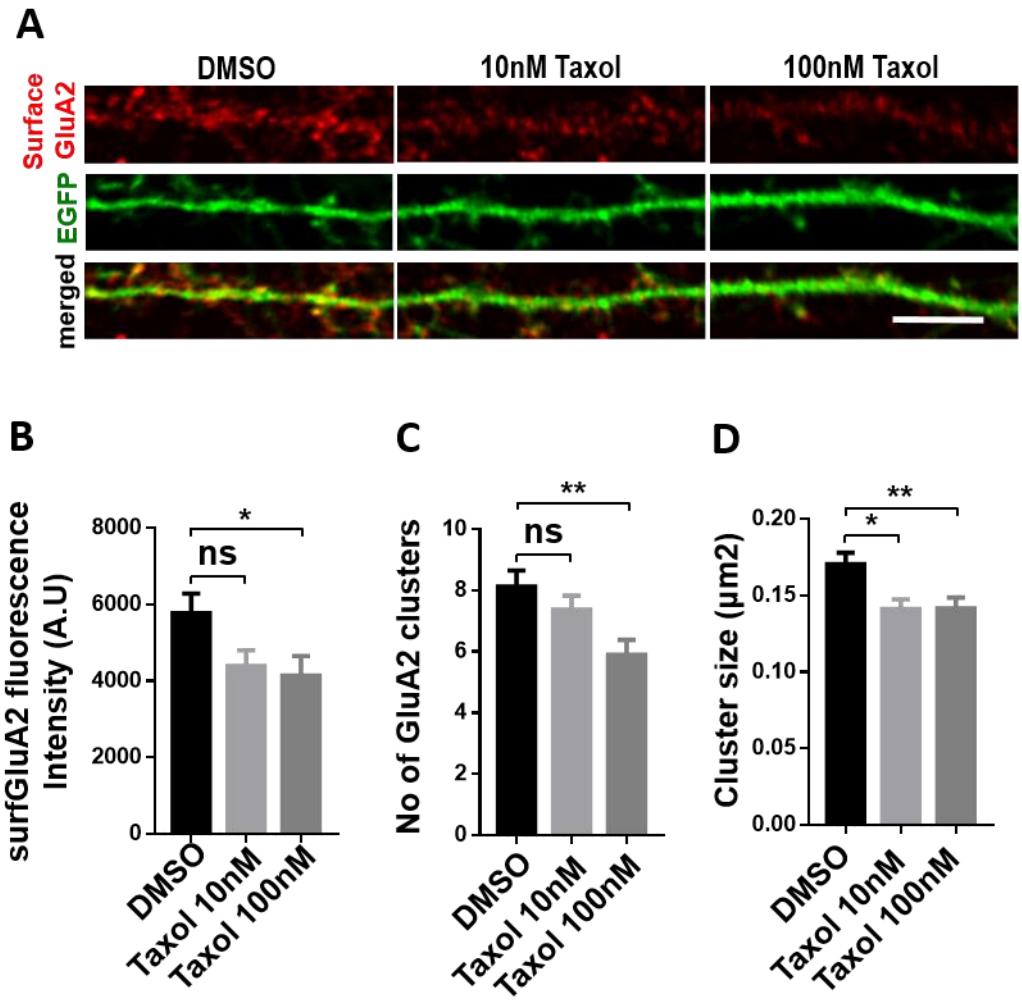

Figure 3.16: Reduced surface GluA2 levels upon treatment with 100 nM taxol. (A) Representative surface immunostainings using an antibody against the extracellular domain of GluA2. Hippocampal neurons were treated with vehicle (DMSO), 10 nM taxol and 100 nM taxol. (B) The highest concentration of taxol reduced the surface expression as well as the number of GluA2 clusters (C). Both concentrations of taxol led to a reduction in GuA2 cluster size (D). Scale is 5 µm. Statistical significance was determined by one-way ANOVA followed by pairwise comparisons. Data represented as mean ± sem.

Chapter 4

Discussion

4. Discussion

4.1 Characterization of spastin knockout mouse

Two mouse models carrying spastin mutations have been generated in the past years in order to understand the pathophysiological mechanisms that underlie hereditary spastic paraplegia [33, 68].

Evaluation of these two mouse models have furthered our understanding of changes that occur at the molecular and tissue levels. Moreover, they are important tools for development of future therapeutic approaches. Despite this, previously generated mouse models have been limited, either due to a mild phenotype, or because they lack some of the characteristic hallmarks of hereditary spastic paraplegia (HSP).

In this research work, I characterized a recently generated spastin knockout mouse model with the aim of understanding the cellular, pathophysiological, and behavioral alterations found in HSP patients [120].

Adult male and female spastin knockout mice exhibited normal body weight and, no gross changes in brain anatomy as related to normal layering of the cortex and normal hippocampal morphology. The microtubule-severing enzyme spastin is reported to direct axon pruning at the neuromuscular junction during the early stages of neurodevelopment [120] . Moreover, it has been recently associated with lipid metabolism: namely lipid droplet generation and controlling triacylglycerol levels [67]. As the correct innervation of muscles is important for normal motor performance and maintenance of total muscle volume/mass, a reduction in the body weight of spastin knockout mice, either due to loss of muscle mass or defective lipid storage was expected. However, such changes were not evident in the spastin knockout mice investigated in this thesis. Since the malfunction of katanin p60 subunit A-like 1 (KATNAL1), another microtubule-severing enzyme, has been linked to impaired neuronal proliferation and migration leading to abnormal layering of the cortex, I also expected similar changes in brain morphology of spastin knockout mice [122] . However, this was not the case, prompting me to suggest that spastin and katnal1 play different roles in the development and maintenance of these brain structures, or, that there are

compensatory mechanisms by other microtubule-severing enzymes that are sufficient to maintain the normal anatomy of the brain.

In order to generate mice for biochemical, live-cell imaging and behavioral experiments, matings between spastin heterozygous mice were set up. Interestingly, spastin homozygous matings did not generate offspring, which might be due to defective meiosis since spastin in reported to be important for spindle pole organization and cytokinesis. Alternatively, this may stem from defective sperm cell movement, as the sperm cell flagellum is composed of microtubules [123]. This issue was however not addressed further in this work.

4.2 Implications of spastin depletion on motor neuron function

HSP is characterized by a progressive retrograde axonal degeneration of nerve fibers from the ascending and descending tracts of the spinal cord with virtually no effect on the peripheral nervous system. Studies from the available mouse models of *SPAST* -related HSP describe axonal swellings, impaired intracellular transport, and accumulation of different motor protein cargoes such as organelles and cytoskeleton components. In addition, the studies report age-dependent progressive impairments in motor neuron performance [33].

In order to validate the recently generated mouse model, I assessed the performance of spastin homozygous, heterozygous knockouts, and their wild type littermates in several behavioral motor assays, which include: pole test, grip strength test, horizontal grid test and rotarod. In line with previously described motor deficits in human patients and mouse models, mice lacking spastin showed poorer performance in motor function, which include: the 14-month old spastin mutant (+/- and -/-) mice took longer to make a turn on the pole test compared to their WT littermates, suggesting a defect in movement coordination. Besides coordination, the performance in this assay depends on muscle strength. To further assess muscle strength, I tested the animals in the grip strength test. 14-month old spastin mutant (+/- and -/-) mice showed

decreased muscle strength in this motor test. These data are in line with the reduced muscle strength and increased muscle tonus of the legs in HSP patients [124]. When the same mutant mice were tested on the horizontal grid test, which assesses both coordination and muscle strength, they spent less time hanging onto the metallic grid compared to WT mice. Interestingly, when the same motor behavioral tests were performed in younger mice (8 months old), no motor phenotype was observed. Finally, spastin knockout (-/-), heterozygous (+/-) and wild type (+/+) mice were tested on the rotarod, a behavioral motor task that requires proper coordination, muscle strength, and endurance in order to maintain balance on a rod rotating at increasingly higher speeds. As expected, mutant (+/- and -/-) mice spent less time on the rotating rod when compared to wild type littermates, but this phenotype was only present in older mice (14 months of age).

In a different mouse model that contains a splice site mutation in spastin (c.1092 + 2T>G), Kasher and colleagues showed that axonal swellings in the spinal cord were more frequent in aged mice. They also described gait abnormalities in heterozygous and homozygous mice for the spastin mutation at the age of 12 months [68].
Taken together, these data suggest that spastin is required for normal motor performance by regulating both coordination and muscle strength. It is noteworthy to mention that this impairment is age-dependent and it resembles the progressive degeneration of the long fibers of the ascending and descending tracts in HSP patients.

4.3 Impact of spastin depletion on cognitive function

Besides the progressive mobility problems, the co-occurrence of mental retardation, progressive cognitive impairment and dementia over the ageing process has been reported in HSP patients with mutations in the *SPAST* gene [24, 25]. The neuropathological assessment of the described cases of patients with cognitive deficits revealed close similarities to the sporadic form of Amyotrophic Lateral Sclerosis (ALS). Both sporadic ALS and HSP patients have increased numbers of α-synuclein, ubiquitin-positive and tau-negative

inclusions, as well as abnormal dendritic morphology in postmortem tissue. Some HSP patients carrying mutations in the *SPAST* gene displayed cerebellar alterations followed by mental retardation. However, there are documented cases of impaired cognitive function without a cerebellar phenotype.Onset of the first symptoms associated with altered cognitive function has been described in *SPAST* -related HSP patients at different ages: a childhood onset in patients whose mental retardation causes social dependency, during adulthood or after the age of 60 years [19].

Based on the cumulative studies showing impaired memory function in SPAST-related patients, I examined cognitive function in spastin mutant mice using several behavioral paradigms. I investigated spatial working memory, which requires proper functioning of the hippocampus and prefrontal cortex; brain regions that are frequently affected in several disorders associated with defective cognitive function such as Alzheimer´s disease [125].
In this work, I reported for the first time impairments in spontaneous alternation in spastin mutant (+/- and -/-) mice when tested in the Y-maze. Interestingly, this behavioral phenotype was only present at the age of 14 months, suggesting that there may be an age-related progressive cognitive decline in mice lacking spastin. It is noteworthy that the decreased alternation was not due to decreased motor activity since the mutants showed comparable arm entries (activity) to the wildtype littermates. Thus, decreased alternation may be due to deficits in cognitive function.

An alternative test that can be used to study alternation behavior is the confined T-maze alternation test. Although the level of complexity of the maze remains the same (3 arms), the possibility of restricting the mouse to a specific starting arm makes the association of a previously visited arm versus an unvisited arm easier to interpret. Similar to the phenotype observed in the Y-maze, spastin mutant mice (+/- and -/-) showed normal alternation at 8 months, which is lost at the age of 14 months in comparison to wildtype littermates.

4.4 Impact of a lack of spastin on contextual fear learning

It is known that the brain receives various inputs from the environment, and conveys them to the hippocampus (namely to the ventral hippocampus) to generate a unified contextual representation that is stored as a memory and can be recalled later [126]. Contextual fear learning is a form of associative learning present in all mammalians and is of crucial importance for the survival of the animal. When a certain context (e.g. open spaces) is associated with a life-threatening situation or adverse stimulus (e.g. pain), it rapidly elicits a fear response and long lasting memories. This form of learning can be studied in the laboratory using the hippocampal-dependent contextual fear conditioning paradigm. Here, a neutral training context [Conditioned stimulus (CS)] is paired with an aversive foot shock stimulus [unconditioned stimulus (US)]. The animal learns to associate the CS with the US such that when it is returned to the context in the absence of the shock, it demonstrates a fear response [conditioned response (CR)]. The CR parameter of interest in mice is freezing behavior. Freezing or absence of all visible motion, except for respiration, is a common innate fear response described in animals challenged by a potential treat.

In order to study the impact of the lack of spastin on fear learning over the ageing process, spastin knockout (-/-), heterozygous (+/-) and their wild type littermates (+/+) at the age of 8 months and 14 months were tested for the formation and retrieval of contextual fear memory. .

Data from the contextual fear conditioning training showed that in both cohorts (8 months and 14 months) all the mice learned to associate a specific context (context A) with the unconditioned stimulus (foot shock) as seen by increased freezing after receiving the foot shock. This suggests that spastin is not involved in the mechanisms underlying contextual fear learning. Contextual memory was tested one day after acquisition by re-introducing the mice to the context. Spastin mutant mice (+/- and -/-) spent less time freezing compared to their wild type littermates (+/+) at the age of 14 months. These data suggest that spastin is involved in the biological mechanisms underlying the recall of fear memory. Interestingly, the same phenotype was not observed in spastin mutant mice at the age of 8 months. In order to determine whether

the elicited fear response (freezing time) was specific to the training contextual, the mice were placed into a completely new context (context B) without receiving any foot shock. Spastin mutant mice (+/- and -/-) showed normal freezing levels at the age of 8 and 14 months.

These results are in line with published data on several behavioral deficits described in tau knockout mouse models. Tau is a microtubule-associated protein that stabilizes microtubules and is predominantly found in the axon where it regulates the motor-driven intracellular transport [127].

Evaluation of mice lacking tau showed that only aged mice (one-year-old mice) displayed behavioral alterations. These mice exhibit motor deficits that consist of muscle weakness, impaired coordination in the rotarod test, and hyperactivity when exposed to novel contexts/environments. Additionally, they exhibit impairments in fear conditioning. One possible explanation for age-dependent deficits might be due to loss of compensatory mechanisms by other microtubule associated proteins, such as Map1A. In fact, Map1A levels increase during embryonic development, but decrease upon brain maturation [128] Based on the behavioral data from tau knockout mice, one could hypothesize that compensatory mechanisms may occur during early development and in early adulthood of spastin mutant mice. Later on, such compensation may be lost or incomplete.

The extinction of contextual fear memory was also assessed in both cohorts by re-introducing the animals to context A (conditioning box) for 4 consecutive days. At the age of 8 months, WT mice re-learned that the context was no longer paired with an adverse stimulus (foot shock) and therefore decreased their freezing response. By contrast, spastin homozygous (-/-) and spastin heterozygous (+/-) knockout mice showed unchanged freezing responses across the four days of testing. These data provide evidence that spastin modulates the processing of contextual information in the hippocampus.

Studies have shown a biphasic shift in the stability of microtubules during fear conditioning. During the acquisition of fear, there is an increase in the labile fraction of microtubules in the hippocampus in order to cope with these initial plastic changes. Later on, during the consolidation of the acquired memories, there is an increase in the stable population of microtubules. As previously

described, spastin is involved in the generation of new microtubule fragments from pre-existing microtubules. These newly generated microtubules can be transported to new cellular compartments or growing branches in order to modify the final neuronal structure/morphology. Since learning requires extensive remodeling of the microtubule cytoskeleton, the lack of spastin, one of the major microtubule severing enzymes in the neuron, may have an impact on the intracellular mechanisms underlying cognitive function [104, 129].

4.5 Role of spastin in synapse formation and maintenance

The role of the microtubule cytoskeleton in axons and dendrites has been extensively described. By contrast, little is known about the function of the microtubule cytoskeleton during synapse formation (synaptogenesis) and maintenance.

Some studies have reported that the *D. Melanogaster* spastin-variant, a microtubule-severing enzyme, regulates the stability of microtubules in synapses and is present in the pre-synaptic terminal. The most studied synapse in flies, the glutamatergic neuromuscular junction, displayed morphological and functional alterations due to spastin depletion. Depletion of spastin through interference RNA decreased the synaptic area, impaired synaptic transmission and increased the amount of stable microtubules at the presynaptic bouton [130].

In this work, I showed that lack of spastin has an impact on the organization of the synapse in hippocampal neurons. Spastin knockout mice (-/-) had fewer undocked vesicles in the presynaptic terminals of CA1 synapses and fewer CA1 synapses in comparison to wild type mice. Protein analysis by western blotting also showed reduced levels of synaptophysin in hippocampal neurons lacking spastin suggesting that spastin is also important for the recruitment of presynaptic components.

Altogether, these data suggest that spastin is important for the proper organization of the presynaptic terminal.

Recent studies using live cell imaging have reported transient entries of microtubules into spines. The invasion of spines by microtubules was more

frequent upon induced neuronal activity. One possibility is that microtubule invasions may be alternative mechanism of delivery of cargoes transported along the microtubules into the spines [131].

A detailed analysis of the spine morphometry in cultured hippocampal neurons isolated from spastin knockout mice (-/-) showed that they had fewer mature mushroom-shaped spines, , but more immature thin- and filamentous-like spines. Overall, there was a reduced number of spines. PSD95, a component of the postsynaptic density, was also reduced in the membrane-enriched fraction following differential centrifugation of hippocampal lysates from spastin knockout mice. These data were also corroborated by fewer PSD95-positive puncta in hippocampal neurons lacking spastin.

Interestingly, another family member of the microtubule severing proteins, katnal1 (Katanin Catalytic Subunit A1 Like 1), has been associated with intellectual disability and schizophrenia. A mouse model bearing a mutation causing loss of function of *Katnal1* showed impaired learning and memory, among other phenotypic alterations. A detailed analysis of Golgi stained cortical neurons also revealed altered neuronal morphometry, decreased length and width of the axon, increased area of the soma and decreased number of synaptic spines [122].

Since I observed changes in both presynaptic and postsynaptic sites in spastin knockout neurons, a quantification of the number of excitatory synapses was performed. As expected, hippocampal neurons from spastin knockout mice had fewer excitatory synapses per dendritic length.

Altogether, these data suggest that spastin is important for synapse formation and maintenance by severing of microtubules; the dynamic scaffolds for concentrating proteins at the presynaptic and postsynaptic sites. The changes in the synapses of hippocampal neurons might account for the cognitive phenotypes seen in spastin knockout mice in this study.

4.6 Impact of microtubule deletion on microtubule dynamics

In order to examine the impact of spastin deletion on the microtubule cytoskeleton, I performed electron micrograph ultrastructural analysis of microtubules in spastin knockout (-/-) and WT neurons. Dendrites of

hippocampal neurons lacking spastin showed longer and more tightly bundled microtubules compared to wild type neurons, with no change in the total length of microtubules. These observations are in line with the described function of spastin as a microtubule-severing enzyme. When spastin is absent, the microtubule breakdown or severing is incomplete, leading to longer microtubules and further compaction, which is associated with more stable microtubules.

It is also reported that the most stable and persistent population of microtubules are a frequent substrate for posttranslational modifications such as polyglutamylation and detyrosination.

I showed by western blot analysis and immunostainings that the tubulin polyglutamylation levels were increased in hippocampal neurons from spastin knockout mice compared to wild types. However, the levels of tubulin detyrosination, tubulin tyrosination and total tubulin levels remained unchanged.

Cumulative evidence in recent years suggests that posttranslational modifications of microtubules can serve as cues to guide motor proteins; affecting not only motor protein activity but also the directionality of transport. Polyglutamylation, the most frequent posttranslational modification of tubulin in neurons, is known to regulate the binding of KIF5 to microtubules. Side chains of up to three glutamate units enhance the binding of this motor protein to microtubules. However in side chains that contain more than 7 glutamate units, the binding of KIF5 is inhibited. (see chapter 1).

Overall, these data indicate that the loss spastin leads to an overall stabilization of the microtubule cytoskeleton. Due to incomplete severing of microtubules, they grow more and have a longer lifetime. These long-lived persistent microtubules can then undergo posttranslational modifications such as polyglutamylation. If this is the case, one would expect a reduction in microtubule dynamics in spastin knockout neurons.

Microtubules have been described as highly dynamic structures undergoing stochastic episodes of growth (polymerization) or catastrophe (depolymerization). When microtubules undergo a phase of growth, members of the microtubule-plus-end-binding protein family, such as EB3, bind to the growing tip. When the microtubule undergoes an episode of depolymerization,

EB3 falls off the growing tip. By investigating the binding and detachment of EB3, one can determine the dynamics of microtubules in cultured hippocampal neurons.

As expected, hippocampal neurons from spastin knockout mice had fewer EB3 comets per dendritic length, and travelled longer distances compared to wild type neurons. These results might be explained by the absence of severing activity by spastin. Since microtubules can no longer be severed by spastin, this leads to the generation of fewer microtubule fragments and thus, fewer available growing tips to which the EB3 can bind.

Interestingly, there are reports that microtubule plus-end binding proteins (+TIPs) are involved in the initiation of intracellular transport in the neuron. Moughamian *et al.* showed that plus-end-binding proteins EB1 and EB3, together with cytoplasmatic linker protein-170 (CLIP-170), bind to dynamic microtubules and then recruit dynactin. The interaction between dynactin and dynein facilitates the formation of the complex cargo-motor protein, which is an important step for the initiation of retrograde transport mediated by dynein [132].

These data prompted me to hypothesize that in the absence of spastin, fewer microtubules are severed, generating fewer growing tips and less binding of EB3. Since these proteins are important for the recruitment of motor proteins to the growing tip and the initiation of the transport, this would mean less loading capability by motor proteins, such as kinesins, leading to altered intracellular transport.

4.7 Microtubule stabilization affects the surface distribution of AMPA receptors

To investigate the impact of microtubule stabilization on the surface distribution of GluA2-containing AMPA receptors, hippocampal neurons were treated with the microtubule stabilizing drug, taxol. Taxol is a commonly used drug in the treatment of cancer due to its ability to block the cell cycle at G1 and M phase through stabilization of the microtubule cytoskeleton. This drug binds with high affinity to β-tubulin and stabilizes the αβ-heterodimers bound to GTP; promoting microtubule polymerization at the plus end and inhibiting microtubule depolymerization at the minus end [133, 134].

In addition to the stabilization of the protofilament, taxol also increases the bundling among the protofilaments, which make up a microtubule, resulting in more compact and stable microtubule bundles. Interestingly, the finding of more bundled microtubules was also shownin hippocampal neurons derived from spastin-depleted mice in my research project.

Hippocampal neurons treated with 10nM taxol did not appear to be significantly different from wild type neurons, except with regard to the cluster size of AMPA receptors. One possible explanation may be that at this concentration of taxol, the polymerization of microtubules is enhanced so the microtubule dynamics is not completely blocked [135].

However, a higher concentration of taxol (100nM) reduced the levels of AMPA receptors at the plasma membrane. This indicated that the hyperstabilization of microtubules alone is sufficient to impair the distribution of these receptors.

The effects of microtubule stabilization induced by taxol on the mechanisms of neuronal transport has been investigated. For example, Goshima and colleagues documented reduced retrograde and anterograde transport of chloro-methylbenzamido dialkylcarbocyanine (CM-DiI)-labeled organelles in chick DRG neurons treated with taxol at clinical doses (1, 10 and 100nM). Theiss and *et al.* also observed accumulation of microtubules in axons and decreased anterograde transport of horseradish (HPR) peroxidase in chick DRG neuron upon treatment with 10µM taxol [136, 137].

Another study by Hammond et al. has shown taxol-induced posttranslational modifications of tubulin (detyrosination, acetylation and polyglutamylation) and reduced affinity of the motor protein KIF5 to microtubules [138].

In line with data from the surface distribution of AMPA receptors in the absence of spastin, my data suggest that increased stabilization of microtubules may interfere with the mechanisms underlying transport and distribution of cargoes in the neuron.

In summary, the pharmacological manipulation of microtubule cytoskeleton stability through taxol, corroborate the observations in neurons lacking spastin: an increased stabilization of microtubules, less dynamic microtubule cytoskeleton, and impaired intracellular transport leading to an altered distribution of AMPA receptors. An alternative explanation for the impaired transport observed in this thesis work might be the reduced binding of tau to

microtubules or conformational alterations of the microtubule structure that could affect the binding of motor proteins to the microtubules.

4.8 Regulation of microtubule-dependent intracellular transport by spastin

The polar morphology of neuronal cells requires the transport of a myriad of cargoes; over long distances from the soma to the periphery and also from the periphery back to the soma.

Intracellular transport is a highly regulated process and mobilizes a concerted action by several molecules. This involves motor proteins, adaptor proteins, microtubule associated proteins, microtubule-severing enzymes and a heterogeneous microtubule population that exists due to the numerous tubulin isotypes, which can undergo different posttranslational modifications.

In this study, the surface distribution of the GluA2-containing AMPA receptors in hippocampal neurons lacking spastin was investigated.

Since I observed a reduction in the number of excitatory synapses, which contain predominantly glutamate receptors, I hypothesized that the surface distribution of this family of receptors would be altered in neurons lacking spastin. Indeed, the number of GluA2-containing AMPA receptors at the plasma membrane was significantly reduced in spastin knockout neurons. However, the surface quantification of AMPA receptors was not sufficient to distinguish between the receptors localized specifically to the synapse or expressed on the dendritic shaft. Therefore, by using western blot analysis, I observed that the total levels of GluA2-containing AMPA were unchanged and only decreased in the membrane enriched fraction (P2). These data suggest that spastin does not affect gene expression of these receptors but might be an important regulator in the re-distribution of these proteins.

Microtubules are important tracks along which specific motor proteins transport cargoes. Given that spastin is involved in the severing of microtubules, I hypothesized that the reduction in GluA2-containing AMPA receptor surface levels might be due altered intracellular transport. Since the kinesin motor KIF5 controls the transport of GluA2-containing AMPA

receptors in dendrites, hippocampal neurons were transfected with a KIF5-pex-tomato construct, to investigate the movement and processivity of this motor protein and principally its cargoes. Indeed, KIF5 moved at slower rates and over shorter distances (i.e. lower processivity) in hippocampal neurons lacking spastin. In line with these results, I also documented altered movement of the GluA2-containing AMPA receptor clusters in the absence of spastin by live cell imaging experiments. These findings suggest that spastin might indirectly regulate the transport of cargoes, namely AMPA receptors, which are ultimately targeted to the postsynaptic membrane.

Based on spastin's regulation of the microtubule cytoskeleton, it is likely that altered transport was not specific only to AMPA receptors, but or whether there was a general impairment in transport of other cargoes.

In line with this, Denton *et al*. reported axonal swellings containing mitochondria and tau in a human neuronal model of hereditary spastic paraplegia associated with a mutation in the *SPAST* gene. This reported accumulation of organelles might be due to a spastin-dependent impairment of intracellular transport [139].

Therefore, I also examined the transport of mitochondria, an organelle that moves in both axons and dendrites. By labelling the mitochondria with mitotracker it was possible to investigate the transport of this organelle in hippocampal neurons.

Similar to the results presented by Denton and *et al,* the transport of mitochondria was altered in neurons lacking spastin. I also noted an abnormal distribution of these organelles throughout the neuron. Hippocampal neurons from spastin knockout mice had an accumulation of mitochondria in the soma and less frequent mitochondrial numbers in dendrites. As mitochondria move both toward the periphery and toward the soma, I could study how changes in the microtubule tracks might affect the directionality of intracellular transport. Analysis of the transport of mitochondria showed that the retrograde/anterograde movement ratio of mitochondria is altered in spastin knockout neurons.

Taken together, these data suggest a role of spastin in the regulation of the intracellular transport of various cargoes, by not only affecting the motor

protein activity (speed and processivity), but also the directionality of transport.

Chapter 5

Conclusions

5. Conclusions and future directions

The aim of the current study was to shed light on the function of spastin in microtubule-dependent transport processes and ultimately in the mechanisms underlying learning and memory.

I have shown in this thesis work that increased microtubule stabilization in the absence of spastin significantly contributes to impaired transport and the distribution of various cargoes in neurons. The molecular changes associated with loss of spastin ultimately have an impact *in vivo* as I have shown by the behavioral deficits in spastin (+/-) and (-/-) mice. This is in line with studies showing that neuronal function requires proper and timed intracellular transport to cope with plastic changes occurring at synapses during learning and memory.

Long-range transport poses a particular challenge to neurons. For example, in ascending and descending corticospinal tracts, neurons can grow up to one meter in length. Minor changes in the organization of the microtubule cytoskeleton in these nerve fibers might explain why the first symptoms of HSP are associated with impaired motor neuron function, particularly of the lower limbs.

For the first time, I have described, in a mouse model of HSP, the existence of altered cognitive function, specifically impaired working memory function and conditioned fear memory and extinction. Therefore, this mouse model might be useful for the design of future therapeutic approaches aimed at tackling not only the motor neuron deficits, but also the progressive cognitive decline in HSP patients.

This mouse model showed another potentially interesting, although not fully characterized anxiety-related phenotype. Several reports have described depressive episodes experienced by HSP patients, yet it remains unclear whether this symptom is a consequence of the debilitating impairments in motor function, or due to currently unknown progressive changes in the CNS. The present work indicates that haplo-insufficiency of spastin might be the triggering factor for the alterations observed in SPG4-linked HSP patients.

Indeed, spastin heterozygous mice often displayed the similar behavioral alterations as spastin homozygous knockout mice.

It would be interesting to distinguish between the effects of spastin during prenatal development and postnatal development of the brain using a conditional knockout model for spastin. My current work using a constitutive knockout mouse model has nonetheless confirmed that spastin has an important role *in vitro* and *in vivo*, by maintaining proper neuronal structure and function and modulating cognition, respectively.

References

6. References

1. Herculano-Houzel, S., *The human brain in numbers: a linearly scaled-up primate brain.* Front Hum Neurosci, 2009. **3**: p. 31.
2. Zervas, M., S. Blaess, and A.L. Joyner, *Classical embryological studies and modern genetic analysis of midbrain and cerebellum development.* Curr Top Dev Biol, 2005. **69**: p. 101-38.
3. Lin, Y.C. and A.J. Koleske, *Mechanisms of synapse and dendrite maintenance and their disruption in psychiatric and neurodegenerative disorders.* Annu Rev Neurosci, 2010. **33**: p. 349-78.
4. Harris, K.M. and J.K. Stevens, *Dendritic spines of CA 1 pyramidal cells in the rat hippocampus: serial electron microscopy with reference to their biophysical characteristics.* J Neurosci, 1989. **9**(8): p. 2982-97.
5. Pierce, J.P. and L.M. Mendell, *Quantitative ultrastructure of Ia boutons in the ventral horn: scaling and positional relationships.* J Neurosci, 1993. **13**(11): p. 4748-63.
6. Schikorski, T. and C.F. Stevens, *Quantitative ultrastructural analysis of hippocampal excitatory synapses.* J Neurosci, 1997. **17**(15): p. 5858-67.
7. Biederer, T., et al., *SynCAM, a synaptic adhesion molecule that drives synapse assembly.* Science, 2002. **297**(5586): p. 1525-31.
8. Garner, C.C., et al., *Molecular mechanisms of CNS synaptogenesis.* Trends Neurosci, 2002. **25**(5): p. 243-51.
9. Yamada, S. and W.J. Nelson, *Synapses: sites of cell recognition, adhesion, and functional specification.* Annu Rev Biochem, 2007. **76**: p. 267-94.
10. Zhai, R.G., et al., *Assembling the presynaptic active zone: a characterization of an active one precursor vesicle.* Neuron, 2001. **29**(1): p. 131-43.
11. Shapira, M., et al., *Unitary assembly of presynaptic active zones from Piccolo-Bassoon transport vesicles.* Neuron, 2003. **38**(2): p. 237-52.
12. Hering, H. and M. Sheng, *Dendritic spines: structure, dynamics and regulation.* Nat Rev Neurosci, 2001. **2**(12): p. 880-8.
13. Petroff, O.A., *GABA and glutamate in the human brain.* Neuroscientist, 2002. **8**(6): p. 562-73.
14. Chechik, G., I. Meilijson, and E. Ruppin, *Synaptic pruning in development: a computational account.* Neural Comput, 1998. **10**(7): p. 1759-77.
15. Varoqueaux, F., et al., *Total arrest of spontaneous and evoked synaptic transmission but normal synaptogenesis in the absence of Munc13-mediated vesicle priming.* Proc Natl Acad Sci U S A, 2002. **99**(13): p. 9037-42.
16. Verhage, M., et al., *Synaptic assembly of the brain in the absence of neurotransmitter secretion.* Science, 2000. **287**(5454): p. 864-9.
17. Sudhof, T.C., *The synaptic vesicle cycle.* Annu Rev Neurosci, 2004. **27**: p. 509-47.
18. Traynelis, S.F., et al., *Glutamate receptor ion channels: structure, regulation, and function.* Pharmacol Rev, 2010. **62**(3): p. 405-96.

19. Fink, J.K., *Hereditary spastic paraplegia: clinico-pathologic features and emerging molecular mechanisms.* Acta Neuropathol, 2013. **126**(3): p. 307-28.
20. Boukhris, A., et al., *Tunisian hereditary spastic paraplegias: clinical variability supported by genetic heterogeneity.* Clin Genet, 2009. **75**(6): p. 527-36.
21. Erichsen, A.K., et al., *Prevalence of hereditary ataxia and spastic paraplegia in southeast Norway: a population-based study.* Brain, 2009. **132**(Pt 6): p. 1577-88.
22. Filla, A., et al., *Prevalence of hereditary ataxias and spastic paraplegias in Molise, a region of Italy.* J Neurol, 1992. **239**(6): p. 351-3.
23. Byrne, P.C., et al., *Linkage of AD HSP and cognitive impairment to chromosome 2p: haplotype and phenotype analysis indicates variable expression and low or delayed penetrance.* Eur J Hum Genet, 1998. **6**(3): p. 275-82.
24. Reid, E., et al., *Subclinical cognitive impairment in autosomal dominant "pure" hereditary spastic paraplegia.* J Med Genet, 1999. **36**(10): p. 797-8.
25. Uttner, I., et al., *Cognitive performance in pure and complicated hereditary spastic paraparesis: a neuropsychological and neuroimaging study.* Neurosci Lett, 2007. **419**(2): p. 158-61.
26. Webb, S., et al., *Autosomal dominant hereditary spastic paraparesis with cognitive loss linked to chromosome 2p.* Brain, 1998. **121 (Pt 4)**: p. 601-9.
27. McDermott, C., et al., *Hereditary spastic paraparesis: a review of new developments.* J Neurol Neurosurg Psychiatry, 2000. **69**(2): p. 150-60.
28. Goldstein, L.S., *Kinesin molecular motors: transport pathways, receptors, and human disease.* Proc Natl Acad Sci U S A, 2001. **98**(13): p. 6999-7003.
29. Klebe, S., et al., *KIF1A missense mutations in SPG30, an autosomal recessive spastic paraplegia: distinct phenotypes according to the nature of the mutations.* Eur J Hum Genet, 2012. **20**(6): p. 645-9.
30. Reid, E., et al., *A kinesin heavy chain (KIF5A) mutation in hereditary spastic paraplegia (SPG10).* Am J Hum Genet, 2002. **71**(5): p. 1189-94.
31. Butler, R., et al., *Genetic and chemical modulation of spastin-dependent axon outgrowth in zebrafish embryos indicates a role for impaired microtubule dynamics in hereditary spastic paraplegia.* Dis Model Mech, 2010. **3**(11-12): p. 743-51.
32. Sherwood, N.T., et al., *Drosophila spastin regulates synaptic microtubule networks and is required for normal motor function.* PLoS Biol, 2004. **2**(12): p. e429.
33. Tarrade, A., et al., *A mutation of spastin is responsible for swellings and impairment of transport in a region of axon characterized by changes in microtubule composition.* Hum Mol Genet, 2006. **15**(24): p. 3544-58.
34. Fassier, C., et al., *Microtubule-targeting drugs rescue axonal swellings in cortical neurons from spastin knockout mice.* Dis Model Mech, 2013. **6**(1): p. 72-83.
35. Baas, P.W., et al., *Polarity orientation of microtubules in hippocampal neurons: uniformity in the axon and nonuniformity in the dendrite.* Proc Natl Acad Sci U S A, 1988. **85**(21): p. 8335-9.

36. Baas, P.W., M.M. Black, and G.A. Banker, *Changes in microtubule polarity orientation during the development of hippocampal neurons in culture.* J Cell Biol, 1989. **109**(6 Pt 1): p. 3085-94.
37. Baas, P.W. and S. Lin, *Hooks and comets: The story of microtubule polarity orientation in the neuron.* Dev Neurobiol, 2011. **71**(6): p. 403-18.
38. Akhmanova, A. and M.O. Steinmetz, *Control of microtubule organization and dynamics: two ends in the limelight.* Nat Rev Mol Cell Biol, 2015. **16**(12): p. 711-26.
39. Harada, A., et al., *MAP2 is required for dendrite elongation, PKA anchoring in dendrites, and proper PKA signal transduction.* J Cell Biol, 2002. **158**(3): p. 541-9.
40. Bartolini, F. and G.G. Gundersen, *Generation of noncentrosomal microtubule arrays.* J Cell Sci, 2006. **119**(Pt 20): p. 4155-63.
41. Folker, E.S., B.M. Baker, and H.V. Goodson, *Interactions between CLIP-170, tubulin, and microtubules: implications for the mechanism of Clip-170 plus-end tracking behavior.* Mol Biol Cell, 2005. **16**(11): p. 5373-84.
42. Kapitein, L.C. and C.C. Hoogenraad, *Building the Neuronal Microtubule Cytoskeleton.* Neuron, 2015. **87**(3): p. 492-506.
43. Dehmelt, L. and S. Halpain, *The MAP2/Tau family of microtubule-associated proteins.* Genome Biol, 2005. **6**(1): p. 204.
44. Kapitein, L.C., K.W. Yau, and C.C. Hoogenraad, *Microtubule dynamics in dendritic spines.* Methods Cell Biol, 2010. **97**: p. 111-32.
45. Merriam, E.B., et al., *Synaptic regulation of microtubule dynamics in dendritic spines by calcium, F-actin, and drebrin.* J Neurosci, 2013. **33**(42): p. 16471-82.
46. Matamoros, A.J. and P.W. Baas, *Microtubules in health and degenerative disease of the nervous system.* Brain Res Bull, 2016. **126**(Pt 3): p. 217-225.
47. Sharp, D.J. and J.L. Ross, *Microtubule-severing enzymes at the cutting edge.* J Cell Sci, 2012. **125**(Pt 11): p. 2561-9.
48. Vale, R.D., *Severing of stable microtubules by a mitotically activated protein in Xenopus egg extracts.* Cell, 1991. **64**(4): p. 827-39.
49. McNally, F.J. and R.D. Vale, *Identification of katanin, an ATPase that severs and disassembles stable microtubules.* Cell, 1993. **75**(3): p. 419-29.
50. Roll-Mecak, A. and F.J. McNally, *Microtubule-severing enzymes.* Curr Opin Cell Biol, 2010. **22**(1): p. 96-103.
51. Evans, K.J., et al., *Linking axonal degeneration to microtubule remodeling by Spastin-mediated microtubule severing.* J Cell Biol, 2005. **168**(4): p. 599-606.
52. Roll-Mecak, A. and R.D. Vale, *The Drosophila homologue of the hereditary spastic paraplegia protein, spastin, severs and disassembles microtubules.* Curr Biol, 2005. **15**(7): p. 650-5.
53. Salinas, S., et al., *Human spastin has multiple microtubule-related functions.* J Neurochem, 2005. **95**(5): p. 1411-20.
54. Salinas, S., et al., *Spastin and microtubules: Functions in health and disease.* J Neurosci Res, 2007. **85**(12): p. 2778-82.
55. Solowska, J.M. and P.W. Baas, *Hereditary spastic paraplegia SPG4: what is known and not known about the disease.* Brain, 2015. **138**(Pt 9): p. 2471-84.

56. Cox, G.A., et al., *The mouse fidgetin gene defines a new role for AAA family proteins in mammalian development.* Nat Genet, 2000. **26**(2): p. 198-202.
57. Leo, L., et al., *Vertebrate Fidgetin Restrains Axonal Growth by Severing Labile Domains of Microtubules.* Cell Rep, 2015. **12**(11): p. 1723-30.
58. White, S.R., et al., *Recognition of C-terminal amino acids in tubulin by pore loops in Spastin is important for microtubule severing.* J Cell Biol, 2007. **176**(7): p. 995-1005.
59. Roll-Mecak, A. and R.D. Vale, *Structural basis of microtubule severing by the hereditary spastic paraplegia protein spastin.* Nature, 2008. **451**(7176): p. 363-7.
60. Lacroix, B., et al., *Tubulin polyglutamylation stimulates spastin-mediated microtubule severing.* J Cell Biol, 2010. **189**(6): p. 945-54.
61. Valenstein, M.L. and A. Roll-Mecak, *Graded Control of Microtubule Severing by Tubulin Glutamylation.* Cell, 2016. **164**(5): p. 911-21.
62. Sudo, H. and P.W. Baas, *Acetylation of microtubules influences their sensitivity to severing by katanin in neurons and fibroblasts.* J Neurosci, 2010. **30**(21): p. 7215-26.
63. Ma, D.L., et al., *Spastin in the human and mouse central nervous system with special reference to its expression in the hippocampus of mouse pilocarpine model of status epilepticus and temporal lobe epilepsy.* Neurochem Int, 2006. **49**(7): p. 651-64.
64. Connell, J.W., et al., *Spastin couples microtubule severing to membrane traffic in completion of cytokinesis and secretion.* Traffic, 2009. **10**(1): p. 42-56.
65. Yu, W., et al., *The microtubule-severing proteins spastin and katanin participate differently in the formation of axonal branches.* Mol Biol Cell, 2008. **19**(4): p. 1485-98.
66. Ye, B., et al., *Differential regulation of dendritic and axonal development by the novel Kruppel-like factor Dar1.* J Neurosci, 2011. **31**(9): p. 3309-19.
67. Papadopoulos, C., et al., *Spastin binds to lipid droplets and affects lipid metabolism.* PLoS Genet, 2015. **11**(4): p. e1005149.
68. Kasher, P.R., et al., *Direct evidence for axonal transport defects in a novel mouse model of mutant spastin-induced hereditary spastic paraplegia (HSP) and human HSP patients.* J Neurochem, 2009. **110**(1): p. 34-44.
69. Miki, H., Y. Okada, and N. Hirokawa, *Analysis of the kinesin superfamily: insights into structure and function.* Trends Cell Biol, 2005. **15**(9): p. 467-76.
70. Vallee, R.B., et al., *Dynein: An ancient motor protein involved in multiple modes of transport.* J Neurobiol, 2004. **58**(2): p. 189-200.
71. Mandelkow, E. and E.M. Mandelkow, *Kinesin motors and disease.* Trends Cell Biol, 2002. **12**(12): p. 585-91.
72. Hirokawa, N. and Y. Noda, *Intracellular transport and kinesin superfamily proteins, KIFs: structure, function, and dynamics.* Physiol Rev, 2008. **88**(3): p. 1089-118.
73. Hirokawa, N., et al., *Submolecular domains of bovine brain kinesin identified by electron microscopy and monoclonal antibody decoration.* Cell, 1989. **56**(5): p. 867-78.
74. Scholey, J.M., et al., *Identification of globular mechanochemical heads of kinesin.* Nature, 1989. **338**(6213): p. 355-7.

75. Yang, J.T., R.A. Laymon, and L.S. Goldstein, *A three-domain structure of kinesin heavy chain revealed by DNA sequence and microtubule binding analyses.* Cell, 1989. **56**(5): p. 879-89.
76. Morii, H., et al., *Identification of kinesin neck region as a stable alpha-helical coiled coil and its thermodynamic characterization.* Biochemistry, 1997. **36**(7): p. 1933-42.
77. Tripet, B., R.D. Vale, and R.S. Hodges, *Demonstration of coiled-coil interactions within the kinesin neck region using synthetic peptides. Implications for motor activity.* J Biol Chem, 1997. **272**(14): p. 8946-56.
78. Seiler, S., et al., *Cargo binding and regulatory sites in the tail of fungal conventional kinesin.* Nat Cell Biol, 2000. **2**(6): p. 333-8.
79. Asbury, C.L., *Kinesin: world's tiniest biped.* Curr Opin Cell Biol, 2005. **17**(1): p. 89-97.
80. Woehlke, G., et al., *Microtubule interaction site of the kinesin motor.* Cell, 1997. **90**(2): p. 207-16.
81. Maday, S., et al., *Axonal transport: cargo-specific mechanisms of motility and regulation.* Neuron, 2014. **84**(2): p. 292-309.
82. Sirajuddin, M., L.M. Rice, and R.D. Vale, *Regulation of microtubule motors by tubulin isotypes and post-translational modifications.* Nat Cell Biol, 2014. **16**(4): p. 335-44.
83. Lakamper, S. and E. Meyhofer, *Back on track - on the role of the microtubule for kinesin motility and cellular function.* J Muscle Res Cell Motil, 2006. **27**(2): p. 161-71.
84. Westermann, S. and K. Weber, *Post-translational modifications regulate microtubule function.* Nat Rev Mol Cell Biol, 2003. **4**(12): p. 938-47.
85. Rosenbaum, J., *Cytoskeleton: functions for tubulin modifications at last.* Curr Biol, 2000. **10**(21): p. R801-3.
86. Magiera, M.M. and C. Janke, *Post-translational modifications of tubulin.* Curr Biol, 2014. **24**(9): p. R351-4.
87. Song, Y. and S.T. Brady, *Post-translational modifications of tubulin: pathways to functional diversity of microtubules.* Trends Cell Biol, 2015. **25**(3): p. 125-36.
88. Ikegami, K., et al., *Loss of alpha-tubulin polyglutamylation in ROSA22 mice is associated with abnormal targeting of KIF1A and modulated synaptic function.* Proc Natl Acad Sci U S A, 2007. **104**(9): p. 3213-8.
89. Boucher, D., et al., *Polyglutamylation of tubulin as a progressive regulator of in vitro interactions between the microtubule-associated protein Tau and tubulin.* Biochemistry, 1994. **33**(41): p. 12471-7.
90. Larcher, J.C., et al., *Interaction of kinesin motor domains with alpha- and beta-tubulin subunits at a tau-independent binding site. Regulation by polyglutamylation.* J Biol Chem, 1996. **271**(36): p. 22117-24.
91. Lafanechere, L. and D. Job, *Preparation of pure tyrosinated or detyrosinated tubulin isoforms.* Methods Mol Biol, 2011. **777**: p. 71-86.
92. Janke, C. and J.C. Bulinski, *Post-translational regulation of the microtubule cytoskeleton: mechanisms and functions.* Nat Rev Mol Cell Biol, 2011. **12**(12): p. 773-86.
93. Wloga, D. and J. Gaertig, *Post-translational modifications of microtubules.* J Cell Sci, 2010. **123**(Pt 20): p. 3447-55.

94. Brown, A., et al., *Composite microtubules of the axon: quantitative analysis of tyrosinated and acetylated tubulin along individual axonal microtubules.* J Cell Sci, 1993. **104 (Pt 2)**: p. 339-52.
95. Dunn, S., et al., *Differential trafficking of Kif5c on tyrosinated and detyrosinated microtubules in live cells.* J Cell Sci, 2008. **121**(Pt 7): p. 1085-95.
96. Reed, N.A., et al., *Microtubule acetylation promotes kinesin-1 binding and transport.* Curr Biol, 2006. **16**(21): p. 2166-72.
97. Rajmohan, V. and E. Mohandas, *The limbic system.* Indian J Psychiatry, 2007. **49**(2): p. 132-9.
98. Shrager, Y., et al., *Spatial memory and the human hippocampus.* Proc Natl Acad Sci U S A, 2007. **104**(8): p. 2961-6.
99. O'Keefe, J. and J. Dostrovsky, *The hippocampus as a spatial map. Preliminary evidence from unit activity in the freely-moving rat.* Brain Res, 1971. **34**(1): p. 171-5.
100. Wilson, M.A. and B.L. McNaughton, *Dynamics of the hippocampal ensemble code for space.* Science, 1993. **261**(5124): p. 1055-8.
101. Ming, G.L. and H. Song, *Adult neurogenesis in the mammalian central nervous system.* Annu Rev Neurosci, 2005. **28**: p. 223-50.
102. Squire, L.R., *The legacy of patient H.M. for neuroscience.* Neuron, 2009. **61**(1): p. 6-9.
103. Jahn, H., *Memory loss in Alzheimer's disease.* Dialogues Clin Neurosci, 2013. **15**(4): p. 445-54.
104. Dent, E.W., *Of microtubules and memory: implications for microtubule dynamics in dendrites and spines.* Mol Biol Cell, 2017. **28**(1): p. 1-8.
105. Shumyatsky, G.P., et al., *stathmin, a gene enriched in the amygdala, controls both learned and innate fear.* Cell, 2005. **123**(4): p. 697-709.
106. Barnes, S.J., et al., *Stable mossy fiber long-term potentiation requires calcium influx at the granule cell soma, protein synthesis, and microtubule-dependent axonal transport.* J Neurosci, 2010. **30**(39): p. 12996-3004.
107. Fanara, P., et al., *Changes in microtubule turnover accompany synaptic plasticity and memory formation in response to contextual fear conditioning in mice.* Neuroscience, 2010. **168**(1): p. 167-78.
108. Uchida, S., et al., *Learning-induced and stathmin-dependent changes in microtubule stability are critical for memory and disrupted in ageing.* Nat Commun, 2014. **5**: p. 4389.
109. Henley, J.M. and K.A. Wilkinson, *AMPA receptor trafficking and the mechanisms underlying synaptic plasticity and cognitive aging.* Dialogues Clin Neurosci, 2013. **15**(1): p. 11-27.
110. Henley, J.M. and K.A. Wilkinson, *Synaptic AMPA receptor composition in development, plasticity and disease.* Nat Rev Neurosci, 2016. **17**(6): p. 337-50.
111. Gerges, N.Z., D.S. Backos, and J.A. Esteban, *Local control of AMPA receptor trafficking at the postsynaptic terminal by a small GTPase of the Rab family.* J Biol Chem, 2004. **279**(42): p. 43870-8.
112. Zhang, H., et al., *Regulation of AMPA receptor surface trafficking and synaptic plasticity by a cognitive enhancer and antidepressant molecule.* Mol Psychiatry, 2013. **18**(4): p. 471-84.

113. Passafaro, M., V. Piech, and M. Sheng, *Subunit-specific temporal and spatial patterns of AMPA receptor exocytosis in hippocampal neurons.* Nat Neurosci, 2001. **4**(9): p. 917-26.
114. Harris, K.M., F.E. Jensen, and B. Tsao, *Three-dimensional structure of dendritic spines and synapses in rat hippocampus (CA1) at postnatal day 15 and adult ages: implications for the maturation of synaptic physiology and long-term potentiation.* J Neurosci, 1992. **12**(7): p. 2685-705.
115. Cendelin, J., *From mice to men: lessons from mutant ataxic mice.* Cerebellum Ataxias, 2014. **1**: p. 4.
116. Wang, L. and A. Brown, *A hereditary spastic paraplegia mutation in kinesin-1A/KIF5A disrupts neurofilament transport.* Mol Neurodegener, 2010. **5**: p. 52.
117. van Swieten, J.C., S.M. Rosso, and P. Heutink, *MAPT-Related Disorders*, in *GeneReviews(R)*, R.A. Pagon, et al., Editors. 1993: Seattle (WA).
118. Inoue, H., H. Nojima, and H. Okayama, *High efficiency transformation of Escherichia coli with plasmids.* Gene, 1990. **96**(1): p. 23-8.
119. Kohrmann, M., et al., *Fast, convenient, and effective method to transiently transfect primary hippocampal neurons.* J Neurosci Res, 1999. **58**(6): p. 831-5.
120. Brill, M.S., et al., *Branch-Specific Microtubule Destabilization Mediates Axon Branch Loss during Neuromuscular Synapse Elimination.* Neuron, 2016. **92**(4): p. 845-856.
121. Gu, J., B.L. Firestein, and J.Q. Zheng, *Microtubules in dendritic spine development.* J Neurosci, 2008. **28**(46): p. 12120-4.
122. Banks, G., et al., *A missense mutation in Katnal1 underlies behavioural, neurological and ciliary anomalies.* Mol Psychiatry, 2017.
123. Goyal, U., et al., *Spastin-interacting protein NA14/SSNA1 functions in cytokinesis and axon development.* PLoS One, 2014. **9**(11): p. e112428.
124. Fink, J.K., *Hereditary Spastic Paraplegia Overview*, in *GeneReviews(R)*, R.A. Pagon, et al., Editors. 1993: Seattle (WA).
125. Kirova, A.M., R.B. Bays, and S. Lagalwar, *Working memory and executive function decline across normal aging, mild cognitive impairment, and Alzheimer's disease.* Biomed Res Int, 2015. **2015**: p. 748212.
126. Rudy, J.W. and P. Matus-Amat, *The ventral hippocampus supports a memory representation of context and contextual fear conditioning: implications for a unitary function of the hippocampus.* Behav Neurosci, 2005. **119**(1): p. 154-63.
127. Ebneth, A., et al., *Overexpression of tau protein inhibits kinesin-dependent trafficking of vesicles, mitochondria, and endoplasmic reticulum: implications for Alzheimer's disease.* J Cell Biol, 1998. **143**(3): p. 777-94.
128. Ikegami, S., A. Harada, and N. Hirokawa, *Muscle weakness, hyperactivity, and impairment in fear conditioning in tau-deficient mice.* Neurosci Lett, 2000. **279**(3): p. 129-32.
129. Kaganovsky, K. and C.Y. Wang, *How Do Microtubule Dynamics Relate to the Hallmarks of Learning and Memory?* J Neurosci, 2016. **36**(22): p. 5911-3.
130. Bodaleo, F.J. and C. Gonzalez-Billault, *The Presynaptic Microtubule Cytoskeleton in Physiological and Pathological Conditions: Lessons from Drosophila Fragile X Syndrome and Hereditary Spastic Paraplegias.* Front Mol Neurosci, 2016. **9**: p. 60.

131. Gu, J. and J.Q. Zheng, *Microtubules in Dendritic Spine Development and Plasticity.* Open Neurosci J, 2009. **3**: p. 128-133.
132. Moughamian, A.J., et al., *Ordered recruitment of dynactin to the microtubule plus-end is required for efficient initiation of retrograde axonal transport.* J Neurosci, 2013. **33**(32): p. 13190-203.
133. Schiff, P.B., J. Fant, and S.B. Horwitz, *Promotion of microtubule assembly in vitro by taxol.* Nature, 1979. **277**(5698): p. 665-7.
134. Schiff, P.B. and S.B. Horwitz, *Taxol stabilizes microtubules in mouse fibroblast cells.* Proc Natl Acad Sci U S A, 1980. **77**(3): p. 1561-5.
135. Derry, W.B., L. Wilson, and M.A. Jordan, *Substoichiometric binding of taxol suppresses microtubule dynamics.* Biochemistry, 1995. **34**(7): p. 2203-11.
136. Theiss, C. and K. Meller, *Taxol impairs anterograde axonal transport of microinjected horseradish peroxidase in dorsal root ganglia neurons in vitro.* Cell Tissue Res, 2000. **299**(2): p. 213-24.
137. Goshima, Y., T. Hida, and T. Gotoh, *Computational analysis of axonal transport: a novel assessment of neurotoxicity, neuronal development and functions.* Int J Mol Sci, 2012. **13**(3): p. 3414-30.
138. Hammond, J.W., et al., *Posttranslational modifications of tubulin and the polarized transport of kinesin-1 in neurons.* Mol Biol Cell, 2010. **21**(4): p. 572-83.
139. Denton, K.R., et al., *Loss of spastin function results in disease-specific axonal defects in human pluripotent stem cell-based models of hereditary spastic paraplegia.* Stem Cells, 2014. **32**(2): p. 414-23.

Appendix

7. Appendix

7.1 List of figures

Figure 1.1: The tubulin assembly-disassembly cycle……18
Figure 1.2: Dynamics of microtubule polymerization and cargo transport……19
Figure 1.3: Schematic representation of the spastin domains……..21
Figure 1.4: Subunit composition of KIF5 motor protein. ……..26
Figure 1.5: Most common tubulin posttranslational modifications……..…28
Figure 1.6: Alternative routes of AMPA receptor trafficking to the synapse……34
Figure 2.12.8: Experimental design for contextual fear conditioning test.....60
Figure 3.1: General phenotypical characterization of the spastin knockout mouse……..63
Figure 3.2: Progressive impairment of motor performance in spastin -/- mice……66
Figure 3.3: Spontaneous and confined alternation behavior tested in spastin-depleted ice……..69
Figure 3.4: Altered contextual fear learning in spastin-depleted mice at 8 and 14 months……72
Figure 3.5: Spastin deficiency alters synaptic density……74
Figure 3.6: Spastin deficiency alters spine morphology……..75
Figure 3.7: Altered distribution of KIF1a cargo, synaptic vesicles, in spastin-depleted mice……..76
Figure 3.8: Spastin depletion reduces cell surface expression of GluA2-containing receptors……78
Figure 3.9: Spastin regulates microtubule stability……...80
Figure 3.10:ultrastructural analysis of microtubule cytoskeleton from spastin deficient mice (-/-) and their WT littermates (+/+)……..81
Figure 3.11: The microtubule-severing enzyme spastin regulates microtubule dynamics……...82
Figure 3.12. Visualization of mCherry-GluR2 particles by time lapse imaging……..83

Figure 3.13: The effect of spastin deficiency on KIF5c motility in dendrites……84
Figure 3.14: Altered intracellular transport of mitochondria in spastin -/- neurons……..….86
Figure 3.15: Altered axonal transport of synaptophysin in neurons lacking spastin……...87
Figure 3.16: Reduced surface GluA2 levels upon treatment with 100nM taxol……..89

7.2 List of tables

Table 2.4.1: List of used primary antibodies in this study…….44
Table 2.4.2: List of used secondary antibodies……..44
Table 2.5: List of used vectors……..45
Table 2.6: List of used unmodified oligonucleotides for PCR genotyping..45
Table 2.7.6: Components of the master mix reaction mixture for genotyping PCR of spastin knockout mice……48
Table 2.11.1: Chronological representation of the behavior experiments and duration……. 56

7.3 Abbreviations

α	Anti/alpha
AAA	Triple-A A*TPases*
ADP	Adenosine diphosphate.
ALS	Amyotrophic lateral sclerosis
AMP-PNP	Adenylyl-imidodiphosphate
AMPA	α-amino-3-hydroxy-5-methyl-4-isoxazolepropionic acid
APP	Amyloid precursor protein
ATP	Adenosine triphosphate
bidest.	Distilled twice
C-terminal	carboxy terminal
CA1	Cornu ammonis 1
CA3	Cornu ammonis 3
CAM	Cell surface adhesion molecule

CAMKIIα	Calcium/calmodulin-dependent protein kinase type II alpha chain
CAMSAP	Calmodulin-regulated spectrin-associated protein
CCP	Carboxypeptidase
CLASP2	CLIP-associating protein 2
CLIP-170	Cytoplasmatic linker protein-170
CNS	Central nervous system
Cy3	Indocarbocyanine
Cy5	Indodicarbocyanine
DG	Dentate gyrus
DIV	Days *in vitro*
dNTP	Deoxynucleoside triphosphate
DRG	Dorsal root ganglia
EB3	End-binding protein 3
ER	Endoplasmatic reticulum
ESCRT-III	Endosomal sorting complexes required for transport-III
GABA	Gamma-aminobutyric acid
GDP	Guanosine diphosphate
GluA1/2	Glutamate receptor subunit 1/2
GRIP1	Glutamate receptor-interacting protein 1
GTP	Guanosine-5'-triphosphate
HR	Hydrophobic region
HRP	Horseradish peroxidase
HSP	Hereditary spastic paraplegia
JIP1	c-Jun N-terminal kinase-*interacting protein 1*
K252	Lysine 252
K40	Lysine 40
KATNAL1	Katanin catalytic subunit A1 like 1
KHC	Kinesin heavy chain
KIF5	Kinesin-related protein 5
KIF5A	Kinesin-related protein 5A
KLC	Kinesin light chain
LTP	Long-term potentiation
MAP	Microtubule-associated protein

MAP2 Microtubule-associated protein 2

MAPT Microtubule-associated protein tau

MIT Microtubule Interacting and Trafficking

mRNA Messenger ribonucleic acid

MT Microtubule

MTBD Microtubule binding domain

NMDAN-Methyl-D-aspartic acid

NR1 NMDA receptor 1

NSE Neuron specific enolase

PCR Polymerase chain reaction

PGS1 Phosphatidylglycerophosphate Synthase 1

PSD95 Postsynaptic density 95

PTM Posttranslational modification

PVDF Polyvinylidene fluoride

Q15 Glutamine 15

REEP1 Receptor expression-enhancing protein 1

RPM Rounds per minute

S172 Serine 172

SEM Standard error of the mean

SNAP23 Synaptosomal-associated protein 23

SNARE Soluble N-ethylmaleimide-sensitive-factor attachment receptor

SPAST Spastin

SPG10 Spastic paraplegia-10

SPG4 Spastic gait gene 4

SYNCAM Synaptic cell adhesion molecule

TBST Tris buffered saline Tween-20

+TIP Microtubule plus-end-tracking proteins

TTL Tubulin tyrosine ligase

TTLL Tubulin tyrosine ligase like

TUBA4A Tubulin alpha 4a

TUBA8 Tubulin alpha 8

US Unconditioned stimulus

VPS4 Vacuolar protein sorting-associated protein 4

WT Wildtype

Units	
%	Percent
Da	Dalton
g	gram
°C	degree Celcius
l	liter
h	hour
min	minute
s	second
m	meter
mol	Mol
V	Volt

Prefixes	
n	nano (10^{-9})
µ	micro (10^{-6})
m	mili (10^{-3})
k	kilo (10^{3})

8. Acknowledgements

I would like to express my sincere gratitude towards all the people, who contributed to the success of this work. At first, I would like to thank my supervisor Prof. Dr. Matthias Kneussel for the time he has invested on me. I have learnt a lot from him in the last three years.

I am also truly grateful to my co-supervisor Dr. Torben Hausrat for his guidance and suggestions during the course of this study.

I am also truly grateful to my thesis committee member Prof. Dr. Christian Lohr, for his help and support.

I especially thank, the coordinator of the Research Training Group 1459, Dr. Thomas Braulke and his secretary Dr. Dorthe Labonté for their valuable support over these years.

I am grateful to all the members of the Molecular Neurogenetics institute.

Last but not least, I would like to thank my parents for all the love and support they gave me.

This study was financially supported by the DFG, German research foundation.